Artemisinin Optimization based on Malaria Therapy: Algorithm and Applications to Medical Image Segmentation

Chong Yuan [1], Dong Zhao [1,*], Ali Asghar Heidari [2], Lei Liu [3], Yi Chen [4], Zongda Wu[5], Huiling Chen [4,*]

[1] College of Computer Science and Technology, Changchun Normal University, Changchun, Jilin 130032, China (yc18338414794@163.com, zd-hy@163.com)

[2] School of Surveying and Geospatial Engineering, College of Engineering, University of Tehran, Tehran, Iran (as_heidari@ut.ac.ir)

[3] College of Computer Science, Sichuan University, Chengdu, Sichuan 610065, China (liulei.cx@gmail.com)

[4] Key Laboratory of Intelligent Informatics for Safety & Emergency of Zhejiang Province, Wenzhou University, Wenzhou 325035, China (kenyoncy2016@gmail.com, chenhuiling.jlu@gmail.com)

[5] Department of Computer Science and Engineering, Shaoxing University, Shaoxing 312000, China (zongda1983@163.com)

*Corresponding Author: Dong Zhao, Huiling Chen

E-mail: zd-hy@163.com (Dong Zhao), chenhuiling.jlu@gmail.com (Huiling Chen)

Abstract: This study proposes an efficient metaheuristic algorithm called the Artemisinin Optimization (AO) algorithm. This algorithm draws inspiration from the process of artemisinin medicine therapy for malaria, which involves the comprehensive eradication of malarial parasites within the human body. AO comprises three optimization stages: a comprehensive eliminations phase simulating global exploration, a local clearance phase for local exploitation, and a post-consolidation phase to enhance the algorithm's ability to escape local optima. In the experimental, this paper conducts qualitative analysis experiments on the AO, explaining its characteristics in searching for the optimal solution. Subsequently, AO is then tested on the classical IEEE CEC 2014, and the latest IEEE CEC 2022 benchmark function sets to assess its adaptability to various function types. Comparative analyses are conducted against eight well-established algorithms and eight high-performance improved algorithms. Statistical analyses of convergence curves and qualitative metrics revealed AO's robust competitiveness. Lastly, the AO is incorporated into breast cancer pathology image segmentation applications. Using fifteen authentic medical images at six threshold levels, AO's segmentation performance is compared against eight distinguished algorithms. Experimental results demonstrated AO's superiority in terms of image segmentation accuracy, Feature Similarity Index (FSIM), Peak Signal-to-Noise Ratio (PSNR), and Structural Similarity Index (SSIM) over the contrast algorithms. These comparative findings emphasize AO's efficacy and its potential in real-world optimization applications. The source codes of this paper will be available in https://aliasgharheidari.com/AO.html and other public websites.

Keywords: Meta-heuristic algorithms; Artemisinin Optimization; Medical applications; Multi-threshold image segmentation

1. Introduction

The current industrial problems are more complex than before, involving many variables, which this fact force us to develop more efficient methods [1]. These problems typically involve intricate scenarios with many decision variables, making it challenging to

identify the global optima swiftly. Due to multiple local optima and the high computational costs associated with these problems, finding a practical solution has become a significant challenge [2, 3]. Researchers have proposed various optimization methods to address this difficulty over the years.

We can differentiate between optimization methods by categorizing them as either deterministic or non-deterministic. Deterministic methods typically rely on established rules, mathematical models, or iterative processes for optimization. Classic examples of deterministic techniques include the Newton method [4] and gradient descent [5], which often employ deterministic rules or gradient information to compute parameters in the direction of the optimal solution. However, deterministic methods may get trapped in local optima when dealing with complex problems, especially those involving multiple peaks. Non-deterministic methods introduce randomness or probabilistic search strategies during the search process, typically employed to address situations with complex search spaces, multiple local optima, or unclear problem structures. Optimization problems in the real world often exhibit intricate characteristics, challenging the efficacy of deterministic approaches and thereby rendering stochastic methods, particularly metaheuristic algorithms, as viable solutions for tackling such problems.

Metaheuristic Algorithms (MAs) constitute a classic category of non-deterministic methods inspired by nature, biological populations, and human societies. They utilize various intelligent computational strategies to guide the search for solutions [6, 7]. Because MAs rely on stochastic search techniques to find optimal solutions [8], they reduce sensitivity to initial conditions, allowing a focus on input and output without overly concerning the problem's internal structure.

The widespread acceptance of metaheuristic algorithms is largely due to their simple conceptual structure, straightforward implementation, and effectiveness in complex, nonlinear settings. These methods typically initiate the optimization process with randomized initial solutions. Through iterative cycles guided by unique computational directives, candidate solutions are iteratively updated and refined. Eventually, the most optimal candidate solution emerges as the solution to the problem. The simplicity of MAs, derived from foundational theories and mathematically inspired by natural phenomena, renders them highly adaptable to real-world scenarios. They can be regarded as versatile "black boxes," capable of producing specific outcomes for diverse inputs and problem sets. Researchers can tailor these algorithms to address various optimization challenges by adjusting their structural configurations and parameters [9, 10]. Moreover, the stochastic nature of these algorithms enables them to explore the entirety of the search space, mitigating the risk of being confined within local optima and facilitating the discovery of ideal solutions. However, due to their problem-agnostic nature, solutions derived from MAs do not always guarantee global optimality. The stochastic nature of their search processes often yields near-optimal rather than globally optimal solutions. The performance of MAs exhibits substantial variability based on the processes involved in searching for and updating candidate solutions. As a result, researchers persistently work to create better solutions and tailor these algorithms to tackle optimization problems. Metaheuristic algorithms stand out in handling a wide range of optimization issues by leveraging their flexibility and adaptability, including complexities, nonlinearities, and non-differentiability in numerical problems. Their successful applications transcend various domains, rendering them invaluable tools for researchers and practitioners [11].

Despite the significant roles that numerous algorithms play in addressing problems across various domains, limitations persist:

(1) Achieving optimal performance in metaheuristic algorithms requires balancing exploration and exploitation. Each algorithm unavoidably encounters the issue of exploring and utilizing the unknown space when searching for the best answer. Exploration involves extensive probing of the search space to discover unknown regions, while exploitation focuses on finding the optimal solution within known regions. To attain the best results, algorithms must balance exploration and exploitation, preventing premature convergence and enhancing robustness [12].

(2) No algorithm can address all optimization problems in best fashion, as per NFL theory [13]. Therefore, an ongoing imperative exists for the continual refinement of novel optimization algorithms to surpass the constraints and exceed the capabilities of current algorithms. Numerous formidable optimization conundrums persistently emerge with the rapid evolution witnessed across various sectors. Current optimization methods might not adequately resolve these issues, necessitating the creation of novel optimization technologies to tackle these challenges..

(3) Although many researchers have been diligently striving to explore various avenues for enhancing and refining existing algorithms, aiming to overcome the limitations [14], these strategies encompass the implementation of optimization modules, refining algorithmic structures, and harnessing parallel computing or distributed systems, among others. With the passage of time and the continual advancement of technology, these strategies may become increasingly intricate, potentially narrowing the scope for performance enhancements. Furthermore, at times, further improvements may encounter the issue of diminishing returns, wherein the performance gains from each iteration gradually diminish, possibly failing to meet the anticipated standards.

Developing new optimization algorithms can alleviate such stagnation and serve as an efficient source of inspiration for enhancing existing algorithms.

To address the aforementioned challenges, there is a drive to conduct research and development on new algorithms, aiming to strike a balance between algorithm specialization and adaptability [15]. The design and analysis of new algorithms have been an active research topic [16]. By studying the wisdom of predecessors through academic literature and interdisciplinary crossroads, drawing inspiration, and accumulating experience, we introduce an efficient metaheuristic algorithm in this paper named Artemisinin Optimization (AO). It is inspired by the curative process of a medicine (artemisinin) against a disease (malaria), simulating the eradication of malarial parasites in the human body. AO primarily comprises three processes:

(1) Simulating the use of a higher dose of artemisinin in the early stages of treatment to eliminate a large number of malarial parasites in the human body, we propose a comprehensive elimination phase strategy for global exploration. This strategy uniquely follows pharmacokinetics, simulating the diffusion of medicines in the human body. Flowing the algorithm's progression, it adjusts the search step size, smoothly transitioning into the local exploitation phase.

(2) Simulating the gradual reduction of drug dosage in the mid to late stages of treatment to eliminate the remaining small number of malarial parasites in the human body, this paper proposes a local clearance phase strategy. This strategy incentivizes the algorithm to perform precise solutions within known regions, thereby augmenting its local exploitation capabilities.

(3) Considering the possibility of malaria recurrence in the late stages of treatment and introducing a post-consolidation strategy. This strategy furnishes the algorithm with mechanisms to counteract entrapment in local optima, thereby enhancing its ability to escape from the trap.

In the experimental section, this paper conducts a comprehensive performance analysis of the AO. Firstly, qualitative analysis experiments were designed to elucidate the algorithm's characteristics and adaptability. To verify its competitiveness among similar outstanding algorithms, AO is compared with eight widely acknowledged algorithms and eight high-performance improved algorithms on both the classic benchmark function set of the IEEE CEC 2014 and the latest set of the IEEE CEC 2022.

Following these efforts, it was applied to a classic scenario in MAs: Multi-threshold Image Segmentation (MTIS) to validate AO's optimization performance in real-world applications. Real pathology images from breast cancer patients were segmented using AO. In the context of image segmentation, due to the imbalance between exploration and exploitation, the likelihood of the algorithm getting stuck in local minima increases with the number of thresholds, reducing efficiency and segmentation accuracy. Combining AO with the MTIS techniques, optimal threshold sets were computed, reducing the complexity of threshold set computation and improving segmentation accuracy. A comprehensive comparison is designed for the experimental results, evaluating AO's segmentation performance meticulously against 8 other MAs at 6 threshold levels. In summary, the contributions of this paper are as follows:

(1) Drawing inspiration from the curative properties of artemisinin against malaria, an efficient Metaheuristic Algorithm is devised. This algorithm aims to establish a well-balanced exploration and exploitation paradigm akin to the dynamics observed in the treatment process of artemisinin. This innovative approach introduces a fresh solution for addressing optimization problems.

(2) In-depth study of AO's exploration and exploitation capabilities is undertaken through a comprehensive set of qualitative analysis experiments. These experiments aimed to unveil the fundamental reasons behind the performance of this technology.

(3) This paper conducted numerical optimization experiments to validate the performance of AO. A comprehensive assessment was conducted on representative IEEE CEC 2014 and the latest IEEE CEC 2022 benchmark function sets, with thorough comparisons against eight well-established and highly improved algorithms.

(4) Integration of AO with MTIS technology enhanced the segmentation accuracy of breast cancer images, leveraging the performance advantages of the AO algorithm. The balance between exploration and exploitation in AO exhibited strong adaptability at different threshold levels.

The subsequent sections of this manuscript encompass the following segments: Section 2 delves into the process of artemisinin's curative efficacy against malaria and elucidates inspirations derived from it. Section 3 introduces the design of AO, explicating its conceptualization and implementation. Section 4 showcases experiments conducted to assess AO's performance, followed by a meticulous analysis of the obtained results. Section 5 demonstrates AO's application in the context of MTIS issues. Finally, Section 6 summarizes the entirety of the work undertaken in this paper, providing an overview of prospective avenues and approaches for further research.

2. Literature review

Metaheuristic Algorithms are specific strategies crafted to effectively tackle complex optimization dilemmas, especially in cases involving insufficient or flawed data, or restricted computational capabilities. They are advanced algorithms or heuristic procedures capable of discovering, generating, adjusting, or selecting strategies to yield satisfactory solutions to optimization problems. In the research landscape of MAs, based on theoretical backgrounds, they can be primarily categorized into four types: evolution-based, physical phenomena-based, swarm intelligence-based, and human societies-based algorithms.

Algorithms based on biological evolution principles essentially implement the notion of incremental optimization search by imitating the mechanisms that are inherent in the process of biological evolution. Examples include genetic algorithm (GA) [17], genetic programming (GP) [18], differential evolution algorithm (DE) [19], biogeography-based optimizer (BBO) [20], evolution strategy (ES) [21], gradient evolution algorithm (GVA) [22], and others. These algorithms use crossover, mutation, and selection procedures to find global optimums, thus being appropriate for complicated domains and high-dimensional problems.

In swarm intelligence-based algorithms, researchers focus on instincts observed in animal populations, such as the instinct to seek advantages and avoid harm, and such behaviors are beneficial for individual or collective survival. These algorithms iterate and update by simulating cooperation or information exchange among individuals in a population, aiming to search for global optima. Examples include particle swarm optimization (PSO) [23], artificial bee colony (ABC) [24], ant colony optimization (ACO) [25], grey wolf optimizer (GWO) [26], and grasshopper optimization algorithm (GOA) [27], slime mould algorithm (SMA) [28, 29], colony predation algorithm (CPA) [30], Harris hawks optimization (HHO) [31], salp swarm algorithm(SSA) [32], bat algorithm (BA) [33], cat optimization algorithm (COA) [34], parrot optimizer (PO) [35], and hunger games search (HGS) [36].

Physics-based algorithms involve researchers drawing inspiration from physical principles like inertia, electromagnetic forces, and gravity. Within these algorithms, search agents interact and navigate the search space based on these physical rules. Examples include gravitational search algorithm (GSA) [37], the earlier proposed black hole optimization (BHO) [38], the galaxy-based search algorithm (GbSA) [39], equilibrium optimizer (EO) [40], simulated annealing (SA) [41], multi-verse optimizer (MVO) [42], central force optimization (CFO) [43], RIME algorithm (RIME) [15], weighted mean of vectors (INFO) [44], and Runge-kutta optimizer (RUN) [45].

The final category of algorithms draws inspiration from the intricate dynamics of human societies. These algorithms are designed to imitate various interactive behaviors and organizational activities observed in human societies, such as cooperation, competition, and information transmission, to address diverse problems. Examples include teaching–learning–based optimization (TLBO) [46], political optimizer (PO) [47], harmony search (HS) [48], exchange market algorithm (EMA) [49], social group optimization (SGO) [50], Jaya algorithm (JAYA) [51], and liver cancer algorithm (LCA) [52].

Over the past two decades, MAs have captured significant attention from researchers. Firstly, they are relatively straightforward to implement and involve very basic concepts. Secondly, they outperform local search algorithms. Thirdly, they find wide-ranging applications across various domains, including economic emission [53, 54], feature selection [55, 56], scheduling difficulties [57-59], bankruptcy prediction [60], medical diagnostics [61, 62], engineering design applications [63].

3. Inspiration from the malaria treatment

One of the most dreaded illness is one caused by a species of parasitic protozoa known to man as Malaria caused by the Plasmodium falciparum and others in the Plasmodium family. [64]. Malaria is now a global pandemic and is a major public health problem in tropical and subtropical areas of the world such as Asia, Africa and Central and South America [65]. Among the many steps to control malaria epidemic, in the area of malaria drug treatment, under the leadership of Tu Youyou, in 2015 several Chinese scientists were able to make an important contribution in malaria treatment when they isolated and extracted a compound artemisinin from a plant artemisia annua. They purified and performed crystallographic analysis of artemisinin. This is just the first time Artemisinin was extracted by Chinese in early 1970s. Artemisinin has exceptional abilities to quickly clear the parasite load from the patient's blood, rapidly reduce clinical manifestations of malaria and give relief to the malaria patient [64, 66].

Artemisinin medications travel throughout different parts of the body and cells once they enter the human bloodstream. It's worth mentioning that red blood cells carry a significant amount of ferrous ions (Fe2+), especially in those infected by malaria parasites [67]. The artemisinin molecule has certain active groups that react chemically when they come into contact with ferrous ions. This interaction harms the biological membrane of the malaria parasite and internal biomolecules, leading to the disruption of cellular membrane integrity and causing the membrane to rupture. At the same time, artemisinin messes with the internal biochemical workings of the malaria parasite, messing up its ability to survive. When someone gets malaria, the journey from getting infected to finally finding relief with artemisinin follows a certain path [65, 68, 69]:

1. Infection: Malaria generally starts when the parasite is passed on by a mosquito's bite. After entering the bloodstream, the malaria parasite moves to liver cells, goes through various stages of development, and then invades red blood cells.
2. Malaria symptoms onset: After the malaria parasite enters red blood cells, there is a quick growth that results in the release of toxins and the start of malaria symptoms in the infected person. These signs frequently consist of elevated body temperature, shivering, head pain, and muscle soreness, indicating the start of the illness presentation.
3. Medical consultation and diagnosis: When individuals show symptoms of malaria, they usually go to a doctor for diagnosis and treatment. Healthcare providers use blood tests to verify the existence of malaria parasites in the blood.
4. Initial treatment (Attack phase): Treatment begins with the initial phase of attack, where medical professionals give artemisinin medications in higher amounts to promptly relieve malaria symptoms.
5. Subsequent medication: Patients have regular appointments for blood tests to track the advancement of the illness and guarantee successful therapy, ultimately lowering the chances of a recurrence.
6. Mid-to-Late treatment (Maintenance phase): After the initial phase of treatment, patients move on to the maintenance phase, during which they receive reduced amounts of artemisinin in order to ensure full elimination of the malaria parasites. The length of this stage changes based on the specific situations of each patient and medical advice given.
7. Complete recovery: Malaria is deemed completely healed once all malaria parasites have been eliminated from the patient's system, and all symptoms have disappeared. This marks the end of the malaria life cycle in the host, with no parasites left.

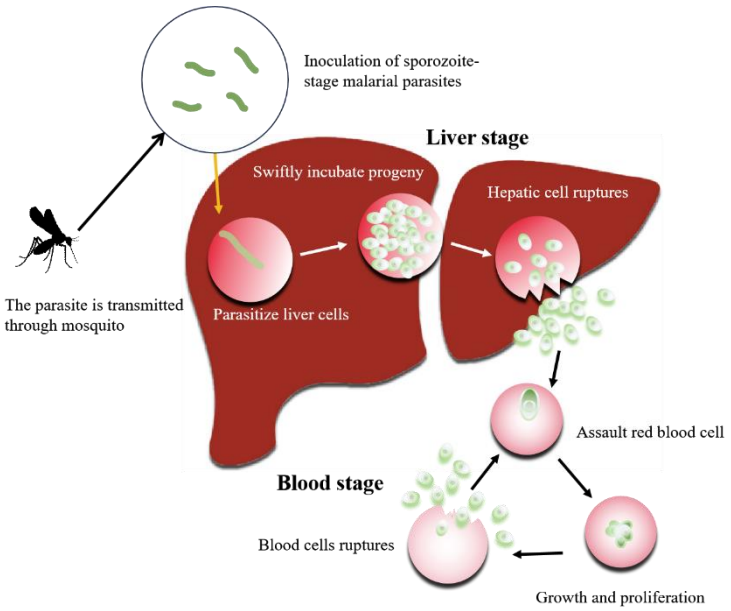


Figure 1. Malarial parasites parasitize human body cells.

The outlined process incorporates nuanced details: initially, upon invasion into the human body, parasites do not immediately trigger symptoms; rather, they infiltrate hepatocytes, undergoing continuous replication (the incubation period). Following a series of lifecycle stages, a substantial population of parasites enters the bloodstream, rampant infection of red blood cells, further replication, and toxin release (the active period), as shown in Figure 1. Upon seeking medical attention and receiving a confirmed diagnosis of malaria, patients commence artemisinin treatment. Prior to diagnosis, during the period of parasitization until

symptomatic manifestation, malaria parasites persistently replicate and invade additional red blood cells, potentially concealing themselves at any location within the intricate spatial confines of the human body—a "complex space." Within this realm, each "unraveling" of symptoms signifies an unfolding chapter in the intricate narrative of the malaria parasite's presence. Given the dispersion of malaria parasites throughout diverse bodily regions, the purpose of employing artemisinin is to seek out and eliminate all malaria parasites, serving as a comprehensive strategy to address the complexity of their concealment within the human body.

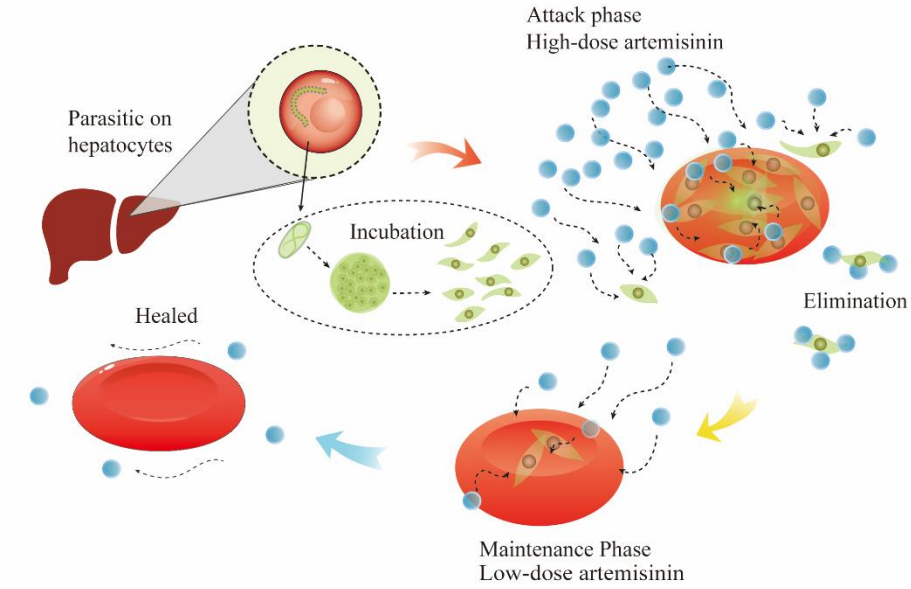


Figure 2. Artemisinin cures malaria

In Figure 2, in the initial treatment phase, higher doses of artemisinin medicines are employed to control malaria symptoms and reduce the parasite count swiftly. A substantial amount of the medication diffuses rapidly through the bloodstream, permeating the entire space (human body) to search for the ultimate solution (parasite). Subsequently, the treatment progresses gradually into the maintenance phase. During this stage, the medicine dosage is decreased, aiming to persist in clearing any remaining malaria parasites within the body until reaching the most concealed "solution." The ultimate objective is the complete eradication and cure of malaria. Through an analysis of the entire process and leveraging its intricate details, this study proposes the Artemisinin Optimization (AO).

4. The Artemisinin optimization algorithm

Drawing upon the analysis presented earlier, three distinct strategies have been devised based on the various stages of artemisinin treatment for malaria. The amalgamation of these three strategies forms the foundation of the AO. This section comprehensively explains the inspirations behind the design and the mathematical model.

4.1 Initialization phase

A patient introduces artemisinin medicines into the body through oral ingestion or injection. Drawing inspiration from this reality, this paper conceptualizes medicine microparticles as search agents for the algorithm, with the entire ensemble of these search agents constituting the algorithm's solution set. Initially, the entire population, denoted as A, is initialized. As described by Eq. (1), the complete population comprises N search agents, where D signifies multiple-dimensional components within a search agent. This abstraction mirrors the decomposition and absorption of drugs in the human body, dispersing through the bloodstream to various locations throughout the body.

$$A_{N,D} = B + R \times (T - B) = \begin{bmatrix} a_{1,1} & a_{1,2} & \cdots & a_{1,D} \\ a_{2,1} & a_{2,2} & \cdots & a_{2,D} \\ \vdots & \vdots & \ddots & \vdots \\ a_{N,1} & a_{N,2} & \cdots & a_{N,D} \end{bmatrix} \quad (1)$$

In the equation, T and B represent the boundaries of the solution space, while R denotes a set of random number sequences, with values ranging between $[0, 1]$. AO employs a common approach found in metaheuristic algorithms by utilizing random number sequences to generate initial solutions.

4.2 Comprehensive elimination phase

During the initial phase of malaria treatment, patients are administered larger doses of medication to control the progression of the disease swiftly. Artemisinin, once absorbed, diffuses throughout the human body as blood is transported to various regions. The distribution of the drug within the body is influenced by factors such as blood flow, vascular permeability, and the drug's binding affinity to proteins. Moreover, the intricate structure of the human body poses a labyrinthine challenge for artemisinin medicines. Considering these considerations, this section introduces a unique search model to simulate the process of drug diffusion, as depicted in Eq. (2):

$$\begin{cases} \mathrm{a}_{\mathrm{i,j}}^{\mathrm{t+1}} = \mathrm{a}_{\mathrm{i,j}}^{\mathrm{t}} + \mathrm{c} \times \mathrm{a}_{\mathrm{i,j}}^{\mathrm{t}} \times (-1)^{\mathrm{t}}, \mathrm{rand} < 0.5 \\ \mathrm{a}_{\mathrm{i,j}}^{\mathrm{t+1}} = \mathrm{a}_{\mathrm{i,j}}^{\mathrm{t}} + \mathrm{c} \times \mathrm{best}_{\mathrm{j}}^{\mathrm{t}} \times (-1)^{\mathrm{t}}, \mathrm{rand} > 0.5 \end{cases} \quad (2)$$

In this strategy, search agents exhibit characteristics of large-scale dispersion, serving as guides to explore the intricate solution space. Here, $a_{i,j}^{t+1}$ and $a_{i,j}^{t}$ respectively represent the search agent before and after the update, and best is the current optimal. Simultaneously, the diffusion of artemisinin drugs in the human body adheres to the principles of pharmacokinetics. This strategy considers the fact that drug concentration diminishes over time. In Eq. (2), c represents the decay exponent of drug concentration in the human body. The decay of artemisinin drug concentration can be described using a one-compartment model, as follows:

$$\frac{dC}{dt} = -k \times C \quad (3)$$

$$C(t) = C_0 \times e^{(-k \times t)} \quad (4)$$

In Eq. (3), the variable C represents the concentration of the drug, and k denotes the rate constant. Solving this differential equation yields Eq. (4): $C(t)$ signifies the drug concentration at time t. Within this model, as time progresses, the drug concentration $C(t)$ undergoes exponential decay. Consequently, the exponent c of the artemisinin drug concentration can be calculated using Eq. (5):

$$c = 1 \times e^{-(4 \times \frac{f}{Maxf})} \quad (5)$$

In this strategy, assuming the initial drug concentration of 1 and the drug decay rate of 4, the algorithm's evaluation process is utilized to simulate the progression of time in the model. Here, f and $Maxf$ represent the current and maximum evaluation iterations of the algorithm. Acknowledging variations in the severity of patients' conditions and differences in physiological factors, which lead to distinct dosages and durations of medication, patients may spend varying durations in this phase. To encapsulate this inherent variability, a probabilistic coefficient K is introduced, as depicted in Eq. (6):

$$K = 1 - \frac{f^{1/6}}{Maxf^{1/6}} \quad (6)$$

In this equation, K serves as a probabilistic coefficient, incorporating the algorithm's evaluation progress to simulate the objective scenario where patients exhibit diverse responses and durations during this stage based on individual conditions. This section provides a brief simulation of the motion process for each particle, as illustrated in Figure 3. Ultimately, the comprehensive elimination phase strategy can be expressed by Eq. (7):

$$\begin{cases} a_{i,j}^{t+1} = a_{i,j}^{t} + c \times a_{i,j}^{t} \times (-1)^{t}, \mathrm{rand} < 0.5 \\ a_{i,j}^{t+1} = a_{i,j}^{t} + c \times best_{j}^{t} \times (-1)^{t}, rand > 0.5 \end{cases}, r_1 < K \quad (7)$$

where r_1 is a random number with a range of $[0, 1]$. Following the initial phase of treatment, as the disease is under control, the treatment transitions into the maintenance phase to ensure the complete cure of malaria.

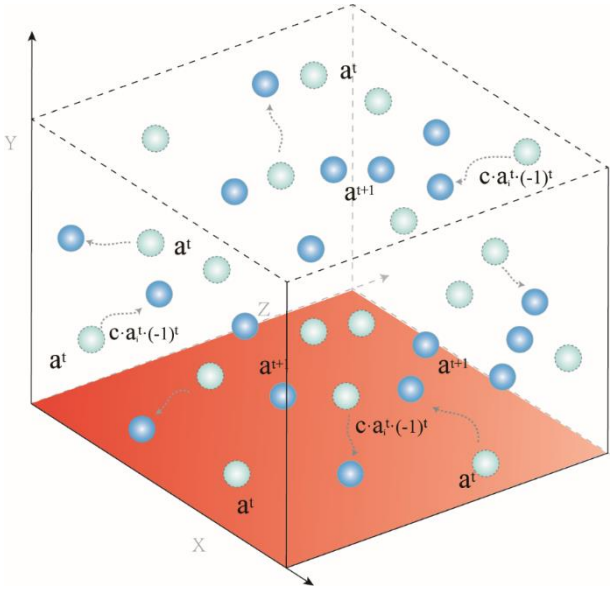


Figure 3. Comprehensive elimination phase of particle motion.

4.3Local clearance phase

The objective of the maintenance phase is to eliminate any remaining malaria parasites in the body, preventing their reproduction and the recurrence of malaria symptoms. While early-stage treatment typically swiftly alleviates symptoms, a small number of malaria parasites may persist in the body, especially in cases of severe infection. During this phase, patients continue to receive treatment with lower doses of artemisinin and its derivatives to ensure the complete eradication of malaria parasites, minimizing the risk of adverse reactions in the human body. Inspired by this, the paper has designed a Local clearance phase strategy. In this strategy, the particle's movement process is depicted in Figure 4, calculated using Eq. (8) to determine the particle's position.

$$a_i^{t+1} = a_{b_3}^t + d \times \left(a_{b_1}^t - a_{b_2}^t\right), if\ rand < Fit_{norm}(i) \quad (8)$$

$$Fit_{norm}(i) = \frac{fit(i) - \min(fit)}{\max(fit) - \min(fit)} \quad (9)$$

$$b_1, b_2, b_3 \sim U(1, N), b_1 \neq b_2 \neq b_3 \quad (10)$$

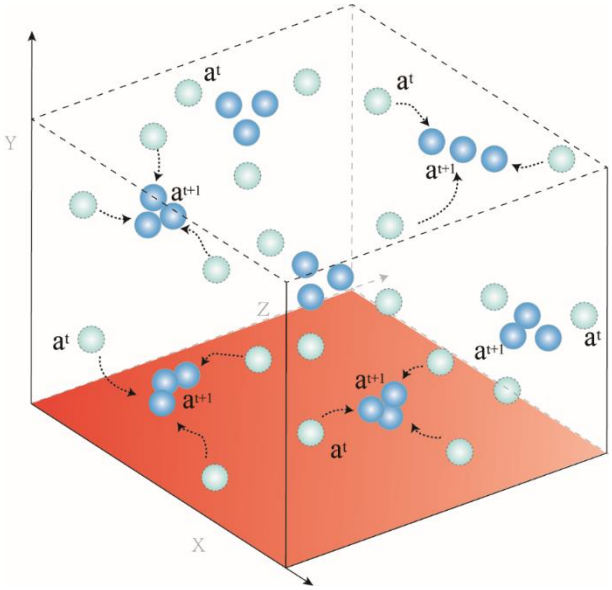


Figure 4. Local clearance phase of particle motion.

In this equation, $Fit_{norm}(i)$ represents the normalized fitness value, transforming the fitness values into a probability

distribution to serve as relative weights among individuals. This ensures that individuals with higher fitness have a larger corresponding probability. This aids in retaining excellent individuals to a certain extent while providing lesser-performing individuals with a chance, adjusting the algorithm's focus on different individuals. The d represents the coefficient, taking a random value between $[0.1, 0.6]$. This strategy simulates the process of a small amount of artemisinin clearing potential malaria parasites in the human body. The maintenance phase strategy allows the algorithm to exploit and exchange local information. In MAs, information exchange among individuals occurs during the iterative process. If an algorithm's information exchange is thorough, its performance might be notably enhanced [24, 70].

4.4 Post-consolidation phase

Indifference to the severity of the illness and laxity during treatment represent perilous detrimental factors. Due to the improvement of their condition, patients might gradually become less vigilant against malaria, reducing medication frequency, dosage, or even discontinuing treatment, potentially leading to a recurrence of the disease. Despite having passed through the attack and maintenance phases, where most malaria parasites in the body have been eradicated, there remains a possibility that a small fraction of parasites may gradually develop resistance to artemisinin. They may even enter a dormant phase, referred to as the "dormant form," significantly diminishing their biological activity and making it challenging for drugs to exert an effective killing effect. If treatment is discontinued, malaria parasites, after passing through the dormant form, may cause a relapse of the disease. Patients should strictly follow to the plan to have a chance to get ride of malaria.

This part presents the post-consolidation, recognizing the chance of unexpected situations and simulating this particular circumstance. It is hypothesized in this strategy that inactive parasite forms remain in the human body. Unfortunately, some patients may suffer a reappearance of malaria despite the continued presence of these dormant parasites. The model for this strategy is expressed by Eq. (11):

$$\begin{cases} a_{i,j}^{t+1} = a_{i,j}^{t}, if\ rand < 0.05 \\ a_{i,j}^{t+1} = best_{i,j}, if\ rand < 0.2 \end{cases} \tag{11}$$

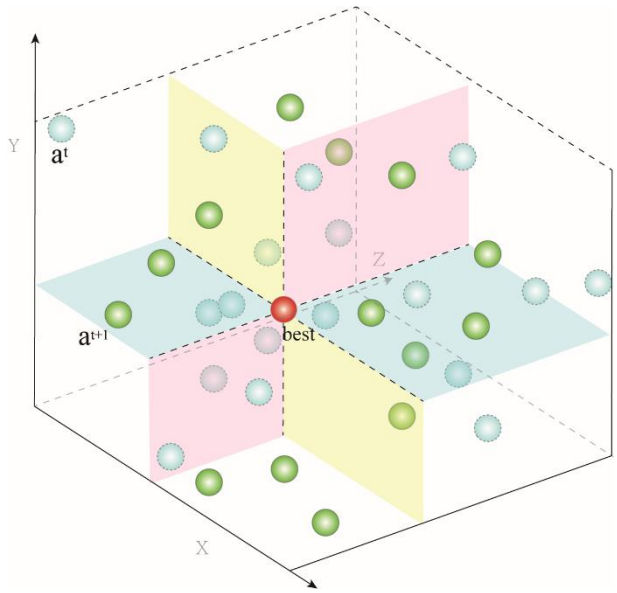


Figure 5. Post-consolidation of particle motion.

In this equation, $best_{i,j}$ represents a sub-vector of the current best solution in the jth dimension. Eq. (11) representing malaria parasites that have not been eliminated due to entering the dormant phase. As depicted in Figure 5, this strategy enhances the ability of search agents to escape from local optima.

4.5 The proposed algorithm

The entire process of treating malaria patients with artemisinin inspires the introduction of the AO. Through an examination of

the treatment process for malaria and the integration of metaheuristic algorithm principles, this paper analyzes different stages, drawing inspiration to propose distinct strategies of the AO. These strategies include the comprehensive elimination phase strategy, encouraging the algorithm to perform global exploration; the local clearance phase strategy, promoting local exploitation, and the post-consolidation phase strategy, enhancing the algorithm's ability to escape local optima.

Specifically, the inspiration behind AO and the algorithm's operational flow can be outlined as follows: Initially, drawing inspiration from the parasitic nature of malaria parasites in the human body, the human body is metaphorically considered a 'space' with constraints. The invading malaria parasites are viewed as 'solutions' to be explored, and artemisinin drugs are regarded as search agents in the algorithm. Inspired by the process of controlling the disease with higher doses of medication in the initial stages of treatment, the comprehensive elimination phase strategy is introduced. Under this strategy, the AO gains global search capabilities, rapidly exploring the entire space and discovering potential regions of optimal solutions. Drawing inspiration from the gradual control of the disease in the later stages of treatment and the reduction in medication dosage, the local clearance phase strategy is proposed. This strategy allows the algorithm to explore potential local optimal solutions. Lastly, anticipating the possibility of symptom recurrence due to the awakening of dormant malaria parasites during treatment, the post-consolidation phase strategy is introduced, reinforcing the algorithm's ability to escape local optima. The pseudocode in Algorithm 1 provides a clearer understanding of the AO's operational process. The flowchart in Figure 6 visually illustrates the structure of the algorithm.

Algorithm 1 Artemisinin Optimization pseudo-code

/* Starting phase */
Parameters initializing: Fitness evaluation f, Max fitness evaluation $MaxF$, Population size N, Dimension D.
Randomly initialize the agent population $A_{N,D}$ and evaluate their fitness fit_i,
Find the current optimal A_{best}.
$f = f + N$.
/* Main loop*/
While $f < MaxF$
Calculate the probability K, exponent c.
For each agent $i = 1 : N$
  For each dimension $j = 1 : D$
    /* Comprehensive elimination phase */
    If rand<K
      Update search agent $a_{i,j}$ using Eq. (7).
    End If
    /* Local clearance phase */
    Update search agent $a_{i,j}$ using Eq. (8)
    /* Post-consolidation phase */
    Search agent information crossover by Eq. (11)
  End For
End For
Calculate the fitness fit.
Update the population and find the optimal.
  $f = f + N$
End While
Return the optimal solution

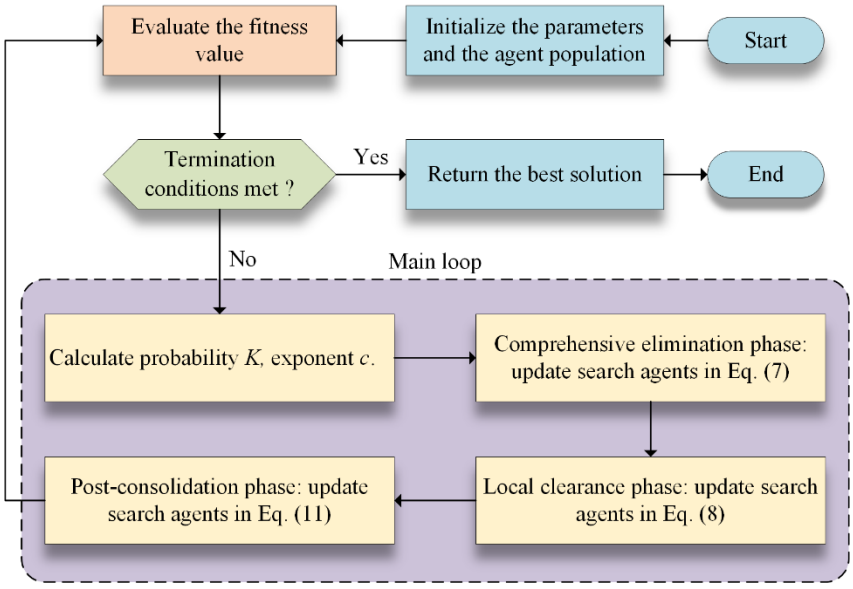


Figure 6. Flowchart of the AO

The computation of AO's algorithmic time complexity is contingent upon the maximum iteration count (T), population size (n), and problem dimensionality (dim). Simultaneously, AO's complexity primarily encompasses the comprehensive elimination phase, local clearance phase, post-consolidation phase, and fitness value evaluation. Firstly, the complexity of generating the initial population is $O(n \times dim)$. Subsequently, due to the algorithm's straightforward design, the combined complexity of the three strategies during the main stages is $O(n \times dim)$. Furthermore, the fitness value calculation then demands $O(n \times \log n)$ computation time. Consequently, the overall complexity of AO is expressed as $O(AO) = O((n \times dim) \times \log n \times (T + 1))$.

5. Experiment

This section encompasses a comprehensive examination of the performance of AO. Initially, to delve into a nuanced understanding of the optimization process of AO, an experiment is established to scrutinize the advantages of AO in optimal exploration and feature search. Subsequently, AO was compared with eight widely acknowledged algorithms and eight high-performance improved algorithms to substantiate the superiority of AO compared to peer algorithms.

5.1 Experimental settings

In AI-based research, precise experimental design and a fair testing environment are key prerequisites to ensure reliable research results [71, 72]. Thus, in this experiment, to ensure the fairness of the trial, a set of 30 search agents was established in the initial population of all participating algorithms, with each algorithm terminating after 300,000 evaluations. Additionally, each algorithm underwent 30 individual runs to mitigate the impact of random conditions, preventing any single run from skewing the true performance understanding of the algorithm. In this manner, fair testing not only aids in the accurate assessment of algorithm performance but also significantly reduces the impact of biases in the testing environment, thereby providing more reliable and consistent results [73, 74].

The datasets employed during testing encompass the classical IEEE CEC 2014 and the latest IEEE CEC 2022 benchmark function datasets. These two benchmark datasets are commonly used to test algorithm performance in the field of evolutionary computing. Within the IEEE CEC 2014 benchmark functions presented in Table A.1, the efficacy of these functions in assessing the convergence, diversity, and adaptability of algorithms has been widely acknowledged. As depicted in Table A.2 for the IEEE CEC 2022 benchmark functions, heightened demands are placed on the accuracy and stability of algorithmic exploration, featuring improvements in comprehensiveness and diversity. This renders them more challenging and facilitates a more robust evaluation and comparison of the performance of different optimization algorithms. AO and its competitors will undergo comparative testing in both function sets, allowing for a thorough assessment of their respective performances.

During the evaluation and comparison of results, the non-parametric significance test standard, the Wilcoxon Signed-Rank Test

(WSRT) [75], was employed to score the performance of each algorithm involved in the comparisons. As each algorithm produces a result for each function it runs on, WSRT compares and ranks the differences between the testing outcomes of AO and the other algorithms. In WSRT, the null hypothesis posits no significant difference between two results, and the relationship between the p-value and 0.05 indicates the validity of the hypothesis: when the p-value is less than 0.05, there is a significant difference between the two results; when the p-value is greater than or equal to 0.05, the two results are considered highly similar. Additionally, based on the significance of the differences and the superiority or inferiority relationship between the two results, counting statistics are performed using the "+/-/=" symbols. Furthermore, the Friedman Test (FT) [76] was utilized to calculate the average results of each algorithm across all benchmark functions, and rankings were assigned based on performance to present the comparative outcomes in a more intuitive manner visually. By using the WSRT and FT, it is possible to compare the performance of different algorithms on benchmark functions and accurately detect significant differences between the results [54, 77, 78].

5.2 Optimization process and adaptive analysis

Due to the limitations of solely relying on model and theory exposition for a clear understanding of the proposed method's search process, this section visually illustrates the process of AO searching for the optimal solution within the solution space. This graphical representation offers a more intuitive insight into the algorithm's operational principles and internal mechanisms.

In this section, a set of experiments is conducted within the IEEE CEC 2014 to explore the iterative process of the AO algorithm. The focus is on a particle within the set of agents, and its trajectory is recorded. Initially, the historical trajectory is reflected by recording the position of the particle after each iteration. Subsequently, attention is directed towards the updating process of this agent, analyzing the trajectory and magnitude of particle changes along the lateral dimension vector of the agent. Finally, a comprehensive analysis of the entire iteration process is conducted by examining the changes in fitness values.

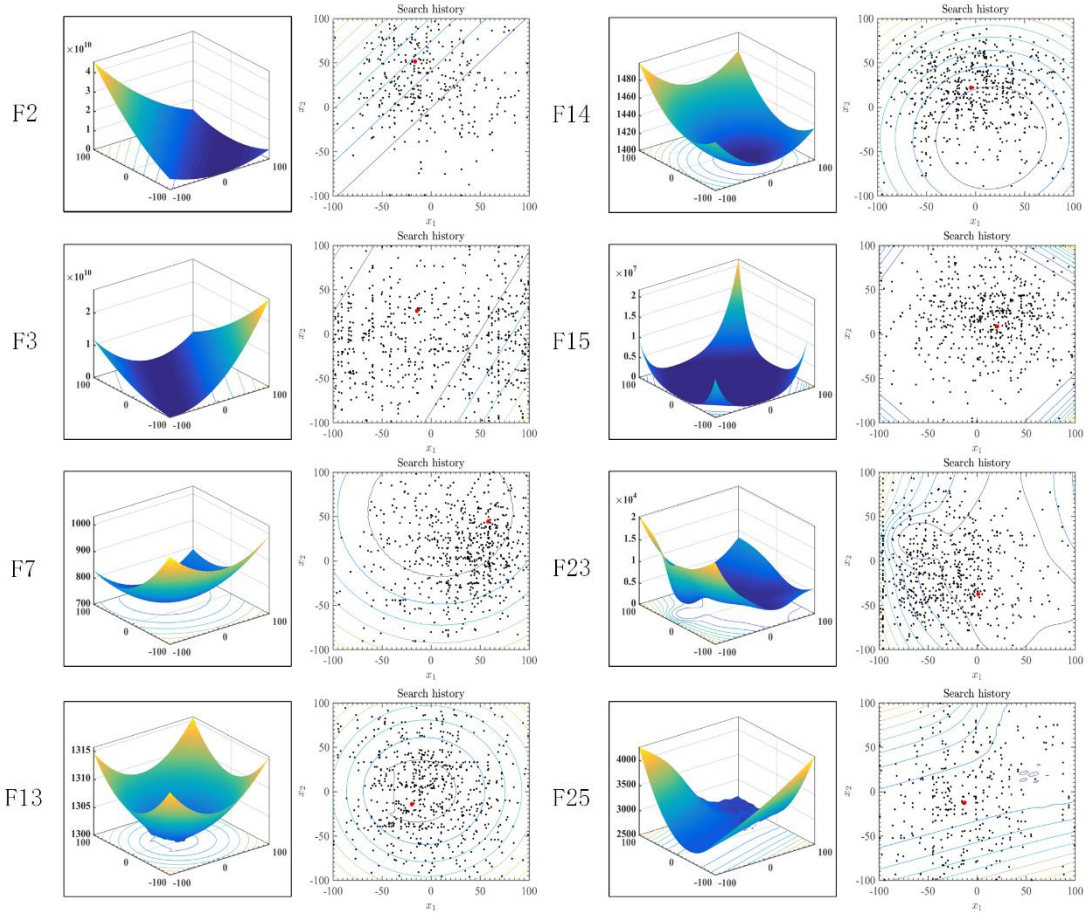


Figure 7. The 3D image of benchmark functions and AO's solution distribution

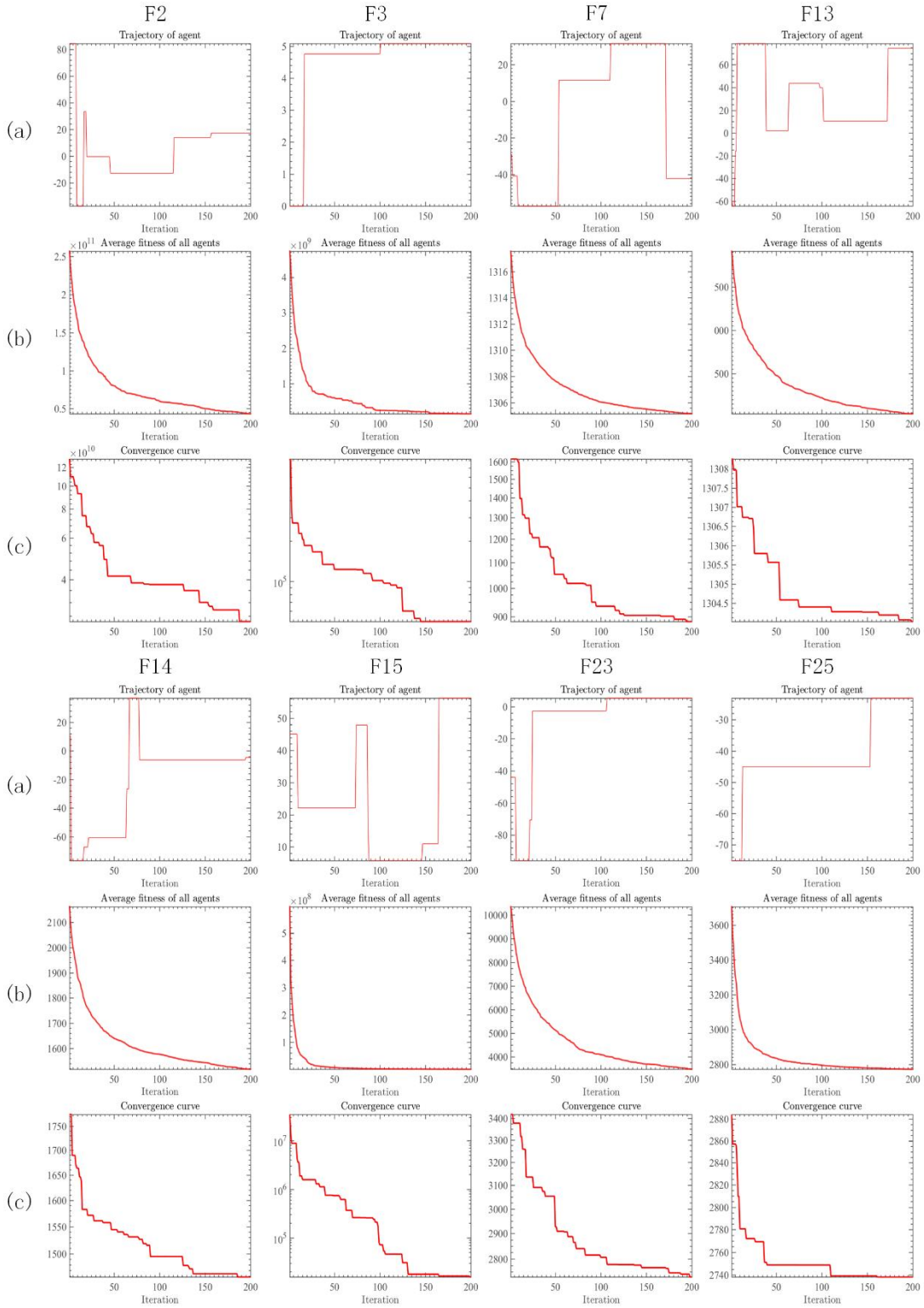


Figure 8. Qualitative analysis experiment of AO

In Figure 7, the first column presents the three-dimensional visualization of benchmark functions used for testing, aiding in a better understanding and observation of the distribution within the solution space. The second column displays the distribution of historical search record points (depicted as black dots) of AO's exploration for the optimal solution within the solution space on a two-dimensional plane. Upon observation, it is evident that AO's agents span almost the entire solution space, with the historical traces exhibiting a remarkably high coverage of the solution set, demonstrating AO's robust global exploration capabilities. Moreover, agents are more densely clustered near the optimal solution (red dot), indicating a converging state and reflecting the continuous development towards the global optimum.

In Figure 8, the (a) column displays the trajectory of a single agent dimension within AO. In the graph, the trajectory of this search agent exhibits significant variations in step size. This indicates that AO has a large global exploration range during the search process, resulting in higher efficiency in exploring. Additionally, in the later stages, the step size of trajectory changes diminishes, eventually converging to a single point. This suggests that AO gradually transitions into local exploitation, ultimately pinpointing

the optimal solution. Moreover, in some functions, the trajectory of the search agent experiences sudden jumps in the later stages, indicating AO's strong capability to escape local optima and break free from them.

The (b) column records the average fitness values calculated for all agents after iterations. Clearly, in multiple functions, the curves of average fitness values exhibit a relatively smooth convergence trend. This indicates that the algorithm transitions from an initial phase of global exploration, searching valuable regions with large step sizes, to gradually adjusting the balance between exploration and exploitation strategies, converging towards the optimal solution, and eventually converging to a single point. In AO, the fitness values of each iteration align with the fluctuating trajectory, as the adopted search mode compels the agents to continuously update their positions and progressively explore until reaching the optimal solution, aligning with the design philosophy of the algorithm.

The (c) column presents the iterative convergence curves of AO. Observing the algorithm's solving process is more intuitive for researchers, wherein the quality of explored solutions improves with increasing iteration counts until optimal or near-optimal solutions are discovered upon iteration termination. Throughout the entire process, the algorithm is expected to explore more finely, avoiding being trapped in local optima. In the (c) column for all functions, AO adheres to the aforementioned description, demonstrating the ability to search for high-quality solutions, maintaining sensitivity to local optima, and quickly escaping from them.

In summary, the design structure of AO aligns with the fundamental principles of metaheuristic algorithms. While ensuring convergence, AO adaptively adjusts the balance between exploration and exploitation during the updating process, dynamically tuning its strategy. Throughout the entire process of seeking the optimal solution, AO effectively coordinates global exploration and local exploitation, achieving a continuous and uninterrupted transition from wide exploration to precise development. Therefore, the search for the optimal solution simultaneously encompasses breadth and depth through AO.

5.3 Performance testing of the AO

4.3.1 Comparison with classical algorithms on IEEE CEC 2014

In this section, AO will be compared with eight classical algorithms in IEEE CEC2014. Table 1 lists all the algorithms participating in the comparison along with their parameter settings. Table 2 presents the average (AVG) and standard deviation (STD) of the results from 30 independent runs for each algorithm.

Table 1. Algorithms involved in the comparison and their parameter settings.

Algorithms	Parameters
Artemisinin Optimization (AO)	~
Particle swarm optimizer (PSO) [79]	$c_1 = 2;\ c_2 = 2;\ V_{max} = 6$
Whale optimization algorithm (WOA)[80]	$a_1 = [2,0]; a_2 = [-2,-1]; b = 1$
Moth-flame optimization algorithm (MFO)[81]	$b = 1$
Harris Hawk optimizer (HHO)[82]	$k = 0$
Ant colony optimization for continuous domains (ACOR)[25]	$k = 10; q = 0.5;\ ibslo = 1$
Sine cosine algorithm (SCA)[83]	$a = 2$
Gravitational search algorithm (GSA)[37]	$Rnorm = 2$
Jaya optimization algorithm (JAYA) [51]	~

Table 2. Optimization results of AO and classical algorithms for IEEE CEC 2014

Fun	F1		F2		F3	
Item	AVG	STD	AVG	STD	AVG	STD
AO	7.99709E+06	6.92039E+06	2.60093E+06	6.85791E+05	7.02929E+03	3.90513E+03
PSO	8.26818E+06	1.95658E+06	1.46964E+08	1.69877E+07	9.57164E+02	1.32723E+02
WOA	2.83812E+07	1.04668E+07	3.16552E+06	3.25583E+06	4.23234E+04	2.83908E+04
MFO	1.05739E+08	1.38512E+08	1.00454E+10	5.81789E+09	9.67456E+04	4.78512E+04
ACOR	6.44089E+06	1.04824E+07	1.22805E+04	1.32849E+04	5.27685E+03	8.21866E+03

HHO	9.30902E+06	5.55005E+06	1.18064E+07	2.15030E+06	5.32870E+03	1.58911E+03
SCA	2.35040E+08	5.91279E+07	1.67936E+10	3.31377E+09	3.71267E+04	5.02912E+03
GSA	1.53372E+06	4.05650E+05	1.95542E+07	2.44149E+06	7.61596E+03	3.19668E+03
JAYA	6.10954E+07	2.36524E+07	5.32355E+09	1.18977E+09	3.27602E+04	7.23848E+03
	F4		F5		F6	
	AVG	STD	AVG	STD	AVG	STD
AO	5.14249E+02	3.01810E+01	5.20177E+02	5.05473E-02	6.12940E+02	2.62929E+00
PSO	4.58610E+02	3.12237E+01	5.20928E+02	5.64797E-02	6.23178E+02	3.81661E+00
WOA	5.84690E+02	4.41531E+01	5.20334E+02	1.78785E-01	6.34612E+02	2.46253E+00
MFO	1.49027E+03	9.33836E+02	5.20276E+02	1.35510E-01	6.23496E+02	3.37465E+00
ACOR	4.73797E+02	3.76781E+01	5.20917E+02	5.79463E-02	6.10628E+02	2.83808E+00
HHO	5.48903E+02	6.20437E+01	5.20221E+02	1.20727E-01	6.29634E+02	3.07476E+00
SCA	1.33629E+03	1.87001E+02	5.20933E+02	5.57415E-02	6.33896E+02	1.87640E+00
GSA	4.46058E+02	5.60596E+01	5.20954E+02	3.97913E-02	6.08438E+02	2.36904E+00
JAYA	1.05960E+03	1.38458E+02	5.20928E+02	6.40442E-02	6.28242E+02	3.95363E+00
	F7		F8		F9	
	AVG	STD	AVG	STD	AVG	STD
AO	7.00979E+02	5.17555E-02	8.00923E+02	4.33169E-01	9.95683E+02	2.63146E+01
PSO	7.02289E+02	1.30136E-01	9.68094E+02	2.03982E+01	1.10998E+03	2.73688E+01
WOA	7.01038E+02	5.56058E-02	9.90677E+02	3.99567E+01	1.14436E+03	7.18540E+01
MFO	8.12609E+02	6.45877E+01	9.51973E+02	4.34687E+01	1.13397E+03	6.36668E+01
ACOR	7.05778E+02	1.34350E+01	8.62425E+02	1.92466E+01	1.01056E+03	6.05590E+01
HHO	7.01104E+02	2.23601E-02	9.03474E+02	1.51416E+01	1.09574E+03	1.61039E+01
SCA	8.31409E+02	2.22640E+01	1.03932E+03	1.47577E+01	1.17770E+03	1.69511E+01
GSA	7.01200E+02	2.55956E-02	8.39218E+02	7.51094E+00	9.63570E+02	1.13977E+01
JAYA	7.10827E+02	2.14767E+00	1.00487E+03	1.74133E+01	1.13720E+03	1.79700E+01
	F10		F11		F12	
	AVG	STD	AVG	STD	AVG	STD
AO	1.00695E+03	2.57079E+00	3.10757E+03	5.48111E+02	1.20021E+03	5.03229E-02
PSO	5.14497E+03	5.88984E+02	5.75941E+03	5.17617E+02	1.20238E+03	2.98948E-01
WOA	4.95500E+03	7.04835E+02	5.86401E+03	6.90030E+02	1.20174E+03	6.20402E-01
MFO	4.11671E+03	8.45878E+02	5.43094E+03	7.98894E+02	1.20047E+03	2.69330E-01
ACOR	2.98826E+03	4.53465E+02	5.37691E+03	2.29537E+03	1.20249E+03	2.74763E-01
HHO	2.71700E+03	7.24657E+02	5.42636E+03	5.72512E+02	1.20145E+03	3.76520E-01
SCA	6.80869E+03	4.97390E+02	8.09091E+03	3.83223E+02	1.20248E+03	3.42345E-01
GSA	2.40165E+03	2.76616E+02	2.92782E+03	3.43008E+02	1.20092E+03	1.33478E-01
JAYA	7.24897E+03	2.81699E+02	7.96492E+03	2.36547E+02	1.20248E+03	2.61738E-01
	F13		F14		F15	
	AVG	STD	AVG	STD	AVG	STD
AO	1.30036E+03	6.75227E-02	1.40054E+03	2.47617E-01	1.50964E+03	2.93635E+00
PSO	1.30041E+03	8.85931E-02	1.40028E+03	1.10043E-01	1.51628E+03	1.28118E+00
WOA	1.30052E+03	1.35004E-01	1.40027E+03	4.96276E-02	1.58241E+03	2.81094E+01
MFO	1.30236E+03	1.22607E+00	1.43270E+03	2.52106E+01	1.55025E+05	3.72008E+05
ACOR	1.30045E+03	8.73998E-02	1.40078E+03	7.64683E-01	1.55852E+03	1.22253E+02
HHO	1.30054E+03	1.18914E-01	1.40035E+03	2.08744E-01	1.54247E+03	1.28367E+01
SCA	1.30289E+03	2.35860E-01	1.44483E+03	7.41809E+00	5.02501E+03	3.04461E+03
GSA	1.30017E+03	2.17429E-02	1.40035E+03	5.51149E-02	1.51309E+03	7.71123E-01
JAYA	1.30144E+03	3.36464E-01	1.40447E+03	3.58230E+00	1.53151E+03	6.21405E+00
	F16		F17		F18	

	AVG	STD	AVG	STD	AVG	STD
AO	1.60996E+03	7.03525E-01	1.47459E+06	9.68065E+05	1.09495E+05	1.01731E+05
PSO	1.61205E+03	4.88560E-01	2.37382E+05	1.03391E+05	2.24851E+06	5.94878E+05
WOA	1.61274E+03	5.12457E-01	3.47644E+06	2.11978E+06	1.89877E+04	5.13832E+04
MFO	1.61277E+03	4.15178E-01	2.45212E+06	2.60924E+06	1.32448E+07	7.18104E+07
ACOR	1.61160E+03	4.03450E-01	1.59610E+05	5.07424E+05	4.83533E+03	5.02905E+03
HHO	1.61231E+03	3.24876E-01	1.80064E+06	1.27003E+06	9.09466E+04	3.94859E+04
SCA	1.61278E+03	3.21737E-01	5.96709E+06	2.78322E+06	1.40450E+08	8.19844E+07
GSA	1.61291E+03	3.88192E-01	2.01483E+05	1.36700E+05	6.22279E+04	2.51066E+04
JAYA	1.61273E+03	1.64278E-01	2.64135E+06	1.04138E+06	3.94425E+07	2.57424E+07
	F19		F20		F21	
	AVG	STD	AVG	STD	AVG	STD
AO	1.91167E+03	1.48738E+01	1.67107E+04	1.12351E+04	7.81944E+05	6.05323E+05
PSO	1.91675E+03	2.96413E+00	2.33050E+03	5.95216E+01	1.24030E+05	7.25773E+04
WOA	1.95807E+03	3.88866E+01	2.69531E+04	1.93732E+04	1.18054E+06	1.22597E+06
MFO	1.97062E+03	6.09155E+01	6.28054E+04	4.29065E+04	1.57727E+06	3.13455E+06
ACOR	1.91738E+03	2.14346E+01	3.76033E+03	2.82457E+03	5.27612E+04	6.04385E+04
HHO	1.93730E+03	3.86349E+01	1.25058E+04	5.53087E+03	5.41651E+05	4.24705E+05
SCA	1.98985E+03	2.05959E+01	1.44013E+04	4.14717E+03	1.48096E+06	1.24473E+06
GSA	1.90759E+03	1.07116E+00	3.69017E+04	1.37812E+04	1.31710E+05	7.91020E+04
JAYA	1.92400E+03	2.75525E+00	4.44044E+03	1.17089E+03	7.17736E+05	2.56957E+05
	F22		F23		F24	
	AVG	STD	AVG	STD	AVG	STD
AO	2.72458E+03	1.84246E+02	2.60394E+03	3.52382E+01	2.60000E+03	5.42123E-07
PSO	2.90626E+03	2.45448E+02	2.61612E+03	6.46513E-01	2.62578E+03	6.11787E+00
WOA	2.92926E+03	2.82432E+02	2.63138E+03	6.86226E+00	2.60511E+03	3.11785E+00
MFO	3.00082E+03	2.94070E+02	2.68220E+03	4.93035E+01	2.68264E+03	3.22619E+01
ACOR	2.53324E+03	1.71659E+02	2.61808E+03	6.73775E+00	2.64113E+03	6.18974E+00
HHO	3.01707E+03	2.46384E+02	2.50000E+03	0.00000E+00	2.60000E+03	1.03246E-04
SCA	2.92043E+03	1.26605E+02	2.66837E+03	1.39127E+01	2.60005E+03	2.52116E-02
GSA	3.10809E+03	2.15988E+02	2.61295E+03	8.39919E+00	2.60822E+03	3.16446E-01
JAYA	2.85582E+03	1.44191E+02	2.64109E+03	5.44557E+00	2.62063E+03	2.17500E+01
	F25		F26		F27	
	AVG	STD	AVG	STD	AVG	STD
AO	2.70038E+03	1.49459E+00	2.78339E+03	3.77702E+01	3.28271E+03	1.58193E+02
PSO	2.71221E+03	5.95572E+00	2.78711E+03	3.46055E+01	3.51737E+03	2.89525E+02
WOA	2.71990E+03	1.77319E+01	2.70375E+03	1.81793E+01	3.67254E+03	3.97808E+02
MFO	2.71476E+03	9.12640E+00	2.70267E+03	1.35215E+00	3.66387E+03	1.61780E+02
ACOR	2.70692E+03	3.70827E+00	2.71378E+03	3.44782E+01	3.36055E+03	9.96760E+01
HHO	2.70000E+03	0.00000E+00	2.76684E+03	4.76903E+01	2.90000E+03	0.00000E+00
SCA	2.72541E+03	8.39690E+00	2.70234E+03	5.92319E-01	3.48113E+03	3.39625E+02
GSA	2.70192E+03	1.00280E-01	2.77378E+03	4.29706E+01	3.33050E+03	4.09514E+02
JAYA	2.71790E+03	3.33650E+00	2.70075E+03	1.11466E-01	3.54026E+03	2.16403E+02
	F28		F29		F30	
	AVG	STD	AVG	STD	AVG	STD
AO	3.84680E+03	2.08016E+02	5.70378E+03	9.03506E+02	7.96402E+03	2.64258E+03
PSO	7.21817E+03	8.08146E+02	5.79332E+04	1.50515E+05	1.48214E+04	6.32058E+03
WOA	5.03384E+03	4.84656E+02	6.30365E+06	4.58108E+06	8.49916E+04	8.94530E+04
MFO	3.85186E+03	7.34991E+01	4.18219E+06	4.28344E+06	4.44922E+04	3.01210E+04

ACOR	3.80635E+03	1.30835E+02	2.84785E+05	1.53373E+06	1.01732E+04	1.05225E+04
HHO	3.00000E+03	0.00000E+00	4.58001E+03	6.22657E+03	6.04157E+03	9.42801E+03
SCA	4.92514E+03	4.03302E+02	9.98325E+06	5.00912E+06	2.34532E+05	9.79239E+04
GSA	4.62512E+03	3.69531E+02	4.90476E+07	6.11502E+07	7.98314E+03	9.98483E+02
JAYA	4.83206E+03	4.86233E+02	5.90456E+06	1.93160E+06	2.01364E+04	6.92944E+03

Table 3. WSRT results and FT rankings for AO and classical algorithmic competitions.

Algorithm	Mean	Rank	+/-/=
AO	2.70	1	~
PSO	4.53	5	22/6/2
WOA	6.03	6	25/3/2
MFO	6.73	8	26/1/3
ACOR	3.57	2	14/11/5
HHO	3.70	3	15/6/9
SCA	7.70	9	28/1/1
GSA	3.83	4	15/9/6
JAYA	6.20	7	27/2/1

In Table 2, the average values of AO are noticeably superior to algorithms such as ACOR, HHO, and GSA in most test functions. This suggests that AO is more likely to find better solutions over 30 independent runs. Additionally, AO exhibits relatively smaller variances in most functions, indicating lower performance fluctuations over multiple runs and demonstrating a higher level of stability. This implies that AO not only finds better optimal solutions among its competitors but also does so more consistently. Subsequently, in Table 3, the FT rankings for all participating algorithms are based on their overall performance across the 30 functions. In the "Mean" column, representing the average ranking across all functions, AO has an average ranking of 2.70, indicating consistently high rankings across individual functions and ultimately securing the top position. Furthermore, the "+/-/=" column metrics indicate that AO outperforms other competitors in multiple functionalities. Therefore, the comprehensive test results suggest that AO possesses superior search capabilities, primarily attributed to its unique exploration and exploitation capabilities, allowing it to search for optimal solutions more effectively.

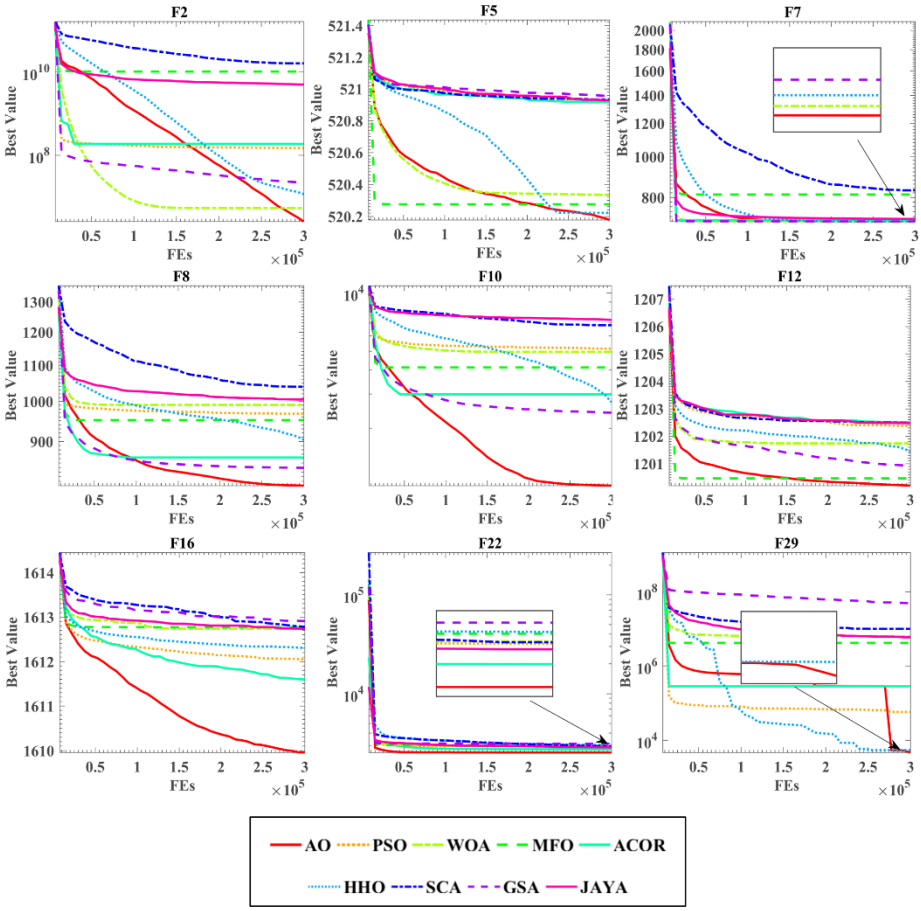


Figure 9. Convergence comparison of AO and classical algorithms.

Subsequently, in order to gain a more profound understanding of the specific performance of AO in its competition with alternative algorithms, we crafted curves illustrating the optimization processes of the competitive counterparts based on numerical values derived from experimental data. Within Figure 9, the term "Best Value" signifies the peak fitness value explored by each algorithm throughout the iterative process, while "FEs" denotes the frequency of fitness evaluations. Analysis of the AO curve compared to its algorithmic counterparts reveals its predominant strength lies in its enduring exploitation capacity. In contrast to alternative algorithms, AO maintains a sustained convergence speed in subsequent iterations, circumventing the gradual reduction in convergence speed and the entrapment of convergence accuracy observed in competing approaches. Even though certain algorithms achieve commendable convergence accuracy in the early stages, their true objective is to achieve a delicate balance between global and local optimization—exploring highly valuable regions in the initial stages but encountering challenges in unearthing optimality in subsequent exploration. This underscores the necessity of focusing on local exploitation strategy [84]. In comparison, AO persistently seeks superior solutions by shifting its focus towards local exploitation, thereby continuously uncovering more optimal solutions.

4.3.2 Comparison with high-performance algorithms on IEEE CEC 2014

To further substantiate the optimization prowess of AO and illustrate its exceptional attributes, this section juxtaposes AO against eight high-performance improved algorithms in IEEE CEC2014. Table 4 enumerates all the algorithms involved in the comparison, along with their corresponding parameter configurations. Table 5 presents the average (AVG) and standard deviation (STD) of the results obtained from 30 independent runs for each algorithm.

Table 4. Algorithms and their parameter settings.

Algorithms	Parameters
Artemisinin Optimization (AO)	~
Hybridizing grey wolf optimization with differential evolution (HGWO) [85]	$\beta_{max} = 0.8, \beta_{min} = 0.2,$ $CR_p = 0.2, a = [0,2]$
JAYA algorithm with Levy flight (LJAYA) [86]	~
Improved grey wolf optimization (IGWO)[87]	$\beta_{num} = 10;\ \Omega_{num} = 15$
Cauchy and Gaussian Sine Cosine Optimization (CGSCA) [88]	$a = 1, \delta = 0.1$
Levy opposition-based learning Grey Wolf Optimizer(OBLGWO)[89]	$P = 0.5$
sine cosine algorithm with differential evolution (SCADE) [90]	$a = 2;\ \beta_{max} = 0.8,$ $\beta_{min} = 0.2;\ CR_p = 0.8$
modified sine cosine algorithm (MSCA) [91]	$JR = 0.1;\ a = 2;\ SR = [0,1]$
Moth-flame optimizer with sine cosine mechanisms (SMFO) [92]	$b = 1$

Table 5. Optimization results of AO and high-performance algorithms

Fun	F1		F2		F3	
Item	AVG	STD	AVG	STD	AVG	STD
AO	2.2735E+06	2.7564E+06	8.7034E+03	9.3286E+03	1.7698E+04	1.4736E+04
HGWO	1.5631E+08	3.9308E+07	8.1099E+09	1.4621E+09	6.5228E+04	6.2117E+03
LJAYA	9.7636E+07	2.5308E+07	6.4044E+09	7.3662E+08	3.9856E+04	6.6413E+03
IGWO	1.6923E+07	5.3929E+06	2.7454E+06	1.6046E+06	6.0414E+03	2.2781E+03
CGSCA	2.6533E+08	6.9017E+07	1.8448E+10	3.4788E+09	4.2247E+04	4.6400E+03
OBLGWO	1.8830E+07	1.0227E+07	1.5871E+07	1.3858E+07	8.4835E+03	2.2330E+03
SCADE	4.3699E+08	9.5082E+07	2.9385E+10	4.4358E+09	5.6480E+04	7.4875E+03
MSCA	6.1133E+07	3.3856E+07	7.1080E+09	3.7914E+09	2.6210E+04	6.5155E+03
SMFO	5.8300E+08	2.2955E+08	4.1069E+10	1.0117E+10	7.5168E+04	8.4295E+03
	F4		F5		F6	
	AVG	STD	AVG	STD	AVG	STD
AO	4.7384E+02	4.9054E+01	5.2069E+02	1.0894E-01	6.0555E+02	1.9113E+00

HGWO	9.1039E+02	6.1329E+01	5.2082E+02	1.2470E-01	6.2613E+02	1.9440E+00
LJAYA	1.2630E+03	1.0150E+02	5.2094E+02	6.6589E-02	6.3232E+02	1.3859E+00
IGWO	5.3001E+02	2.5933E+01	5.2053E+02	1.3073E-01	6.1905E+02	2.6114E+00
CGSCA	1.7143E+03	2.1859E+02	5.2094E+02	3.5013E-02	6.3346E+02	1.7436E+00
OBLGWO	5.5267E+02	4.3863E+01	5.2097E+02	4.4515E-02	6.2070E+02	4.0333E+00
SCADE	2.3774E+03	5.8344E+02	5.2094E+02	5.4345E-02	6.3347E+02	2.6641E+00
MSCA	7.8660E+02	1.4433E+02	5.2058E+02	1.4642E-01	6.2137E+02	2.7453E+00
SMFO	7.0836E+03	1.9341E+03	5.2094E+02	6.0806E-02	6.3773E+02	2.3034E+00
	F7		F8		F9	
	AVG	STD	AVG	STD	AVG	STD
AO	7.0002E+02	3.3382E-02	8.1043E+02	5.0586E+00	9.4760E+02	2.6749E+01
HGWO	7.4366E+02	1.1500E+01	1.0078E+03	1.1355E+01	1.1427E+03	1.3603E+01
LJAYA	7.1413E+02	2.0660E+00	1.0235E+03	1.2886E+01	1.1491E+03	1.5429E+01
IGWO	7.0099E+02	4.9306E-02	8.8561E+02	1.4424E+01	1.0152E+03	1.8689E+01
CGSCA	8.5592E+02	2.9572E+01	1.0553E+03	1.6230E+01	1.1804E+03	1.3502E+01
OBLGWO	7.0116E+02	5.8833E-02	9.1562E+02	3.6524E+01	1.0662E+03	3.3605E+01
SCADE	8.9609E+02	3.8698E+01	1.0735E+03	1.3949E+01	1.2050E+03	1.5663E+01
MSCA	7.4613E+02	2.5595E+01	9.3749E+02	1.8571E+01	1.0499E+03	2.4796E+01
SMFO	9.7422E+02	8.2084E+01	1.0882E+03	3.2693E+01	1.2102E+03	2.3822E+01
	F10		F11		F12	
	AVG	STD	AVG	STD	AVG	STD
AO	1.2465E+03	1.4447E+02	3.1407E+03	1.2092E+03	1.2008E+03	2.8380E-01
HGWO	5.5815E+03	2.7062E+02	6.7318E+03	4.6017E+02	1.2013E+03	3.0530E-01
LJAYA	6.9339E+03	3.5092E+02	7.9182E+03	2.7295E+02	1.2025E+03	3.7038E-01
IGWO	3.3967E+03	6.2858E+02	4.3281E+03	5.5233E+02	1.2007E+03	2.8461E-01
CGSCA	6.8817E+03	4.6926E+02	8.1026E+03	3.4986E+02	1.2025E+03	3.4341E-01
OBLGWO	3.9695E+03	6.8481E+02	5.1134E+03	9.4824E+02	1.2024E+03	6.2125E-01
SCADE	7.3381E+03	3.3867E+02	8.2620E+03	3.1012E+02	1.2026E+03	2.9531E-01
MSCA	4.0081E+03	4.9869E+02	4.7900E+03	6.6196E+02	1.2006E+03	3.2925E-01
SMFO	7.3997E+03	7.2090E+02	8.1202E+03	7.0611E+02	1.2023E+03	5.8046E-01
	F13		F14		F15	
	AVG	STD	AVG	STD	AVG	STD
AO	1.3003E+03	4.9251E-02	1.4003E+03	8.0028E-02	1.5117E+03	2.0982E+00
HGWO	1.3019E+03	4.2079E-01	1.4227E+03	5.2177E+00	1.8070E+03	1.8776E+02
LJAYA	1.3018E+03	3.9868E-01	1.4069E+03	2.8207E+00	1.5445E+03	1.6943E+01
IGWO	1.3006E+03	1.3070E-01	1.4004E+03	2.7949E-01	1.5177E+03	5.7835E+00
CGSCA	1.3032E+03	3.6341E-01	1.4525E+03	8.0849E+00	6.4554E+03	4.5498E+03
OBLGWO	1.3005E+03	9.4262E-02	1.4004E+03	2.4180E-01	1.5171E+03	4.8967E+00
SCADE	1.3039E+03	3.5443E-01	1.4864E+03	1.3165E+01	1.9053E+04	7.6873E+03
MSCA	1.3008E+03	5.8246E-01	1.4141E+03	6.6638E+00	1.8289E+03	4.1414E+02
SMFO	1.3058E+03	8.0789E-01	1.5440E+03	3.5117E+01	4.2152E+04	3.3857E+04
	F16		F17		F18	
	AVG	STD	AVG	STD	AVG	STD
AO	1.6111E+03	6.1494E-01	1.0716E+06	7.0822E+05	4.2527E+03	3.0763E+03
HGWO	1.6125E+03	2.5608E-01	5.6636E+06	2.6618E+06	1.1649E+08	4.4056E+07
LJAYA	1.6127E+03	2.1208E-01	2.9382E+06	1.1159E+06	2.8431E+07	1.6396E+07
IGWO	1.6117E+03	5.8564E-01	8.3159E+05	5.2089E+05	1.9637E+04	2.5555E+04
CGSCA	1.6128E+03	2.1698E-01	7.2906E+06	3.4463E+06	1.8197E+08	1.1428E+08
OBLGWO	1.6121E+03	5.4464E-01	1.6921E+06	1.3287E+06	3.8711E+04	3.0730E+04

SCADE	1.6128E+03	1.8235E-01	1.3589E+07	6.4909E+06	1.7776E+08	1.0031E+08
MSCA	1.6118E+03	6.2215E-01	1.6346E+06	1.4847E+06	3.3665E+07	5.6622E+07
SMFO	1.6126E+03	3.5459E-01	4.0851E+07	3.9766E+07	1.0789E+09	9.4488E+08
	F19		F20		F21	
	AVG	STD	AVG	STD	AVG	STD
AO	1.9122E+03	1.7752E+01	1.2341E+04	8.6995E+03	5.4930E+05	3.9953E+05
HGWO	1.9920E+03	1.0699E+01	6.5077E+04	2.5176E+04	2.2187E+06	1.8770E+06
LJAYA	1.9264E+03	2.6416E+00	7.6840E+03	2.1876E+03	7.0562E+05	2.3361E+05
IGWO	1.9167E+03	1.1670E+01	2.9751E+03	8.6587E+02	2.2032E+05	1.7216E+05
CGSCA	1.9904E+03	1.9249E+01	1.8394E+04	4.5279E+03	1.3880E+06	7.0538E+05
OBLGWO	1.9146E+03	1.1087E+01	6.7346E+03	3.8890E+03	5.7622E+05	4.9633E+05
SCADE	2.0148E+03	1.2664E+01	2.6851E+04	8.2172E+03	2.7484E+06	1.5405E+06
MSCA	1.9515E+03	2.4508E+01	1.1344E+04	4.9956E+03	4.6457E+05	4.7066E+05
SMFO	2.1563E+03	1.0380E+02	7.7902E+04	8.5775E+04	1.9043E+07	1.5747E+07
	F22		F23		F24	
	AVG	STD	AVG	STD	AVG	STD
AO	2.6286E+03	2.0181E+02	2.6152E+03	3.5038E-04	2.6215E+03	7.3848E+00
HGWO	2.9890E+03	1.5941E+02	2.5117E+03	4.4437E+01	2.6000E+03	0.0000E+00
LJAYA	2.8335E+03	1.1530E+02	2.6483E+03	5.3356E+00	2.6569E+03	6.7347E+00
IGWO	2.5438E+03	1.5823E+02	2.6210E+03	3.3631E+00	2.6000E+03	4.4471E-03
CGSCA	3.0348E+03	1.5402E+02	2.5000E+03	0.0000E+00	2.6000E+03	1.2800E-05
OBLGWO	2.6781E+03	1.8649E+02	2.6146E+03	2.1730E+01	2.6000E+03	0.0000E+00
SCADE	3.1207E+03	1.4629E+02	2.5000E+03	0.0000E+00	2.6000E+03	1.4275E-06
MSCA	2.5619E+03	1.5927E+02	2.6386E+03	9.4151E+00	2.6000E+03	6.5869E-04
SMFO	3.4884E+03	7.3630E+02	2.5000E+03	0.0000E+00	2.6000E+03	1.1495E-05
	F25		F26		F27	
	AVG	STD	AVG	STD	AVG	STD
AO	2.7068E+03	1.8865E+00	2.7436E+03	5.0360E+01	3.1721E+03	8.5824E+01
HGWO	2.7000E+03	0.0000E+00	2.7342E+03	4.6421E+01	3.6451E+03	1.0478E+02
LJAYA	2.7249E+03	3.9218E+00	2.7008E+03	1.3454E-01	3.3803E+03	2.1295E+02
IGWO	2.7106E+03	2.4137E+00	2.7007E+03	1.4219E-01	3.1093E+03	3.8275E+00
CGSCA	2.7000E+03	0.0000E+00	2.7029E+03	3.8590E-01	2.9000E+03	0.0000E+00
OBLGWO	2.7000E+03	0.0000E+00	2.7006E+03	1.5249E-01	3.1235E+03	3.2250E+02
SCADE	2.7000E+03	0.0000E+00	2.7038E+03	5.5310E-01	3.2862E+03	2.7641E+02
MSCA	2.7139E+03	3.0029E+00	2.7008E+03	1.5483E-01	3.1629E+03	9.4494E+01
SMFO	2.7000E+03	0.0000E+00	2.7422E+03	4.4769E+01	2.9000E+03	0.0000E+00
	F28		F29		F30	
	AVG	STD	AVG	STD	AVG	STD
AO	3.7174E+03	8.0671E+01	4.2304E+03	4.4857E+02	6.0330E+03	9.3097E+02
HGWO	4.3236E+03	2.8317E+02	4.5982E+06	2.9927E+06	4.3232E+04	1.0876E+05
LJAYA	4.8536E+03	2.8360E+02	5.5222E+06	2.3912E+06	2.9883E+04	7.4050E+03
IGWO	3.9000E+03	2.0882E+02	2.0495E+06	4.6534E+06	2.9535E+04	1.9622E+04
CGSCA	3.0000E+03	0.0000E+00	3.1000E+03	0.0000E+00	1.0492E+04	3.9942E+04
OBLGWO	3.7580E+03	5.1936E+02	4.2897E+06	4.3412E+06	2.2179E+04	1.2261E+04
SCADE	5.2496E+03	6.4983E+02	1.6338E+07	8.0626E+06	4.6663E+05	1.5590E+05
MSCA	3.8955E+03	1.3782E+02	6.5487E+05	1.0123E+06	5.1337E+04	3.6073E+04
SMFO	3.0000E+03	0.0000E+00	1.5108E+06	8.2579E+06	1.0817E+06	8.7055E+05

Table 6. WSRT results and FT rankings for AO and high-performance algorithms

Algorithm	Mean	Rank	+/-/=
AO	2.60	1	~
HGWO	5.57	5	26/3/1
LJAYA	5.83	7	28/1/1
IGWO	2.73	2	20/7/3
CGSCA	5.60	6	23/6/1
OBLGWO	3.37	3	19/5/6
SCADE	7.30	9	25/3/2
MSCA	4.27	4	21/3/6
SMFO	7.20	8	24/5/1

In the data presented in Table 5, AO exhibits a markedly superior average performance in most test functions compared to other algorithms such as IGWO, OBLGWO, and MSCA. This suggests that AO maintains an advantage even when competing against high-performing counterparts. Subsequently, in Table 6, the "Mean" column of comprehensive rankings across all functions shows that AO achieves an average ranking of 2.60, consistently positioning itself prominently in rankings for individual functions and ultimately securing the Rank 1. Additionally, the "+/-/=" column indicators also suggest that AO's results are superior across multiple functions, with noticeable distinctions.

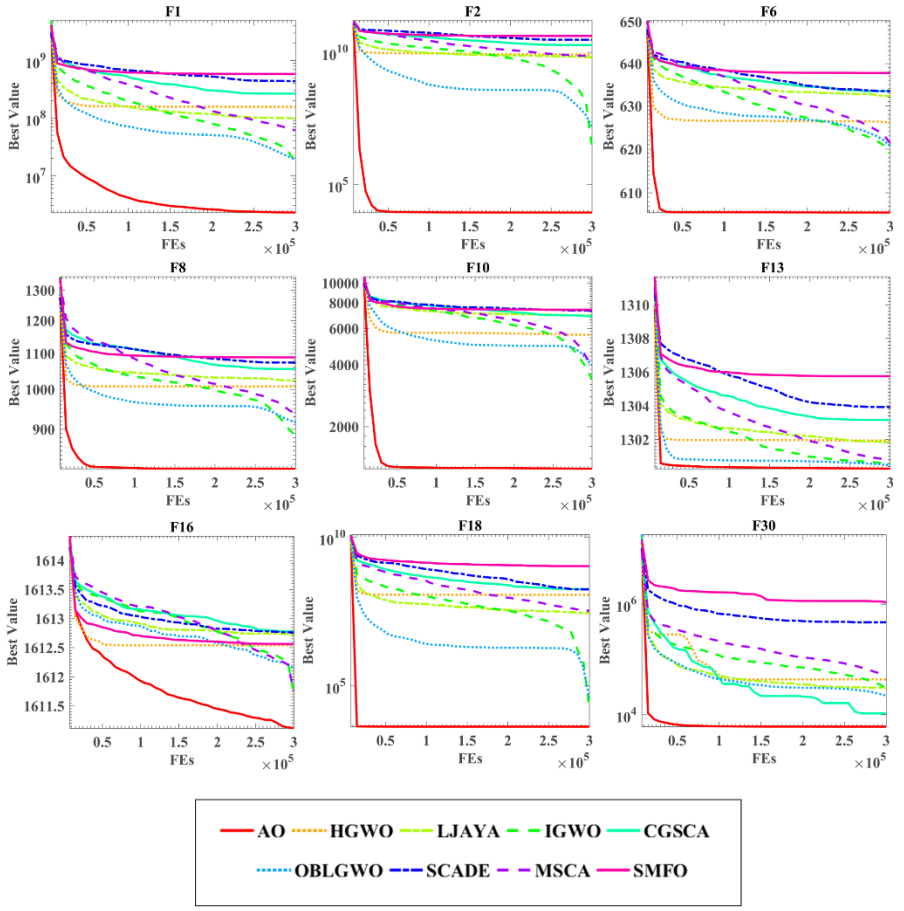


Figure 10. Convergence comparison of AO and high-performance algorithms.

Subsequently, to comprehend the specific performance of the AO in competition with improved algorithms, curves illustrating the optimization processes were generated based on numerical values obtained from experiments, as depicted in Figure 10. A distinct advantage is evident in the convergence trends of the curves, with AO displaying noteworthy superiority. Across single-modal functions F1 and F2, multi-modal functions F6, F8, F10, F13, F16, hybrid function F18, and composite function F30, AO exhibits commendable convergence trends, effectively balancing global exploration and local exploitation to search for the optima. The comprehensive comparison results between AO, classical algorithms, and enhanced algorithms validate its performance in IEEE CEC 2014.

4.3.3 Classical algorithms comparison on IEEE CEC 2022

In the preceding sections, AO demonstrated outstanding performance in comparison with 16 algorithms on IEEE CEC 2014, showcasing its optimization capabilities through contrasts on classical test function sets. This section extends the experimentation by subjecting the algorithm to the latest IEEE CEC 2022 test suite. In contrast to its predecessor, IEEE CEC 2022 imposes higher demands on the accuracy and stability of algorithmic exploration, with improvements in comprehensiveness and diversity, rendering it more challenging and better suited for evaluating and comparing the performance of various optimization algorithms. Therefore, in this study, AO is once again compared with eight classical algorithms to examine its superiority in addressing new challenges in IEEE CEC2022. Table 7 enumerates the competitors involved in the comparison along with their parameter settings. In this experiment, unlike the previous section, the dimensionality of the test functions is set to 20 (default dimension value) due to dimension constraints, and each algorithm is iterated for 200,000 iterations.

Table 7. Algorithms involved in the comparison and their parameter settings.

Algorithms	Parameters
Artemisinin Optimization (AO)	~
Particle swarm optimizer (PSO) [79]	$c_1 = 2;\ c_2 = 2;\ V_{max} = 6$
Whale optimization algorithm (WOA)[80]	$a_1 = [2,0]; a_2 = [-2,-1]; b = 1$
Moth-flame optimization algorithm (MFO)[81]	$b = 1$
Ant colony optimization for continuous domains (ACOR)[25]	$k = 10; q = 0.5;\ ibslo = 1$
Harris Hawk optimizer (HHO)[82]	$k = 0$
Sine cosine algorithm (SCA)[83]	$a = 2$
Multi-verse Optimizer (MVO)[42]	$W_{max} = 1; W_{min} = 0.2$
Jaya optimization algorithm (JAYA) [51]	~

Table 8. Comparison results of AO and peers in IEEE CEC 2022

Fun	F1		F2		F3	
Item	AVG	STD	AVG	STD	AVG	STD
Demo	3.35895E+02	2.34986E+01	4.54938E+02	2.04887E+01	6.00454E+02	8.32234E-02
PSO	3.75904E+02	1.34509E+01	4.41358E+02	2.79380E+01	6.35324E+02	1.38175E+01
WOA	2.64691E+03	2.03047E+03	4.83878E+02	3.83323E+01	6.63441E+02	1.56195E+01
MFO	2.45748E+04	1.91359E+04	5.40992E+02	1.32771E+02	6.19323E+02	9.28611E+00
ACOR	2.28415E+03	6.34142E+03	4.40116E+02	1.75853E+01	6.01365E+02	2.28535E+00
HHO	3.28924E+02	1.28679E+01	4.62901E+02	1.80404E+01	6.53861E+02	8.77329E+00
SCA	8.01472E+03	1.64819E+03	6.33674E+02	5.93129E+01	6.36199E+02	4.80298E+00
MVO	3.00020E+02	8.20511E-03	4.46508E+02	1.64725E+01	6.03205E+02	4.19923E+00
JAYA	7.78702E+03	1.49836E+03	5.43470E+02	2.13640E+01	6.13102E+02	1.98380E+00
	F4		F5		F6	
	AVG	STD	AVG	STD	AVG	STD
Demo	8.60835E+02	1.81085E+01	1.51606E+03	5.22949E+02	5.09879E+04	5.17886E+04
PSO	8.94289E+02	1.93524E+01	1.47943E+03	8.19065E+02	1.21896E+06	3.91441E+05
WOA	9.09113E+02	3.34675E+01	3.45927E+03	1.17681E+03	9.91695E+03	9.78604E+03
MFO	9.10977E+02	3.14849E+01	3.26253E+03	1.10535E+03	3.99670E+06	9.62114E+06
ACOR	8.90632E+02	2.81155E+01	9.71764E+02	1.35222E+02	6.67739E+03	5.99720E+03
HHO	8.83179E+02	1.42429E+01	2.67900E+03	2.25799E+02	6.78555E+04	3.11794E+04
SCA	9.30007E+02	1.03182E+01	1.88624E+03	2.78617E+02	6.67100E+07	3.74250E+07
MVO	8.42313E+02	1.28857E+01	9.01313E+02	2.92690E+00	9.97905E+03	7.44928E+03
JAYA	9.18638E+02	9.03111E+00	1.29292E+03	1.15428E+02	3.20276E+07	1.52615E+07
	F7		F8		F9	
	AVG	STD	AVG	STD	AVG	STD

Demo	2.04921E+03	2.66350E+01	2.22224E+03	6.70457E-01	2.48158E+03	4.73910E-01
PSO	2.11510E+03	3.47318E+01	2.28061E+03	7.01310E+01	2.46583E+03	1.09992E-01
WOA	2.18126E+03	5.59483E+01	2.25546E+03	2.96415E+01	2.49540E+03	1.79462E+01
MFO	2.10794E+03	4.35303E+01	2.23681E+03	1.11124E+01	2.50907E+03	3.66813E+01
ACOR	2.05610E+03	3.79727E+01	2.23408E+03	2.58425E+01	2.48134E+03	3.05582E+00
HHO	2.15210E+03	5.41456E+01	2.25130E+03	3.88309E+01	2.48561E+03	2.32419E+00
SCA	2.11381E+03	1.63772E+01	2.24910E+03	8.55966E+00	2.55352E+03	1.89136E+01
MVO	2.08007E+03	6.02453E+01	2.30200E+03	8.91089E+01	2.48083E+03	2.10838E-02
JAYA	2.09963E+03	1.14643E+01	2.23586E+03	2.91979E+00	2.54210E+03	1.27361E+01
	F10		F11		F12	
	AVG	STD	AVG	STD	AVG	STD
Demo	2.49361E+03	7.27645E+01	2.60411E+03	1.66499E+00	2.86553E+03	3.03125E+00
PSO	4.35614E+03	1.17609E+03	2.79538E+03	1.95710E+02	2.85204E+03	1.12305E+01
WOA	4.30201E+03	1.02543E+03	2.78997E+03	1.37550E+02	2.87520E+03	1.97660E+01
MFO	4.04211E+03	1.17879E+03	2.80115E+03	1.61997E+02	2.86477E+03	2.01682E+00
ACOR	3.42781E+03	6.53016E+02	2.76128E+03	1.78729E+02	2.86517E+03	2.07629E+00
HHO	3.41059E+03	6.76626E+02	2.76332E+03	1.23253E+02	2.89419E+03	3.85740E+01
SCA	2.52668E+03	3.98602E+01	2.76182E+03	8.24780E+00	2.86827E+03	1.24375E+00
MVO	3.57518E+03	6.10863E+02	2.75676E+03	1.85078E+02	2.86059E+03	1.93399E+00
JAYA	2.55059E+03	9.96284E+01	2.61675E+03	3.30387E+00	2.87242E+03	1.51187E+00

Table 9. WSRT results and FT rankings for AO and competitors comparison at IEEE CEC 2022

	Mean	Rank	+/-/=
AO	2.67	1	~
PSO	5.08	4	8/3/1
WOA	6.92	9	11/1/0
MFO	6.50	7	10/0/2
ACOR	2.92	2	5/2/5
HHO	5.67	6	9/0/3
SCA	6.75	8	12/0/0
MVO	3.08	3	6/6/0
JAYA	5.42	5	11/0/1

In Table 8, AO's performance in the latest test suite continues to exhibit outstanding exploration results, indicating its ability to adapt stably to more complex sets of test functions. In Table 9, AO secures the top rank with a "Rank" value of 2.67. Furthermore, AO outperforms its peers in most functions in the "+/-/=" column.

Figure 11 illustrates the exploration process of AO and its competitors in discovering optimal solutions in the latest test suite. During the initial exploration phase, AO rapidly identifies potentially promising regions. As the exploration progresses, it transitions into local exploitation, precisely searching for the optimal solution, ultimately achieving the best convergence accuracy. These convergence plots depict AO striking a balance between exploration and exploitation. Thus, through comparisons on intricate functions, AO maintains a satisfactory level of performance.

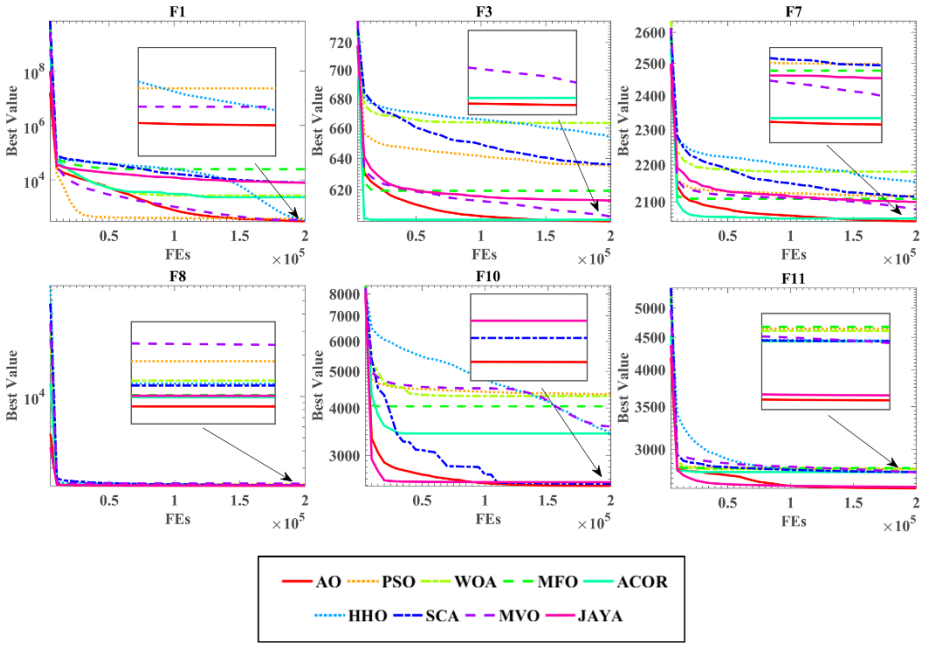


Figure 11. Convergence comparison of AO and competitors in the IEEE CEC 2022.

4.3.4 High-performance algorithms comparison on IEEE CEC 2022

In this section, AO is once again compared with eight high-performance enhanced algorithms on IEEE CEC 2022 to further evaluate its performance in the face of complex challenges. Table 10 enumerates all the algorithms involved in the comparison along with their respective parameter configurations. Table 11 presents the average (AVG) and standard deviation (STD) of the results obtained from 30 independent runs for each algorithm.

Table 10. Algorithms involved in the comparison and their parameter settings.

Algorithms	Parameters
Artemisinin Optimization (AO)	~
Hybridizing grey wolf optimization with differential evolution (HGWO) [85]	$\beta_{max} = 0.8, \beta_{min} = 0.2,$ $CR_p = 0.2, a = [0,2]$
JAYA algorithm with Levy flight (LJAYA) [86]	~
Double adaptive random spare reinforced whale optimization algorithm (RDWOA) [93]	$s = 0; a_1 = [2,0];$ $a_2 = [-2,-1]; b = 1$
Cauchy and Gaussian Sine Cosine Optimization (CGSCA) [88]	$a = 1, \delta = 0.1$
Levy opposition-based learning Grey Wolf Optimizer(OBLGWO)[89]	$P = 0.5$
sine cosine algorithm with differential evolution (SCADE) [90]	$a = 2;\ \beta_{max} = 0.8,$ $\beta_{min} = 0.2;\ CR_p = 0.8$
modified sine cosine algorithm (MSCA) [91]	$JR = 0.1;\ a = 2;\ SR = [0,1]$
Moth-flame optimizer with sine cosine mechanisms (SMFO) [92]	$b = 1$

Table 11. Optimization results of AO and high-performance algorithms.

Fun	F1		F2		F3	
Item	AVG	STD	AVG	STD	AVG	STD
AO	3.0010E+02	4.5618E-01	4.5719E+02	1.5080E+01	6.0004E+02	2.0919E-01
HGWO	2.7213E+04	6.1708E+03	5.6619E+02	2.8309E+01	6.2397E+02	4.9572E+00
LJAYA	1.0908E+04	2.2880E+03	5.5633E+02	2.0311E+01	6.1730E+02	2.4186E+00
RDWOA	1.0317E+03	1.1234E+03	4.6637E+02	2.3890E+01	6.0298E+02	2.3861E+00
CGSCA	9.7005E+03	2.8040E+03	6.9791E+02	7.3253E+01	6.4160E+02	6.3308E+00
OBLGWO	5.4112E+02	1.1984E+02	4.6063E+02	2.3726E+01	6.0680E+02	6.0381E+00

SCADE	2.3704E+04	4.1954E+03	7.5201E+02	8.8059E+01	6.4422E+02	6.5507E+00
MSCA	5.5828E+03	2.7795E+03	5.1459E+02	4.7343E+01	6.1402E+02	4.6127E+00
SMFO	6.8954E+04	4.4745E+04	1.4510E+03	3.9801E+02	6.7012E+02	1.1311E+01
	F4		F5		F6	
	AVG	STD	AVG	STD	AVG	STD
AO	8.7727E+02	2.0451E+01	9.0449E+02	8.1976E+00	5.7467E+03	4.8753E+03
HGWO	9.1787E+02	1.0105E+01	1.3941E+03	1.2469E+02	3.4206E+07	1.2796E+07
LJAYA	9.2406E+02	7.4571E+00	1.4717E+03	1.2492E+02	2.9290E+07	1.1739E+07
RDWOA	9.1185E+02	3.2912E+01	2.3222E+03	4.3059E+02	8.9430E+03	7.2292E+03
CGSCA	9.3317E+02	1.2050E+01	2.2012E+03	3.4257E+02	4.9413E+07	3.4530E+07
OBLGWO	8.7941E+02	2.1529E+01	1.0755E+03	2.1167E+02	2.2698E+04	2.6773E+04
SCADE	9.4916E+02	9.1818E+00	2.6403E+03	4.1515E+02	6.4803E+07	5.2445E+07
MSCA	8.6909E+02	1.2912E+01	1.4140E+03	2.2834E+02	2.0122E+06	7.9045E+06
SMFO	9.5035E+02	1.7299E+01	3.2545E+03	3.7080E+02	3.8535E+08	3.7737E+08
	F7		F8		F9	
	AVG	STD	AVG	STD	AVG	STD
AO	2.0681E+03	4.5425E+01	2.2265E+03	2.1749E+01	2.4808E+03	3.9236E-02
HGWO	2.1515E+03	1.8247E+01	2.2455E+03	8.0953E+00	2.5523E+03	2.4357E+01
LJAYA	2.0976E+03	1.2254E+01	2.2376E+03	3.3126E+00	2.5358E+03	1.0050E+01
RDWOA	2.0681E+03	3.5606E+01	2.2312E+03	3.0175E+01	2.4812E+03	1.0123E+00
CGSCA	2.1247E+03	2.1103E+01	2.2546E+03	7.5544E+00	2.5625E+03	2.4384E+01
OBLGWO	2.0753E+03	2.5814E+01	2.2383E+03	1.3350E+01	2.4818E+03	1.5688E+00
SCADE	2.1569E+03	1.6579E+01	2.2459E+03	3.8859E+00	2.5700E+03	2.2185E+01
MSCA	2.0553E+03	1.2950E+01	2.2297E+03	5.7078E+00	2.5012E+03	1.9056E+01
SMFO	2.2043E+03	4.2043E+01	2.3017E+03	1.0492E+02	2.8322E+03	1.4833E+02
	F10		F11		F12	
	AVG	STD	AVG	STD	AVG	STD
AO	2.5605E+03	9.0696E+01	2.7857E+03	1.5872E+02	2.8713E+03	6.5633E+00
HGWO	2.6950E+03	4.5927E+02	2.8928E+03	1.7908E+02	2.8666E+03	5.1000E+00
LJAYA	2.5052E+03	8.6732E+00	2.6162E+03	2.8583E+00	2.8721E+03	1.4631E+00
RDWOA	2.6446E+03	1.4645E+02	2.7538E+03	1.7752E+02	2.8701E+03	9.6974E+00
CGSCA	2.5250E+03	6.0857E+00	2.7649E+03	1.0066E+01	2.8677E+03	1.2553E+00
OBLGWO	2.8447E+03	6.9650E+02	2.6512E+03	1.3010E+02	2.8638E+03	1.9705E+00
SCADE	2.5526E+03	6.5746E+01	2.7661E+03	9.0700E+00	2.8692E+03	1.2176E+00
MSCA	2.5644E+03	2.4073E+02	2.7162E+03	4.1428E+01	2.8633E+03	1.8446E+00
SMFO	5.8375E+03	1.3331E+03	3.0481E+03	3.5398E+02	2.9497E+03	5.3229E+01

Table 12. WSRT results and FT rankings for AO and high-performance competitors' comparison at IEEE CEC 2022

Algorithms	Mean	Rank	+/-/=
AO	2.50	1	~
HGWO	5.92	6	11/1/0
LJAYA	4.67	5	9/2/1
RDWOA	3.67	4	8/0/4
CGSCA	5.92	6	9/1/2
OBLGWO	3.25	3	6/2/4
SCADE	7.00	8	9/0/3
MSCA	3.08	2	7/3/2
SMFO	9.00	9	12/0/0

In Table 11, AO continues to exhibit outstanding performance in the comparison with high-performance algorithms on IEEE CEC 2022, indicating its ability to adapt more stably to complex sets of test functions compared to enhanced algorithms. In Table

12, AO secures the top rank with a "Rank" value of 2.50. Additionally, AO outperforms its peers in most functions in the "+/-/=" column. Figure 12 illustrates the exploration process of AO and its competitors in discovering optimal solutions in the latest test suite. During the initial exploration phase, AO rapidly identifies potentially promising regions and accurately transitions into local development to search for the optimal solution precisely, achieving the best convergence. These convergence plots indicate that AO attains a balance between exploration and exploitation in line with its design philosophy. Thus, through further comparisons, it can be affirmed that AO is an algorithm capable of better addressing new challenges.

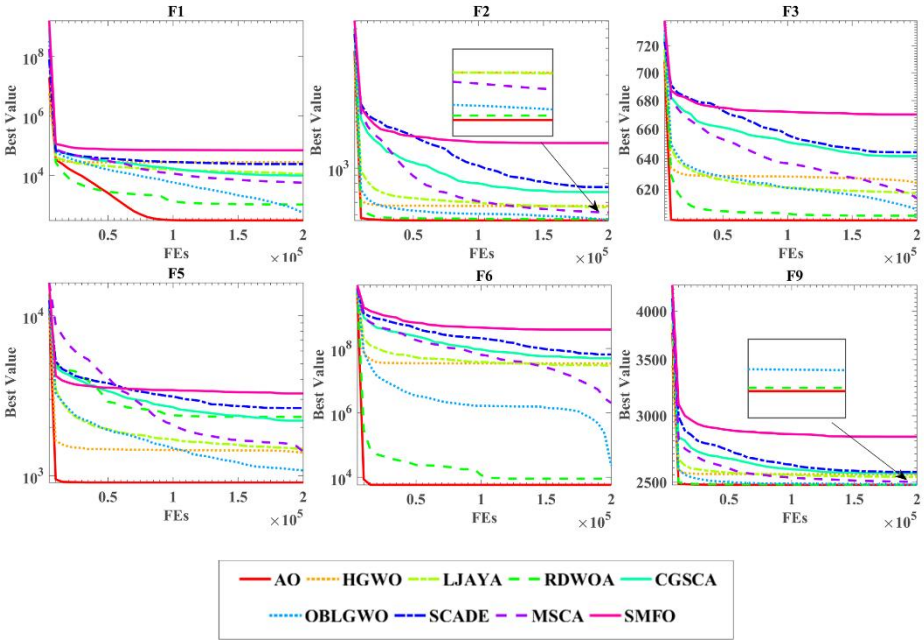


Figure 12. Convergence comparison of AO and high-performance competitors on the IEEE CEC 2022.

6. Application of the AO to multi-threshold image segmentation

In this section, AO is placed in a real-world application scenario of MAs: multi-threshold image segmentation (MTIS). Harnessing AO's optimization capabilities, it provides the MTIS system with an optimal combination of thresholds conducive to the proficient segmentation of images.

MTIS technique segments images into different regions, each determined by one or more thresholds. Compared to traditional binary image segmentation techniques, MTIS excels in effectively handling images with multiple objects or exhibiting discontinuous color or brightness variations [94]. The fundamental concept involves comparing pixel intensity values in the image with a set of thresholds, thereby allocating pixels to different regions. The simplicity and versatility of this approach make it applicable to various types of images. However, general threshold segmentation methods often struggle to utilize spatial positional information in the image effectively.

In cases where objects occupy a relatively small portion of the image, such methods may result in significant segmentation errors, rendering the results susceptible to noise interference. Abutaleba [102] introduced a MTIS method based on a two-dimensional histogram to address this issue. This method integrates the original grayscale histogram with pixel local averages histogram to obtain a two-dimensional histogram of non-local means. Such integration substantially reduces the occurrence of segmentation errors of this nature, markedly enhancing segmentation quality. However, in this method, it is necessary to compute the corresponding two-dimensional entropy for each possible threshold and select the threshold that minimizes the entropy. This exhaustive approach introduces considerable computational complexity [95, 96].

While the two-dimensional histogram-based MTIS proves effective, it still faces limitations. This method necessitates extensive threshold optimization computations, potentially incurring significant computational costs. With the continuous evolution of complexity in digital images, there is an escalating demand for accurate and efficient image analysis. The deficiencies of this

approach, such as overlooking certain image details, gradually become apparent [97]. This paper introduces a MTIS method that integrates non-local mean filtering, two-dimensional histograms, Kapur entropy, and AO to address these challenges. The structure of this section is as follows: Section 5.1 outlines the designed MTIS method. Section 5.2 presents tests of the method at various threshold levels, incorporating comparisons with several analogous algorithms to assess the impact of AO on this segmentation approach.

6.1 Integrating the AO with MTIS system

In the designed MTIS system, four key functional components have been incorporated: non-local mean filtering, two-dimensional histograms, Kapur's entropy, and the AO. Non-local mean filtering, as an image denoising technique, filters each pixel by considering the pixel values in the surrounding region, generating a non-local mean filtered image. This filtered image is then used to synthesize a two-dimensional histogram, enhancing the stability and accuracy of subsequent segmentation steps. The two-dimensional histogram serves as a chart to represent the relationship between two variables, aiding in the observation of relationships between different grayscale levels in the image and facilitating the partitioning process with multiple thresholds. Kapur's entropy is an indicator used to measure the information content of an image, assisting in the selection of optimal thresholds [98]. In the context of MTIS, Kapur's entropy functions as the objective function and is optimized through the AO to determine the optimal combination of multiple thresholds. To provide a clear understanding of the operational flow of MTIS, a flowchart is presented in Figure 13.

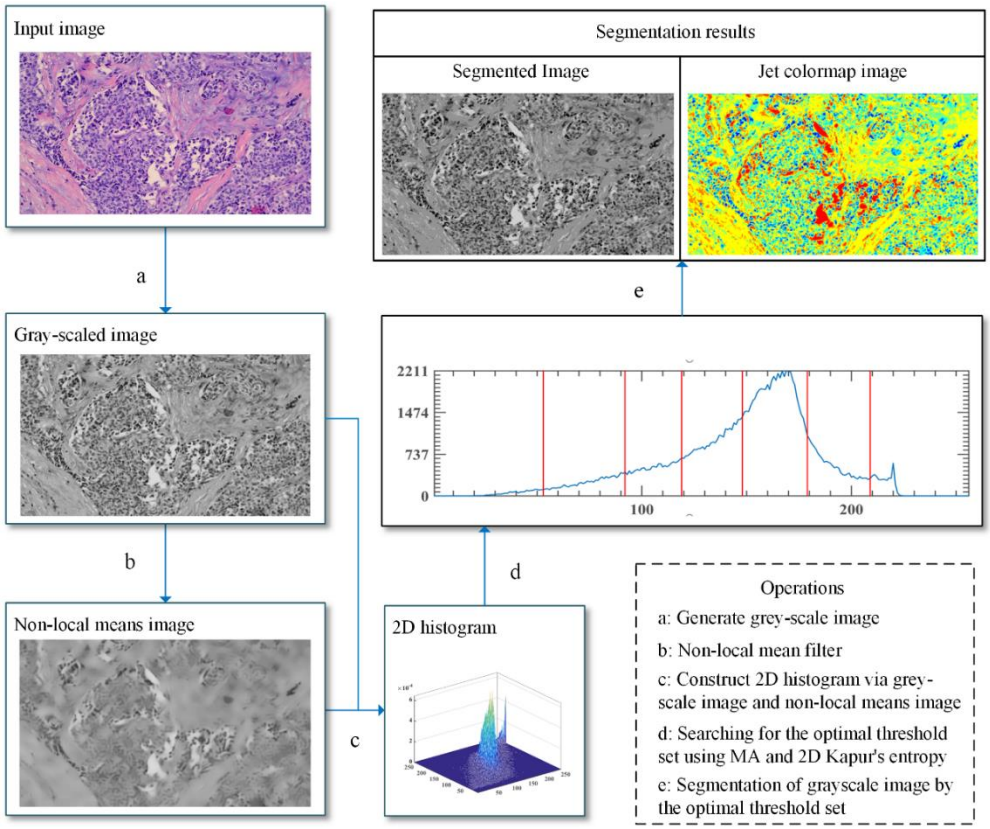


Figure 13. The flowchat of MTIS modeling

Specifically, the steps of this method are as follows: Initially, grayscale the input image to generate a grayscale image. Subsequently, non-local mean filtering is applied to the grayscale image to reduce noise, ensuring greater stability for subsequent processing. The grayscale and non-local mean filtered images are then used to construct a two-dimensional histogram. Employing Kapur's entropy as the evaluation metric, the entropy for each set of thresholds is computed. The objective of this method is to search for a threshold combination that maximizes Kapur's entropy, resulting in the segmented image's maximal entropy and information content. Following this, the AO is employed to optimize the computation of the entropy. Finally, the image is segmented using the optimized set of thresholds, gaining the completed segmented image.

6.2 Segmentation experiments on breast cancer pathology images

Cancer has been a serious disease in the last decade and there is an increasing momentum in medical research to detect it and help diagnosis of cancer more efficiently [99]. Hence, in this study, 15 breast cancer pathology images were utilized as the target images for segmentation, all sourced from the Affiliated Hospital of Wenzhou Medical University. Figure 14 illustrates the original images and their corresponding non-local mean two-dimensional histograms. The experimental objective is to evaluate whether the AO-based MTIS system can consistently maintain excellent segmentation performance when faced with different images. Additionally, the study also aims to assess whether AO's ability to select optimal thresholds in the face of diverse images meets the anticipated standards, as each image is treated as an independent problem associated with the segmentation threshold level [100].

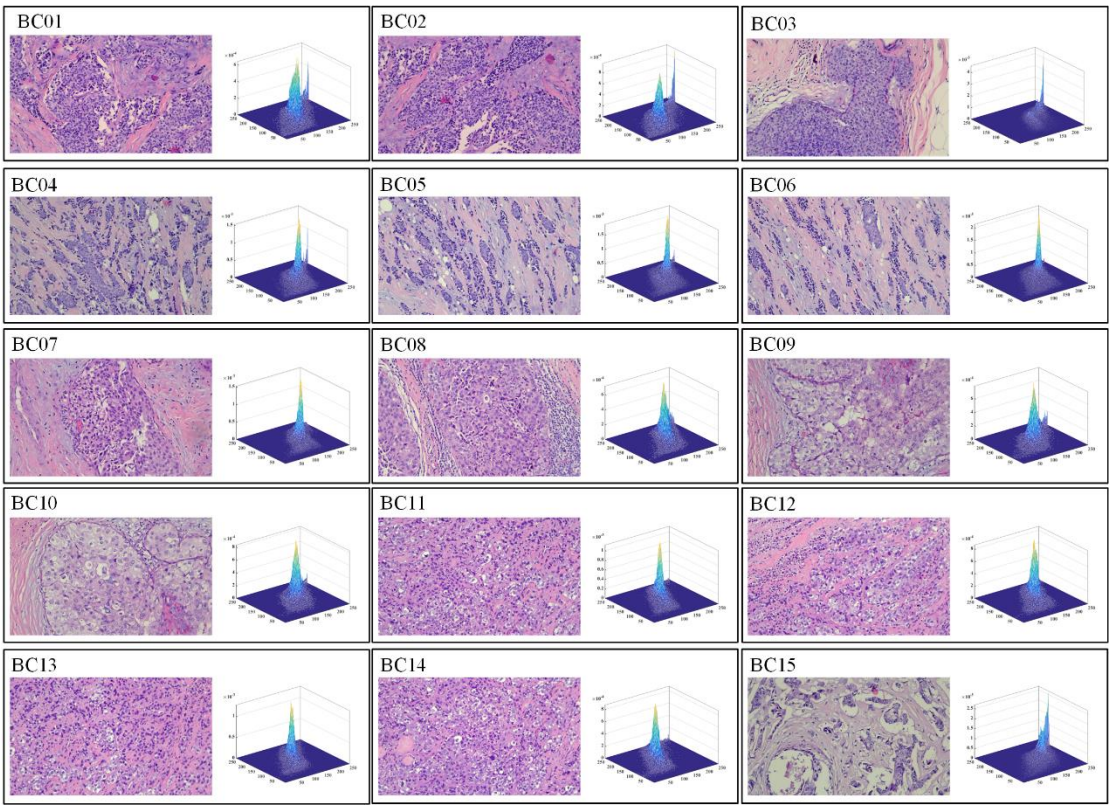


Figure 14. Image samples and 2D histograms

Furthermore, to thoroughly test AO, we engaged in a discussion on the selection of threshold levels. The specific choice of how many thresholds to use for segmenting medical images often depends on the medical application and image characteristics. In practice, this number is typically determined through experimentation and validation. There is no fixed standard number, as different images and applications may require varying numbers of thresholds. This experiment references some general guidelines [95, 101, 102]: for simple applications like basic tumor detection, only one threshold may be needed to segment the image into background and foreground (tumor) categories. For more complex applications like tissue classification, where the image needs to be segmented into multiple tissue types, additional thresholds (usually between 3 and 6) can be chosen based on the image histogram or expert knowledge to delineate corresponding categories. For finer applications, such as distinguishing different types of tissues (muscle, bone, vessels, etc.), more thresholds (between 6 and 10) may be necessary to segment various tissue types accurately. For more intricate tasks like cell and lesion analysis, even more thresholds (usually exceeding 10) may be required to precisely segment structures with different shapes and colors.

Therefore, this study designed two sets of segmentation experiments, including simple segmentation with 2, 4, and 6 threshold levels, and detailed segmentation with 16, 20, and 24 threshold levels. Eight algorithms were included in the segmentation task for comparison with the AO. All the algorithms involved in the comparison and their parameter settings are shown in Table 13.

Table 13. Algorithms involved in the comparison and their parameter settings.

Algorithms	Parameters
Artemisinin optimization (AO)	~
RIME algorithm (RIME) [15]	$W = 5$

Differential evolution (DE) [103]	$\beta_{max} = 0.8, \beta_{min} = 0.2, CR_p = 0.2$
Harris Hawk optimizer (HHO) [82]	$k = 0$
Whale optimization algorithm (WOA) [80]	$a_1 = [2,0]; a_2 = [-2,-1]; b = 1$
Particle swarm optimizer (PSO) [79]	$W_{max=}0.9, W_{min} = 0.2$
Sine cosine algorithm (SCA) [83]	$a = 2$
Salp swarm algorithm (SSA) [32]	~
Cuckoo search (CS) [104]	$Pa = 0.25$

In the experiment, Peak Signal-to-Noise Ratio (PSNR) [105], Structural Similarity Index (SSIM) [106], and Feature Similarity Index (FSIM) [107] were employed as metrics to evaluate the results. Analysis was conducted based on the mean and variance of these metrics, and statistical tests using WSRT [75] and FT [76] were performed. The algorithms underwent 2000 iterations, with image dimensions set at 480x270 pixels. The algorithm's solution set included 30 search agents, and each algorithm was independently run 30 times.

6.2.1 Experimental at low threshold level

This section categorized threshold levels of 2, 4, and 6 as low threshold groups. AO, along with eight algorithms, was utilized to segment the 15 images, and the segmentation results were compared.

Tables A.3 to A.5 present all the thresholds discovered by various methods in 2, 4, and 6-level threshold segmentation for 15 images, along with the corresponding computed fitness values (Kapur's entropy). By observing the results, it is evident that AO successfully identifies threshold sets that maximize Kapur's entropy for all images, demonstrating improved performance as the threshold levels increase.

Figure 15 shows convergence curves for various algorithms during the segmentation experiment with 6-level thresholds for selected images. It is apparent that AO exhibits effective convergence in searching for the optimal threshold set, showcasing a reliable ability to find the maximum Kapur's entropy compared to other algorithms and achieving higher convergence accuracy. Notably, AO demonstrates excellent capability in locating the maximum value of Kapur's entropy, especially at lower threshold levels during image segmentation experiments.

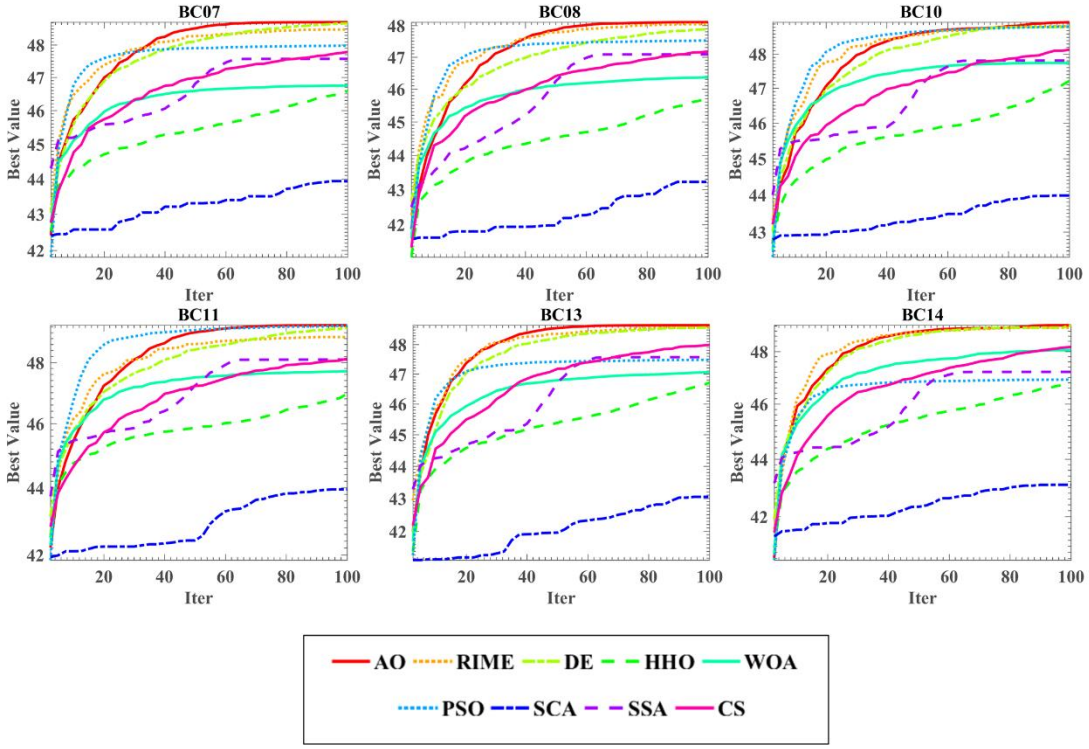


Figure 15. Convergence curves of Kapur's entropy at 6 threshold levels.

Then, Appendices A.6 to A.8 display the average and standard deviation of the three metrics after 30 iterations of segmentation using AO and the other eight algorithms. Clearly, AO achieved the highest averages and the lowest standard deviations in most images, indicating its superior overall performance and relatively stable results in the task of simple segmentation of the targets.

Tables 14, 15, and 16 present the statistical results of these three metrics. The statistical results suggest that the AO outperforms the other algorithms overall for simple segmentation tasks.

Table 14. The FSIM comparison results at low threshold level

	2 thresholds			4 thresholds			6 thresholds		
	Mean	Rank	+/-/=	Mean	Rank	+/-/=	Mean	Rank	+/-/=
AO	2.60	1	~	2.00	1	~	1.53	1	~
RIME	3.20	3	3/1/11	2.53	3	6/0/9	2.67	2	6/0/9
DE	3.13	2	6/4/5	2.07	2	4/3/8	2.80	3	7/1/7
HHO	7.73	9	10/0/5	7.73	8	15/0/0	7.47	8	14/0/1
WOA	6.13	7	8/0/7	6.67	7	14/0/1	7.00	7	15/0/0
PSO	5.07	4	9/2/4	3.67	4	10/1/4	3.33	4	10/0/5
SCA	6.47	8	7/2/6	9.00	9	15/0/0	9.00	9	15/0/0
SSA	5.20	5	4/1/10	6.13	6	13/0/2	5.13	5	14/0/1
CS	5.47	6	7/0/8	5.20	5	12/0/3	6.07	6	13/0/2

Table 15. The PSNR comparison results at low threshold level

	2 thresholds			4 thresholds			6 thresholds		
	Mean	Rank	+/-/=	Mean	Rank	+/-/=	Mean	Rank	+/-/=
AO	1.67	1	~	1.93	1	~	2.07	1	~
RIME	3.47	3	4/1/10	2.47	3	6/1/8	2.80	3	3/2/10
DE	2.53	2	6/2/7	2.40	2	6/1/8	2.33	2	4/2/9
HHO	8.00	9	13/0/2	8.00	8	15/0/0	7.53	8	15/0/0
WOA	6.20	7	10/0/5	6.60	7	15/0/0	6.87	7	14/0/1
PSO	6.67	8	12/0/3	3.53	4	10/1/4	2.80	3	6/3/6
SCA	5.93	6	11/0/4	8.93	9	15/0/0	9.00	9	15/0/0
SSA	5.47	5	10/0/5	6.13	6	14/0/1	5.93	6	14/0/1
CS	5.07	4	8/0/7	5.00	5	12/0/3	5.67	5	13/0/2

Table 16. The SSIM comparison results at low threshold level

	2 thresholds			4 thresholds			6 thresholds		
	Mean	Rank	+/-/=	Mean	Rank	+/-/=	Mean	Rank	+/-/=
AO	1.73	1	~	2.20	1	~	2.07	1	~
RIME	3.13	3	3/0/12	2.20	2	4/2/9	2.80	3	3/2/10
DE	2.60	2	6/1/8	2.27	3	4/3/8	2.53	2	5/2/8
HHO	7.87	9	12/0/3	7.80	8	15/0/0	7.47	8	14/0/1
WOA	6.40	7	12/0/3	6.60	7	14/0/1	6.67	7	14/0/1
PSO	6.07	6	12/0/3	3.73	4	10/0/5	2.80	3	5/3/7
SCA	6.87	8	9/0/6	8.87	9	15/0/0	9.00	9	15/0/0
SSA	5.47	5	9/0/6	6.20	6	14/0/1	5.80	5	12/0/3
CS	4.87	4	8/0/7	5.13	5	12/0/3	5.87	6	13/0/2

In the analysis of the segmentation results, as depicted in Figure 16, the segmentation outcomes of BC15 at 6 threshold levels are presented; this sample image contains a more complex background and iconic tissue, which is relatively challenging in low thresholding. With an increase in the number of thresholds, the image is segmented into more regions, thereby achieving higher accuracy, especially for images with multiple targets, textures, or complex structures. Upon examining the original image, the central region is observed to have a complex and dense structure, while the edges are unclear due to noise interference. After segmentation, these regions are distinctly separated. Upon close observation, the results segmented by AO exhibit vibrant colors and clear contours in the central region. The analysis of these segmentation experiment results clearly indicates the superiority of the proposed AO method over other algorithms in simple segmentation tasks.

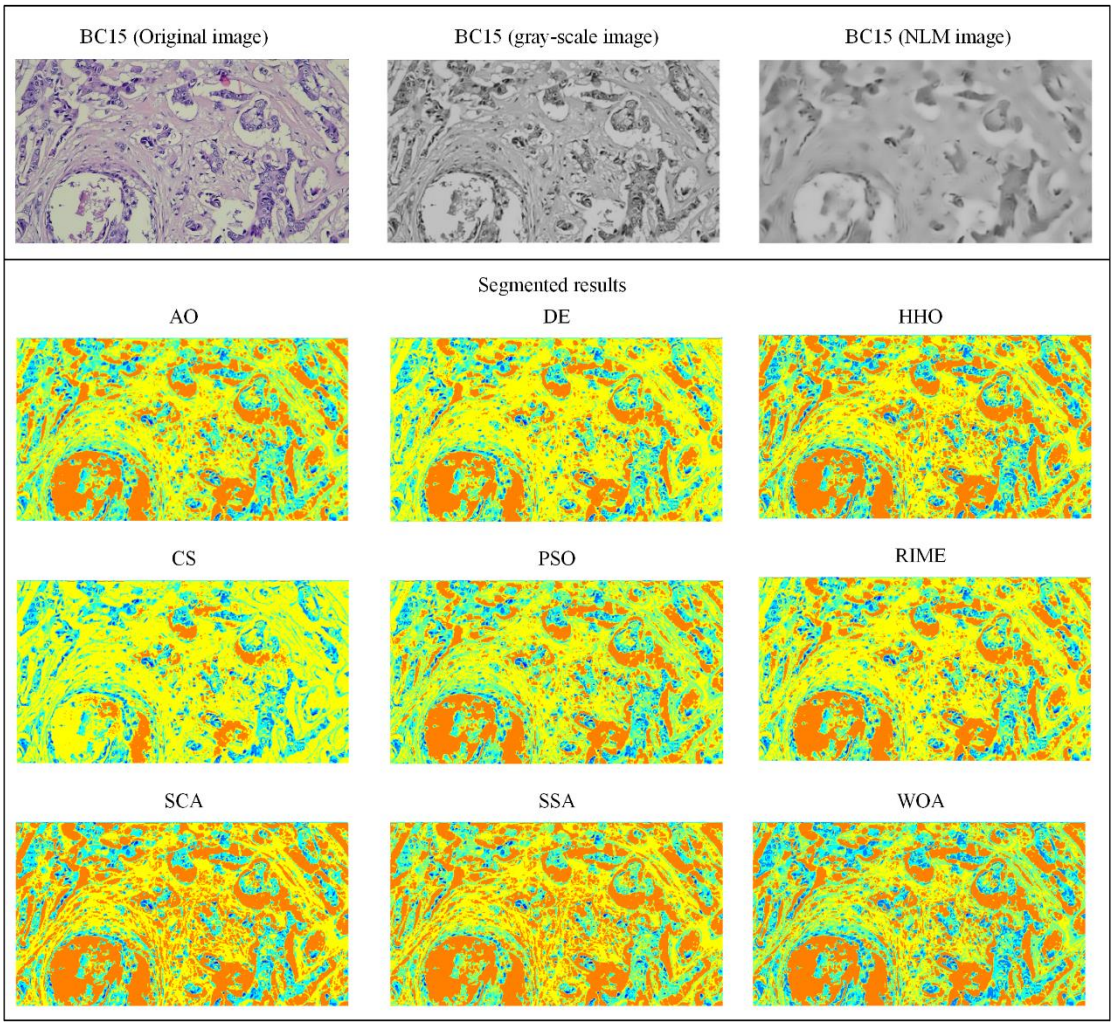


Figure 16. Comparison of segmentation results for BC15 at 6 threshold levels.

6.2.2 Experimental at high threshold level

In this section, segmentation accuracy is enhanced by increasing the threshold levels. AO once again competes with the 8 algorithms, segmenting the same set of 15 images.

Figure 17 presents convergence curves for various algorithms during the segmentation experiment with 24-level thresholds for selected images. It is evident that AO demonstrates superior convergence when searching for the optimal threshold set at higher levels, achieving a faster, more precise ability to find the maximum of Kapur's entropy compared to other algorithms, making it more reliable. Notably, when conducting more refined segmentation experiments, AO is more capable of locating the maximum value of Kapur's entropy than other algorithms.

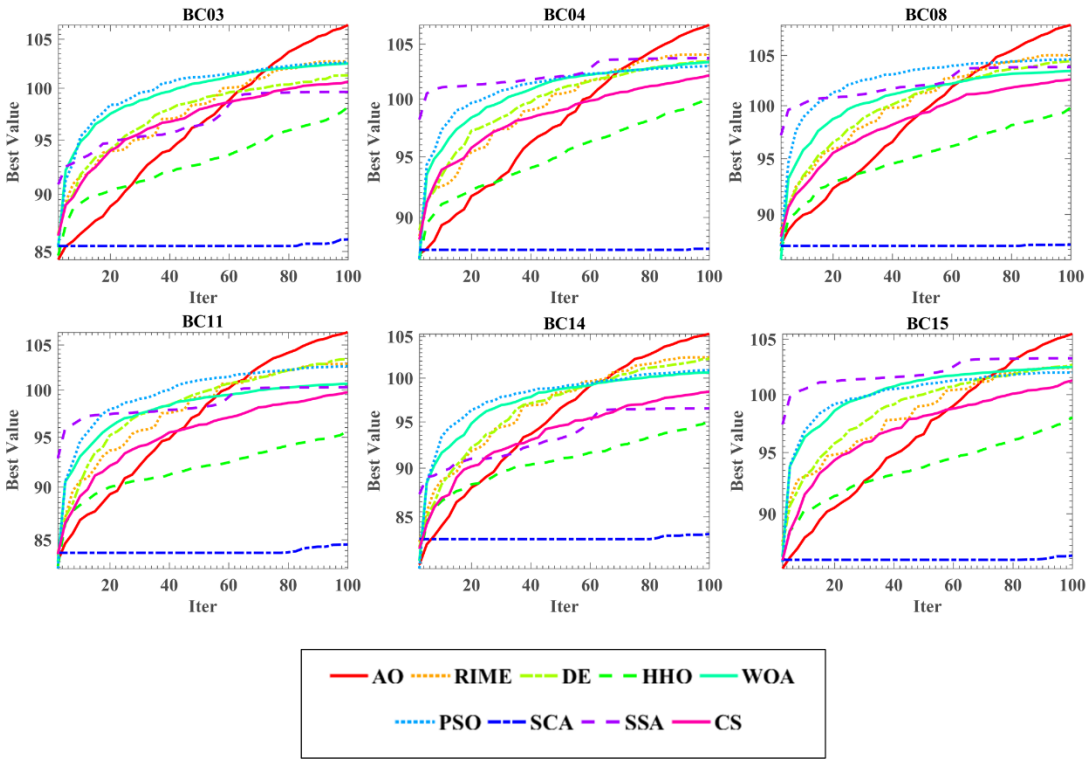


Figure 17. Convergence curves of Kapur's entropy at 24 threshold levels.

Tables A.9 to A.11 in the appendix list the averages and standard deviations of the three metrics after segmentation. Clearly, in most images, AO outperforms other algorithms in both average and standard deviation at high threshold levels. Additionally, Tables 17, 18, and 19 summarize the statistical results of these metrics when using WSRT and FT. The statistical analysis indicates that when facing higher segmentation accuracy requirements, AO continues to outperform other algorithms and exhibits greater stability and adaptability to fine segmentation tasks with higher threshold levels.

Table 17. The FSIM comparison results at high threshold level

	16 thresholds			20 thresholds			24 thresholds		
	Mean	Rank	+/-/=	Mean	Rank	+/-/=	Mean	Rank	+/-/=
AO	1.67	1	~	1.27	1	~	1.60	1	~
RIME	3.67	3	9/0/6	5.07	5	14/0/1	5.13	6	11/0/4
DE	3.73	4	11/0/4	3.73	3	14/0/1	4.20	3	11/0/4
HHO	8.13	8	14/0/1	7.87	8	15/0/0	8.07	8	15/0/0
WOA	6.07	6	13/0/2	5.07	5	12/0/3	4.40	4	6/0/9
PSO	2.33	2	7/0/8	3.93	4	11/0/4	4.40	4	8/0/7
SCA	8.87	9	14/0/1	9.00	9	15/0/0	8.93	9	15/0/0
SSA	3.93	5	11/1/3	2.53	2	8/0/7	1.87	2	3/0/11
CS	6.60	7	13/0/2	6.53	7	14/0/1	6.40	7	13/0/2

Table 18. The PSNR comparison results at high threshold level

	16 thresholds			20 thresholds			24 thresholds		
	Mean	Rank	+/-/=	Mean	Rank	+/-/=	Mean	Rank	+/-/=
AO	1.73	1	~	1.67	1	~	2.27	1	~
RIME	3.00	3	3/1/11	4.67	6	2/0/13	4.87	6	5/0/10
DE	3.93	4	5/1/9	4.40	5	8/0/7	4.60	5	7/0/8
HHO	7.80	8	13/0/2	7.93	8	14/0/1	8.07	8	14/0/1
WOA	4.93	5	5/0/10	4.00	4	3/1/11	3.33	3	3/0/12
PSO	2.53	2	3/0/12	3.00	2	2/0/13	3.73	4	3/0/12
SCA	9.00	9	15/0/0	9.00	9	15/0/0	8.93	9	15/0/0
SSA	5.53	6	9/0/6	3.93	3	5/0/10	2.73	2	3/1/12
CS	6.53	7	11/0/4	6.40	7	11/0/4	6.47	7	9/0/6

Table 19. The SSIM comparison results at high threshold level

	16 thresholds			20 thresholds			24 thresholds		
	Mean	Rank	+/-/=	Mean	Rank	+/-/=	Mean	Rank	+/-/=
AO	2.13	1	~	1.27	1	~	1.80	1	~
RIME	3.47	3	2/0/13	4.33	5	6/0/9	4.87	6	5/0/10
DE	4.00	4	6/0/9	4.47	6	11/0/4	4.80	5	10/0/5
HHO	7.73	8	12/0/3	7.53	8	14/0/1	7.87	8	14/0/1
WOA	4.67	5	4/0/11	4.13	4	3/0/12	3.47	3	3/0/12
PSO	2.27	2	1/1/13	3.67	2	4/0/11	4.33	4	7/0/8
SCA	8.93	9	15/0/0	9.00	9	15/0/0	8.93	9	15/0/0
SSA	5.07	6	10/0/5	3.87	3	6/0/9	2.67	2	4/0/11
CS	6.73	7	10/0/5	6.73	7	11/0/4	6.27	7	10/0/5

Furthermore, Figure 18 shows the original image, grayscale image, and non-local mean image of BC03, where the edges of the cellular tissue are more blurred and challenging for fine segmentation. At 24 threshold levels, each algorithm calculates the optimal threshold set using a 2D histogram composed of grayscale and non-local mean images. After segmenting pixels of the original image, different tissues in the image are precisely delineated with vibrant colors. Upon close observation, the results segmented by the AO preserve more local features of the image and exhibit higher contrast. The analysis of the results from the low threshold image segmentation experiments shows that the proposed AO performs exceptionally well in the segmentation of 24 threshold images in this model, outperforming other algorithms.

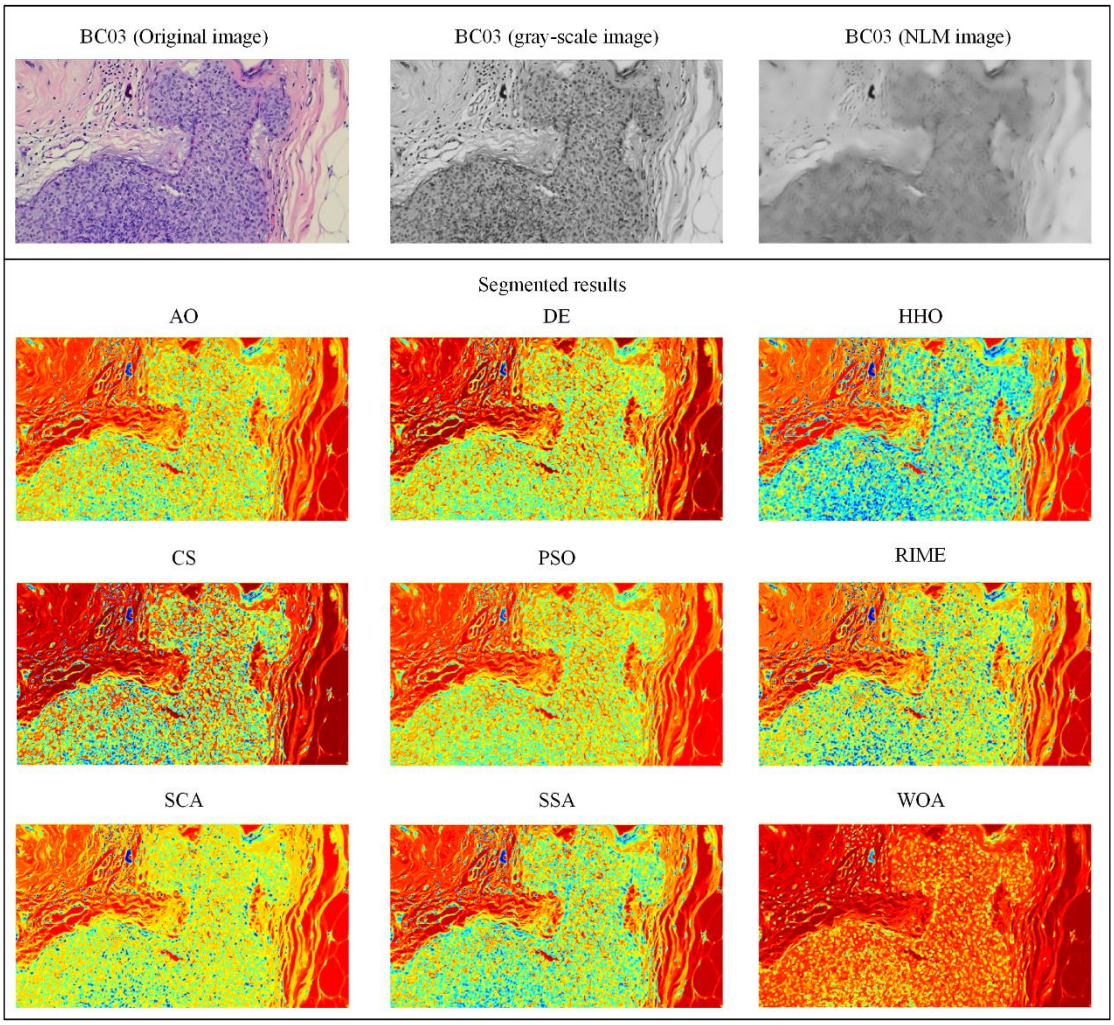


Figure 18. Comparison of segmentation results for BC03 at 24 threshold levels

7. Conclusion and future work

This paper introduces an efficient metaheuristic algorithm, Artemisinin Optimization (AO), aiming to address contemporary complex optimization problems. The inspiration behind AO's design stems from the process of artemisinin medicine treatment for malaria, which involves eradicating the malaria parasites parasitizing the human body. AO is crafted based on three treatment stages, each featuring distinct search strategies. In the design of AO, the intricate human body is conceptualized as the solution space, the malaria parasites residing in the human body are considered potential solutions, and the artemisinin drug serves as search agents. Inspired by the early-stage treatment process involving the administration of higher medicine doses to control the disease, a comprehensive elimination phase strategy is proposed. In this strategy, the algorithm gains global exploration capabilities, aiding in the rapid exploration of the entire space; Drawing inspiration from the later-stage treatment process where the disease is gradually controlled and the dosage is reduced, the AO introduces a local clearance phase strategy, encouraging the algorithm to exploit potential optimal solutions within a local scope. Considering unforeseen circumstances that may arise during treatment, such as disease relapse triggered by the awakening of dormant malaria parasites, a post-consolidation phase strategy is proposed, equipping the search agent with the ability to escape from local optima.

In AO, the harmony between the core strategies of metaheuristic algorithms, exploration, and exploitation is achieved by adjusting their weights appropriately, fostering their collaboration for optimal optimization outcomes. The effectiveness of AO was tested through benchmark function experiments. AO was compared with eight widely acknowledged algorithms and eight high-performance improved algorithms in the IEEE CEC 2014 and IEEE CEC 2022 benchmark function sets. The results were comprehensively analyzed and discussed, providing evidence of the exceptional performance of the proposed algorithm.

Simultaneously, this study integrates AO into a classical application scenario of MAs: Multi-Threshold Image Segmentation (MTIS), aiming to assess its excellent capabilities in handling practical applications. AO is combined with MTIS techniques to compute the optimal threshold set. The performance of AO is experimentally evaluated using real data, conducting a comprehensive comparison with six threshold levels and eight algorithms that exhibit outstanding performance across 15 medical images. The experimental validation confirms its robust capabilities, particularly in real-world applications, especially in the medical field. These findings affirm AO as a powerful optimization tool capable of addressing various challenges in the real world.

In future research, the AO algorithm exhibits considerable potential in several directions. Firstly, it can be extended to tackle large-scale problems in different domains, including feature selection in medical data [108], multi-objective optimization [109], and parameter tuning [110]. Additionally, exploring hybrids with other algorithms presents an exciting avenue for future research.

8. Acknowledgment

This work was supported in part by the Natural Science Foundation of Jilin Province (YDZJ202201ZYTS567), Natural Science Foundation of Zhejiang Province (LZ22F020005), National Natural Science Foundation of China (62301367, 62076185). We acknowledge the comments of the reviewers.

Declaration of AI and AI-assisted technologies in the writing process

During the writing of this work the author(s) used ChatGPT as a grammar checker in order to correct and proofread the English grammar of the paper. After using this tool/service, the author(s) reviewed and edited the content as needed and take(s) full responsibility for the content of the publication.

9. Appendix A

Table A.1.IEEE CEC 2014 function list

Class	Function	Describe	Range	$Fi * = Fi(x *)$
Unimodal Functions	F1	Rotated High Conditioned Elliptic Function	$[-100,100]$	100
	F2	Rotated Bent Cigar Function	$[-100,100]$	200
	F3	Rotated Discus Function	$[-100,100]$	300
Simple Multimodal Functions	F4	Shifted and Rotated Rosenbrock's Function	$[-100,100]$	400
	F5	Shifted and Rotated Ackley's Function	$[-100,100]$	500
	F6	Shifted and Rotated Weierstrass Function	$[-100,100]$	600
	F7	Shifted and Rotated Griewank's Function	$[-100,100]$	700
	F8	Shifted Rastrigin's Function	$[-100,100]$	800
	F9	Shifted and Rotated Rastrigin's Function	$[-100,100]$	900
	F10	Shifted Schwefel's Function	$[-100,100]$	1000
	F11	Shifted and Rotated Schwefel's Function	$[-100,100]$	1100
	F12	Shifted and Rotated Katsuura Function	$[-100,100]$	1200
	F13	Shifted and Rotated HappyCat Function	$[-100,100]$	1300
	F14	Shifted and Rotated HGBat Function	$[-100,100]$	1400
	F15	Shifted and Rotated Expanded Griewank's plus Rosenbrock's Function	$[-100,100]$	1500
	F16	Shifted and Rotated Expanded Schaffer's F6 Function	$[-100,100]$	1600
Hybrid Functions	F17	Hybrid Function 1 (N=3)	$[-100,100]$	1700
	F18	Hybrid Function 2 (N=3)	$[-100,100]$	1800
	F19	Hybrid Function 3 (N=4)	$[-100,100]$	1900
	F20	Hybrid Function 4 (N=4)	$[-100,100]$	2000
	F21	Hybrid Function 5 (N=5)	$[-100,100]$	2100
	F22	Hybrid Function 6 (N=5)	$[-100,100]$	2200
Composition Functions	F23	Composition Function 1 (N=5)	$[-100,100]$	2300
	F24	Composition Function 2 (N=3)	$[-100,100]$	2400
	F25	Composition Function 3 (N=3)	$[-100,100]$	2500
	F26	Composition Function 4 (N=5)	$[-100,100]$	2600
	F27	Composition Function 5 (N=5)	$[-100,100]$	2700
	F28	Composition Function 6 (N=5)	$[-100,100]$	2800
	F29	Composition Function 7 (N=3)	$[-100,100]$	2900
	F30	Composition Function 8 (*N*=3)	$[-100,100]$	3000

Table A.2. IEEE CEC 2022 functions

Class	Functions	Describe	f_i
Unimodal	F1	Shifted and full Rotated Zakharov Function	300

Functions			
Multimodal Functions	F2	Shifted and full Rotated Rosenbrock's Function	400
	F3	Shifted and full Rotated Expanded Schaffer's f6 Function	600
	F4	Shifted and full Rotated Non-Continuous Rastrigin's Function	800
	F5	Shifted and full Rotated Levy Function	900
Hybrid Functions	F6	Hybrid Function 1 (N = 3)	1800
	F7	Hybrid Function 2 (N = 6)	2000
	F8	Hybrid Function 3 (N = 5)	2200
Composition Functions	F9	Composition Function 1 (N = 5)	2300
	F10	Composition Function 2 (N = 4)	2400
	F11	Composition Function 3 (N = 5)	2600
	F12	Composition Function 4 (N = 6)	2700

Table A.3. Threshold values and fitness at 2 threshold levels.

Image	Method	AO	RIME	DE	HHO	WOA	PSO	SCA	SSA	CS
BC01	Thresh1	119	119	119	151	122	119	105	119	119
	Thresh2	209	209	209	209	209	209	211	209	209
	Fitness	27.5208	27.5208	27.5208	27.2687	27.4956	27.5208	27.2400	27.5190	27.5208
BC02	Thresh1	114	114	114	114	106	114	105	107	117
	Thresh2	206	206	206	206	176	206	206	206	206
	Fitness	27.3750	27.3750	27.3750	27.3735	27.2983	27.3750	27.2858	27.3541	27.3720
BC03	Thresh1	128	128	128	159	167	144	116	102	113
	Thresh2	228	228	228	228	228	228	229	228	227
	Fitness	26.7235	26.7235	26.7235	26.1169	26.0992	26.1795	25.9917	26.5928	26.5382
BC04	Thresh1	130	130	130	131	129	130	132	130	130
	Thresh2	190	190	190	190	181	190	181	190	190
	Fitness	28.4505	28.4505	28.4505	28.4174	28.4096	28.4505	28.4009	28.4492	28.4489
BC05	Thresh1	103	103	103	105	82	124	142	124	101
	Thresh2	174	174	174	174	174	174	185	174	174
	Fitness	26.0579	26.0579	26.0579	26.0572	25.9562	25.8838	25.5833	25.8813	26.0547
BC06	Thresh1	82	82	82	75	82	80	73	82	82
	Thresh2	150	150	150	152	150	174	146	150	151
	Fitness	25.3453	25.3453	25.3453	25.3366	25.3453	24.3765	25.3224	25.3453	25.3436
BC07	Thresh1	108	108	108	108	108	113	107	108	107
	Thresh2	153	153	153	153	153	199	153	153	153
	Fitness	25.1519	25.1519	25.1519	25.1519	25.1519	24.2989	25.1091	25.1519	25.1515
BC08	Thresh1	129	129	129	107	107	128	100	107	129
	Thresh2	197	197	197	150	150	197	148	150	197
	Fitness	25.2992	25.2992	25.2992	25.2374	25.2374	25.2989	25.2175	25.2374	25.2992
BC09	Thresh1	117	117	117	91	109	116	118	115	117
	Thresh2	197	197	197	197	197	197	215	186	197
	Fitness	26.3062	26.3062	26.3062	26.1055	26.2228	26.3056	25.9218	26.1804	26.3062
BC10	Thresh1	80	80	80	80	80	105	79	80	80
	Thresh2	144	144	144	146	144	195	144	144	143
	Fitness	25.6556	25.6556	25.6556	25.6530	25.6556	25.5480	25.6206	25.6556	25.6549
BC11	Thresh1	112	112	112	111	130	130	96	83	122
	Thresh2	190	190	190	190	190	190	162	188	190

	Fitness	26.7265	26.7265	26.7265	26.7256	26.1493	26.1485	26.3633	26.5861	26.6636
BC12	Thresh1	98	98	98	98	98	98	90	98	98
	Thresh2	148	148	148	152	148	203	146	148	148
	Fitness	25.4553	25.4553	25.4553	25.4327	25.4553	24.3847	25.4224	25.4553	25.4553
BC13	Thresh1	74	74	74	74	74	92	74	74	74
	Thresh2	132	132	132	132	132	175	129	132	132
	Fitness	25.4532	25.4532	25.4532	25.4532	25.4532	24.1337	25.4461	25.4532	25.4532
BC14	Thresh1	97	97	97	97	78	111	69	85	86
	Thresh2	153	153	153	153	153	153	152	153	153
	Fitness	37.4926	37.4926	37.4926	37.4926	37.4013	36.7233	37.2581	37.4551	37.4608
BC15	Thresh1	112	112	112	125	129	135	111	133	136
	Thresh2	185	185	185	185	185	185	179	185	185
	Fitness	28.1936	28.1936	28.1936	28.1219	28.1376	28.1525	27.7541	28.1516	28.1504

Table A.4. Threshold values and fitness at 4 threshold levels.

Image	Method	AO	RIME	DE	HHO	WOA	PSO	SCA	SSA	CS
BC01	Thresh1	42	42	75	51	50	42	23	68	80
	Thresh2	120	120	132	114	124	118	80	121	128
	Thresh3	170	170	179	151	158	167	155	156	158
	Thresh4	202	202	205	190	185	202	206	197	202
	Fitness	40.7552	40.7552	40.7454	40.4548	39.8013	40.7237	38.8494	40.5000	40.5375
BC02	Thresh1	65	64	64	81	65	67	27	41	69
	Thresh2	114	113	114	118	116	106	111	83	98
	Thresh3	161	161	161	174	174	145	144	143	145
	Thresh4	206	206	206	206	206	206	191	206	206
	Fitness	40.7455	40.7413	40.7449	40.0005	39.7951	40.6789	38.7114	40.1980	40.4556
BC03	Thresh1	99	99	99	88	88	94	108	65	110
	Thresh2	140	140	140	132	140	137	158	148	135
	Thresh3	188	188	188	182	182	171	175	170	188
	Thresh4	228	228	228	212	228	228	206	228	230
	Fitness	39.8598	39.8598	39.8596	38.8201	39.6133	39.8246	37.6524	39.2841	39.3636
BC04	Thresh1	77	77	77	66	73	73	75	44	70
	Thresh2	127	126	127	114	123	123	104	109	121
	Thresh3	168	166	168	146	154	165	154	143	165
	Thresh4	200	200	200	176	190	199	192	200	202
	Fitness	41.3732	41.3699	41.3732	40.8131	40.9895	41.3584	39.1890	40.9695	41.2291
BC05	Thresh1	76	76	76	74	86	72	26	83	76
	Thresh2	124	124	124	111	130	119	88	117	120
	Thresh3	170	170	170	138	187	172	143	148	174
	Thresh4	209	209	209	188	207	209	172	188	209
	Fitness	39.1483	39.1483	39.1483	38.5763	38.4936	39.1031	37.1289	38.6695	39.0823
BC06	Thresh1	75	75	69	78	70	72	50	68	67
	Thresh2	121	127	119	121	116	122	105	116	115
	Thresh3	154	167	153	165	149	178	159	151	152
	Thresh4	182	197	181	182	178	207	184	181	181
	Fitness	37.9646	37.9131	37.9385	37.6723	37.8853	37.4938	36.9299	37.8697	37.8034
BC07	Thresh1	98	99	97	82	87	91	96	8	86
	Thresh2	141	142	140	130	133	132	137	15	128
	Thresh3	170	171	168	157	169	168	148	66	150

	Thresh4	199	200	198	184	199	198	189	169	190
	Fitness	37.4748	37.4737	37.4731	37.3450	37.1979	37.2083	36.2452	37.6309	37.2702
BC08	Thresh1	96	96	98	96	97	95	74	86	93
	Thresh2	142	142	141	134	136	138	127	132	136
	Thresh3	183	183	182	173	174	173	157	167	170
	Thresh4	234	234	234	209	203	205	187	210	197
	Fitness	38.4574	38.4574	38.4361	37.8709	38.3076	38.3623	37.0719	38.2440	38.2614
BC09	Thresh1	78	79	78	78	89	76	36	82	74
	Thresh2	122	125	125	125	130	122	120	132	127
	Thresh3	159	162	163	169	163	164	154	171	159
	Thresh4	197	201	201	217	197	201	188	201	201
	Fitness	39.0450	39.0413	39.0429	38.8270	38.9932	39.0159	37.6022	38.9780	38.9294
BC10	Thresh1	80	80	80	63	64	79	6	66	73
	Thresh2	133	133	133	127	136	131	15	126	125
	Thresh3	179	179	181	187	179	177	48	169	159
	Thresh4	226	226	226	208	215	217	104	217	213
	Fitness	38.8088	38.8088	38.8072	37.9930	38.5629	38.7785	37.9479	38.5626	38.6105
BC11	Thresh1	69	68	69	74	54	67	7	78	73
	Thresh2	125	125	117	134	121	112	98	122	121
	Thresh3	161	162	145	183	171	141	135	151	165
	Thresh4	190	190	190	216	190	173	178	201	190
	Fitness	40.1107	40.0929	40.0408	39.0902	39.6057	36.7226	37.0204	39.8691	39.7641
BC12	Thresh1	78	78	78	77	78	78	111	78	81
	Thresh2	130	131	130	127	128	129	148	128	135
	Thresh3	165	165	165	171	159	166	184	164	165
	Thresh4	197	197	197	202	195	197	201	197	198
	Fitness	38.0460	38.0453	38.0460	37.9784	38.0034	38.0339	37.3107	38.0337	37.9394
BC13	Thresh1	68	68	68	70	66	72	88	63	67
	Thresh2	111	111	111	122	109	119	125	107	119
	Thresh3	146	145	146	157	145	151	152	143	150
	Thresh4	177	177	177	192	177	187	199	176	189
	Fitness	38.0221	38.0220	38.0221	37.9283	38.0189	37.9879	36.9386	38.0076	37.9460
BC14	Thresh1	67	68	70	64	49	68	22	72	53
	Thresh2	107	107	108	108	104	107	117	113	105
	Thresh3	139	139	140	138	133	136	154	145	138
	Thresh4	168	168	168	168	168	168	168	168	168
	Fitness	50.2365	50.2358	50.2358	50.0188	50.0054	50.2222	47.2756	49.8117	50.0064
BC15	Thresh1	42	42	75	51	50	42	23	68	80
	Thresh2	120	120	132	114	124	118	80	121	128
	Thresh3	170	170	179	151	158	167	155	156	158
	Thresh4	202	202	205	190	185	202	206	197	202
	Fitness	40.7552	40.7552	40.7454	40.4548	39.8013	40.7237	38.8494	40.5000	40.5375

Table A.5. Threshold values and fitness at 6 threshold levels.

Image	Method	AO	RIME	DE	HHO	WOA	PSO	SCA	SSA	CS
BC01	Thresh1	53	47	54	83	50	42	40	52	47
	Thresh2	92	87	92	99	66	87	87	75	80
	Thresh3	119	116	119	117	101	117	91	113	122
	Thresh4	148	144	149	148	149	144	160	147	140
	Thresh5	179	176	180	166	180	172	177	182	177

	Thresh6	209	209	209	220	213	209	217	209	210
	Fitness	52.2315	52.2038	52.2179	50.7375	51.2683	52.1397	47.3415	51.6545	51.5506
BC02	Thresh1	42	48	42	49	27	44	24	44	45
	Thresh2	79	80	77	95	63	85	57	81	83
	Thresh3	108	108	109	114	95	113	99	107	114
	Thresh4	138	139	139	137	120	141	151	130	154
	Thresh5	169	169	170	161	176	175	172	175	178
	Thresh6	206	206	206	206	206	206	216	206	207
	Fitness	52.1361	52.1128	52.1283	51.1448	51.0952	52.0129	48.3288	51.9445	51.3995
BC03	Thresh1	48	54	41	31	26	34	21	88	83
	Thresh2	97	95	91	63	86	91	97	115	116
	Thresh3	134	134	137	109	140	140	105	135	146
	Thresh4	166	164	167	132	167	171	122	158	171
	Thresh5	201	197	196	181	211	204	175	214	203
	Thresh6	230	228	230	214	230	230	211	230	230
	Fitness	50.7991	50.7339	50.4350	47.9028	49.6005	50.4454	47.1519	49.6676	49.8509
BC04	Thresh1	44	68	62	29	60	44	28	71	42
	Thresh2	94	105	107	67	98	93	87	116	78
	Thresh3	122	129	131	121	126	121	115	136	121
	Thresh4	149	153	156	149	152	146	141	155	145
	Thresh5	175	177	179	175	173	175	182	179	164
	Thresh6	200	203	203	197	199	201	239	205	199
	Fitness	51.9260	51.8370	51.7811	50.5132	51.0523	51.8024	46.0089	51.0901	51.1312
BC05	Thresh1	62	31	31	19	27	68	25	53	67
	Thresh2	100	98	95	90	105	106	74	99	108
	Thresh3	131	129	128	116	132	139	132	129	128
	Thresh4	163	160	162	144	165	168	153	154	170
	Thresh5	187	185	186	181	187	189	190	182	187
	Thresh6	209	209	209	200	203	209	230	209	217
	Fitness	49.9159	49.9229	49.9352	48.4125	49.4862	49.7576	46.3382	49.3594	49.3466
BC06	Thresh1	50	50	50	50	30	49	48	46	65
	Thresh2	99	97	96	95	103	94	84	106	104
	Thresh3	128	130	128	139	138	125	114	129	129
	Thresh4	154	155	158	174	160	157	142	156	153
	Thresh5	177	177	178	187	178	184	177	180	178
	Thresh6	204	206	207	207	214	211	184	202	201
	Fitness	48.8823	48.8097	48.8444	48.4344	48.1397	48.2349	45.3822	48.6753	48.3276
BC07	Thresh1	50	8	52	20	91	75	3	79	20
	Thresh2	99	15	99	24	126	128	4	125	24
	Thresh3	130	41	134	45	151	157	24	153	44
	Thresh4	159	73	163	97	174	180	47	181	55
	Thresh5	185	120	184	138	191	203	76	204	109
	Thresh6	209	174	213	164	208	221	97	224	142
	Fitness	49.7549	48.1997	48.1118	49.0743	47.8565	48.1221	45.8283	48.0234	48.5875
BC08	Thresh1	48	51	47	85	74	63	39	27	19
	Thresh2	96	101	99	116	111	88	100	82	24
	Thresh3	132	133	129	139	142	123	113	134	51
	Thresh4	159	166	155	161	174	154	153	167	75
	Thresh5	191	194	185	183	200	184	176	195	108

	Thresh6	234	234	234	210	234	234	216	234	168
	Fitness	49.5856	49.5326	49.5051	48.6200	48.7308	49.3563	45.4263	49.1260	49.3876
BC09	Thresh1	43	46	42	42	41	40	88	55	69
	Thresh2	86	87	88	78	77	89	126	106	91
	Thresh3	119	123	117	110	111	119	151	141	126
	Thresh4	147	151	148	137	140	148	175	166	154
	Thresh5	180	181	182	180	176	183	235	194	189
	Thresh6	219	219	217	218	201	215	253	228	217
	Fitness	49.5370	49.5305	49.4668	48.9566	48.7719	49.3897	46.0659	48.7457	48.9524
BC10	Thresh1	7	40	45	11	5	45	28	38	47
	Thresh2	15	78	78	20	15	78	63	79	79
	Thresh3	43	122	113	39	42	117	105	129	106
	Thresh4	72	150	147	58	71	152	119	162	144
	Thresh5	108	180	187	77	107	186	154	192	182
	Thresh6	153	217	217	104	152	217	173	226	217
	Fitness	49.9042	49.6752	49.5779	48.7686	49.4305	49.7079	46.0457	49.6956	49.2163
BC11	Thresh1	65	64	59	50	70	50	45	58	69
	Thresh2	100	100	102	71	98	96	72	90	102
	Thresh3	125	124	126	125	139	122	82	125	128
	Thresh4	146	147	146	153	162	143	110	147	146
	Thresh5	169	172	170	176	175	170	125	171	178
	Thresh6	201	201	201	216	201	201	179	196	205
	Fitness	51.055	51.006	50.983	49.674	50.448	50.881	45.207	50.273	50.146
BC12	Thresh1	68	68	69	70	66	71	41	55	77
	Thresh2	111	113	111	108	112	113	66	110	112
	Thresh3	139	140	139	137	138	140	135	136	144
	Thresh4	164	164	164	161	164	163	175	160	167
	Thresh5	188	188	188	187	188	188	189	186	198
	Thresh6	210	208	208	207	208	209	214	208	217
	Fitness	48.7168	48.7089	48.6786	48.4912	48.7032	48.6962	47.5179	48.5657	48.4052
BC13	Thresh1	52	56	52	70	55	55	28	58	53
	Thresh2	91	91	91	114	93	94	57	99	94
	Thresh3	120	120	120	136	121	122	110	130	120
	Thresh4	146	147	146	156	148	147	155	150	152
	Thresh5	173	174	173	179	173	172	161	173	173
	Thresh6	197	200	197	205	197	198	190	194	208
	Fitness	49.0675	49.0532	49.0666	48.5218	49.0511	47.0537	45.4969	48.8517	48.8580
BC14	Thresh1	34	33	34	47	64	41	15	48	43
	Thresh2	68	66	65	73	88	68	54	102	81
	Thresh3	97	96	96	93	109	101	90	118	107
	Thresh4	122	123	122	113	128	130	98	136	126
	Thresh5	147	151	145	151	151	153	144	146	150
	Thresh6	168	168	168	168	168	168	151	168	169
	Fitness	60.9886	60.9270	60.9553	59.8276	60.4923	60.6613	56.0493	58.9246	59.7111
BC15	Thresh1	42	42	42	31	25	38	40	45	38
	Thresh2	97	99	95	103	107	99	88	79	103
	Thresh3	132	128	128	130	142	131	140	119	137
	Thresh4	160	155	154	156	162	161	145	153	156
	Thresh5	187	188	189	182	180	188	175	175	194

Thresh6	212	212	212	212	205	205	219	212	212
Fitness	51.2677	51.2062	51.0513	50.5180	49.8412	51.1109	48.4555	50.5764	50.6744

Table A.6 FSIM evaluation results at low threshold

		2 thresholds		4 thresholds		6 thresholds	
Image	Method	AVG	STD	AVG	STD	AVG	STD
BC01	AO	0.7308	0.0370	0.8883	0.0221	0.9465	0.0091
	RIME	0.6860	0.0001	0.8828	0.0143	0.9448	0.0056
	DE	0.7033	0.0296	0.8862	0.0090	0.9465	0.0039
	HHO	0.6815	0.0789	0.8323	0.0529	0.8737	0.0518
	WOA	0.7001	0.0564	0.8478	0.0398	0.9038	0.0232
	PSO	0.7085	0.0368	0.8672	0.0133	0.9385	0.0096
	SCA	0.6453	0.1200	0.8103	0.0698	0.8602	0.0471
	SSA	0.7139	0.0527	0.8447	0.0464	0.9165	0.0233
	CS	0.6738	0.0323	0.8672	0.0356	0.9070	0.0339
BC02	AO	0.7568	0.0441	0.9134	0.0174	0.9524	0.0081
	RIME	0.7370	0.0506	0.8941	0.0266	0.9447	0.0078
	DE	0.7279	0.0424	0.8835	0.0181	0.9438	0.0076
	HHO	0.6877	0.1159	0.8433	0.0520	0.9072	0.0280
	WOA	0.7365	0.0638	0.8428	0.0737	0.8930	0.0446
	PSO	0.7751	0.0320	0.8854	0.0196	0.9374	0.0059
	SCA	0.6579	0.1338	0.8400	0.0568	0.8506	0.0566
	SSA	0.7350	0.0682	0.8476	0.0521	0.9125	0.0324
	CS	0.7281	0.0460	0.8643	0.0298	0.9192	0.0176
BC03	AO	0.6687	0.0673	0.8373	0.0297	0.9037	0.0203
	RIME	0.6317	0.0637	0.8341	0.0180	0.8908	0.0242
	DE	0.6343	0.0569	0.8282	0.0093	0.8905	0.0237
	HHO	0.5839	0.1260	0.7732	0.0683	0.8227	0.0744
	WOA	0.5649	0.0991	0.7876	0.0643	0.8245	0.0660
	PSO	0.6009	0.0607	0.8115	0.0280	0.8753	0.0458
	SCA	0.6141	0.1308	0.7447	0.0913	0.7783	0.0992
	SSA	0.5923	0.1168	0.7822	0.0562	0.8615	0.0571
	CS	0.5636	0.0472	0.7834	0.0533	0.8414	0.0531
BC04	AO	0.7121	0.0358	0.8800	0.0095	0.9291	0.0126
	RIME	0.6995	0.0238	0.8677	0.0171	0.9210	0.0171
	DE	0.7045	0.0318	0.8686	0.0092	0.9249	0.0119
	HHO	0.6643	0.0964	0.7922	0.0843	0.8643	0.0605
	WOA	0.6915	0.0588	0.8073	0.0680	0.8926	0.0355
	PSO	0.6972	0.0126	0.8540	0.0187	0.9267	0.0140
	SCA	0.6821	0.0928	0.7755	0.0861	0.8273	0.0786
	SSA	0.6958	0.0377	0.8377	0.0493	0.8952	0.0236
	CS	0.7024	0.0177	0.8376	0.0376	0.8792	0.0449
BC05	AO	0.7537	0.0240	0.8714	0.0211	0.9350	0.0072
	RIME	0.7615	0.0048	0.8776	0.0168	0.9338	0.0121
	DE	0.7615	0.0050	0.8829	0.0074	0.9364	0.0072
	HHO	0.7004	0.0675	0.8440	0.0358	0.8785	0.0428
	WOA	0.7179	0.0570	0.8373	0.0429	0.8902	0.0424
	PSO	0.7419	0.0379	0.8777	0.0147	0.9255	0.0124
	SCA	0.7129	0.0716	0.7999	0.0474	0.8584	0.0373
	SSA	0.7491	0.0373	0.8431	0.0520	0.9064	0.0311

	CS	0.7553	0.0161	0.8607	0.0333	0.9052	0.0195
BC06	AO	0.7761	0.0058	0.8924	0.0087	0.9404	0.0043
	RIME	0.7744	0.0061	0.8891	0.0074	0.9334	0.0108
	DE	0.7761	0.0047	0.8926	0.0041	0.9385	0.0054
	HHO	0.7336	0.0447	0.8566	0.0290	0.8906	0.0352
	WOA	0.7558	0.0307	0.8528	0.0443	0.9010	0.0280
	PSO	0.7239	0.0344	0.8634	0.0172	0.9234	0.0123
	SCA	0.7558	0.0133	0.7932	0.0973	0.8306	0.0936
	SSA	0.7633	0.0132	0.8602	0.0270	0.9050	0.0289
	CS	0.7685	0.0124	0.8798	0.0194	0.8979	0.0535
BC07	AO	0.7207	0.0010	0.8723	0.0056	0.9213	0.0129
	RIME	0.7210	0.0002	0.8615	0.0222	0.9103	0.0251
	DE	0.7211	0.0000	0.8707	0.0057	0.9115	0.0152
	HHO	0.6599	0.0797	0.8129	0.0476	0.8413	0.0711
	WOA	0.6636	0.0731	0.8332	0.0480	0.8657	0.0420
	PSO	0.6657	0.0622	0.8546	0.0272	0.9172	0.0065
	SCA	0.7043	0.0274	0.7675	0.1009	0.7889	0.1132
	SSA	0.6960	0.0419	0.8346	0.0622	0.8966	0.0232
	CS	0.7201	0.0076	0.8491	0.0247	0.8555	0.0870
BC08	AO	0.7274	0.0087	0.8945	0.0452	0.9441	0.0271
	RIME	0.7291	0.0124	0.9033	0.0095	0.9423	0.0138
	DE	0.7284	0.0133	0.9036	0.0130	0.9374	0.0176
	HHO	0.7145	0.0882	0.8448	0.0420	0.9044	0.0410
	WOA	0.7327	0.0218	0.8524	0.0497	0.8972	0.0604
	PSO	0.7530	0.0319	0.9032	0.0108	0.9350	0.0341
	SCA	0.7254	0.0300	0.7980	0.1040	0.8446	0.0707
	SSA	0.7362	0.0213	0.8715	0.0530	0.9172	0.0230
	CS	0.7263	0.0123	0.8849	0.0251	0.9166	0.0326
BC09	AO	0.6560	0.0587	0.8723	0.0238	0.9184	0.0093
	RIME	0.6449	0.0606	0.8579	0.0286	0.9122	0.0211
	DE	0.6206	0.0607	0.8534	0.0239	0.9103	0.0180
	HHO	0.6347	0.0925	0.7775	0.0675	0.8591	0.0684
	WOA	0.6231	0.0808	0.8068	0.0668	0.8760	0.0546
	PSO	0.6043	0.0498	0.8322	0.0208	0.9046	0.0195
	SCA	0.6323	0.0941	0.7565	0.0630	0.7701	0.0734
	SSA	0.6393	0.0995	0.8021	0.0463	0.8618	0.0540
	CS	0.5751	0.0775	0.8053	0.0456	0.8797	0.0294
BC10	AO	0.6661	0.0203	0.8700	0.0427	0.9051	0.0332
	RIME	0.6567	0.0491	0.8581	0.0400	0.9084	0.0183
	DE	0.6552	0.0092	0.8289	0.0413	0.8931	0.0151
	HHO	0.5980	0.0886	0.7543	0.1101	0.8202	0.1295
	WOA	0.6393	0.0712	0.7945	0.0794	0.8542	0.0598
	PSO	0.5773	0.0654	0.7994	0.0710	0.8963	0.0209
	SCA	0.5934	0.7643	0.7225	0.1245	0.7850	0.0715
	SSA	0.6313	0.5346	0.7905	0.0553	0.8756	0.0386
	CS	0.6536	0.0167	0.7871	0.0721	0.8837	0.0387
BC11	AO	0.7361	0.0476	0.8775	0.0142	0.9232	0.0143
	RIME	0.7459	0.0275	0.8763	0.0149	0.9270	0.0126
	DE	0.7558	0.0131	0.8779	0.0142	0.9199	0.0142

	HHO	0.6914	0.0659	0.8152	0.0793	0.8951	0.0404
	WOA	0.6996	0.0583	0.8469	0.0168	0.8853	0.0578
	PSO	0.7224	0.0431	0.8506	0.0054	0.9195	0.0187
	SCA	0.6275	0.1027	0.7776	0.0691	0.8297	0.0523
	SSA	0.7169	0.0491	0.8365	0.0575	0.8964	0.0343
	CS	0.7267	0.0422	0.8608	0.0258	0.9180	0.0178
BC12	AO	0.7084	0.0068	0.8913	0.0092	0.9389	0.0045
	RIME	0.7009	0.0237	0.8912	0.0022	0.9396	0.0042
	DE	0.7130	0.0000	0.8936	0.0011	0.9385	0.0053
	HHO	0.6869	0.0604	0.8614	0.0331	0.9161	0.0203
	WOA	0.6990	0.0506	0.8681	0.0296	0.9180	0.0257
	PSO	0.6814	0.0507	0.8951	0.0044	0.9367	0.0038
	SCA	0.6994	0.0268	0.8065	0.0578	0.8367	0.0624
	SSA	0.6897	0.0484	0.8892	0.0096	0.9302	0.0147
	CS	0.7089	0.0136	0.8744	0.0490	0.9251	0.0181
BC13	AO	0.7122	0.0090	0.8812	0.0040	0.9369	0.0030
	RIME	0.7128	0.0082	0.8829	0.0052	0.9369	0.0083
	DE	0.7102	0.0029	0.8806	0.0038	0.9392	0.0023
	HHO	0.7030	0.0731	0.8601	0.0228	0.9039	0.0199
	WOA	0.7121	0.0174	0.8727	0.0156	0.9239	0.0167
	PSO	0.7136	0.0497	0.8728	0.0075	0.9301	0.0122
	SCA	0.7000	0.0325	0.7741	0.0807	0.8106	0.1225
	SSA	0.7064	0.0242	0.8744	0.0125	0.9264	0.0168
	CS	0.7108	0.0128	0.8783	0.0118	0.9239	0.0157
BC14	AO	0.7081	0.0111	0.7764	0.0341	0.8190	0.0345
	RIME	0.6997	0.0050	0.7756	0.0319	0.8005	0.0238
	DE	0.7004	0.0033	0.8060	0.0171	0.8106	0.0112
	HHO	0.6456	0.0829	0.7316	0.1031	0.8074	0.0531
	WOA	0.6596	0.0913	0.7371	0.0816	0.7994	0.0303
	PSO	0.6943	0.0088	0.7826	0.0215	0.8333	0.0289
	SCA	0.6813	0.1053	0.6048	0.1582	0.7156	0.1290
	SSA	0.6226	0.1037	0.7534	0.0538	0.8241	0.0678
	CS	0.6575	0.0561	0.7650	0.0363	0.8020	0.0364
BC15	AO	0.7056	0.0345	0.8664	0.0228	0.9247	0.0211
	RIME	0.7111	0.0116	0.8724	0.0162	0.9203	0.0251
	DE	0.7122	0.0222	0.8721	0.0270	0.9069	0.0310
	HHO	0.6921	0.0801	0.7923	0.0774	0.8923	0.0531
	WOA	0.6620	0.0736	0.8122	0.0735	0.8794	0.0446
	PSO	0.7116	0.0031	0.8663	0.0221	0.9218	0.0209
	SCA	0.5938	0.1356	0.7427	0.1030	0.8251	0.0829
	SSA	0.6865	0.0697	0.8194	0.0755	0.9016	0.0417
	CS	0.6940	0.0221	0.8416	0.0422	0.8806	0.0413

Table A.7 PSNR evaluation results at low threshold

		2 thresholds		4 thresholds		6 thresholds	
Image	Method	AVG	STD	AVG	STD	AVG	STD
BC01	AO	14.4298	1.4809	19.8827	0.5628	22.9130	0.4972
	RIME	13.0646	0.0021	19.6940	0.5106	22.7632	0.4443
	DE	13.4478	0.9739	19.6409	0.3160	22.9456	0.2724
	HHO	12.7583	2.0591	17.6209	1.8392	20.0550	2.1371

	WOA	13.3573	1.5662	18.3963	1.5344	20.9262	1.3886
	PSO	13.2897	0.4377	19.3380	0.3673	22.5898	0.5931
	SCA	12.3189	2.4586	17.3652	2.1641	19.4766	2.0535
	SSA	13.5769	1.3863	17.9573	1.7689	21.0224	1.1918
	CS	12.8446	0.5248	18.9861	0.9224	21.2389	1.5464
BC02	AO	15.3730	1.5606	20.5369	0.6266	23.1086	0.4062
	RIME	14.0918	1.4217	19.9389	0.7992	22.7834	0.5007
	DE	14.0871	1.4122	19.4070	0.6646	22.9079	0.3791
	HHO	12.9209	2.4898	17.8404	1.9158	21.0338	1.2117
	WOA	14.5603	2.0845	18.0495	2.4716	20.3306	1.9814
	PSO	13.8400	0.2848	19.3875	0.7385	22.5523	0.4864
	SCA	12.9469	2.4395	18.0001	1.8602	18.7874	2.1989
	SSA	14.1159	1.7170	18.2061	1.8977	21.2404	1.6579
	CS	13.3475	0.4426	18.4184	1.4491	21.6519	0.7903
BC03	AO	13.8104	1.9328	18.8532	1.1154	22.0866	0.8871
	RIME	12.8013	1.8023	18.7672	0.6143	21.5914	1.0407
	DE	12.8748	1.6014	18.5174	0.2941	21.6306	0.7835
	HHO	11.5769	3.5694	16.9783	2.0608	19.1233	2.5967
	WOA	10.7799	2.5666	17.4861	1.7467	19.2027	2.1124
	PSO	12.0322	1.6762	18.1969	1.0319	21.1193	1.4223
	SCA	12.8383	2.9767	16.3233	2.4154	17.7176	2.6742
	SSA	11.8276	3.1190	17.3558	1.8459	20.6130	1.9044
	CS	11.0364	1.2309	17.4473	1.5770	19.7682	1.8298
BC04	AO	13.9361	1.3551	20.0958	0.4717	23.1410	0.8055
	RIME	13.3384	0.9560	19.5713	0.7599	22.4973	1.1469
	DE	13.5681	1.2284	19.5326	0.5424	22.8683	0.6439
	HHO	12.8466	2.3489	17.5555	2.8351	20.3224	2.2832
	WOA	13.4299	1.6975	17.6010	2.4757	21.6706	1.8716
	PSO	13.1086	0.2250	19.0900	0.9656	22.7772	0.7891
	SCA	13.8152	2.6886	17.0343	2.3169	18.9965	2.5547
	SSA	13.2744	1.1073	18.6035	1.9194	21.4825	1.2525
	CS	13.1564	0.3299	18.6493	1.4567	21.1282	2.0251
BC05	AO	16.1721	0.9455	20.7040	0.5928	23.4456	0.5056
	RIME	16.2436	0.3235	20.1936	0.6590	23.3030	0.5500
	DE	16.4146	0.2791	20.4114	0.3806	23.4991	0.5681
	HHO	13.9238	2.1781	18.5138	1.6185	20.7455	1.7291
	WOA	14.5748	1.8408	18.6220	1.6993	21.2944	2.0646
	PSO	14.9072	1.9375	19.8753	0.7470	22.7926	0.8940
	SCA	14.9764	1.9566	17.9082	1.7751	20.3016	1.5390
	SSA	15.7078	1.5866	18.5168	1.9729	22.0274	1.3462
	CS	15.8024	0.7203	19.2188	1.2087	21.8236	1.1159
BC06	AO	17.0184	0.3632	21.7094	0.6680	24.3030	0.4363
	RIME	16.9109	0.3813	21.7683	0.7507	23.6717	0.9435
	DE	17.0017	0.3108	21.9045	0.3794	24.1298	0.3920
	HHO	14.9645	1.4916	19.2658	1.2478	21.0919	1.6355
	WOA	16.0440	1.3056	19.7356	2.3713	21.7706	1.5658
	PSO	14.2832	1.4004	19.4815	0.9148	23.0130	0.9081
	SCA	16.3668	0.6476	17.7946	3.2315	19.3399	3.4324
	SSA	16.3755	0.6550	19.8603	1.4267	21.9178	1.6791

	CS	16.7879	0.6396	20.9956	1.2585	21.9577	2.3393
BC07	AO	17.5240	0.0315	20.4829	0.5312	23.0648	0.8380
	RIME	17.5171	0.0091	19.9710	0.8030	22.5715	1.2979
	DE	17.5188	0.0000	20.3844	0.4746	22.5079	1.1124
	HHO	13.8292	2.4122	18.5731	1.7503	20.0723	2.6669
	WOA	14.3617	2.7781	19.2093	1.7489	20.8559	1.8703
	PSO	13.7435	2.1904	19.8888	1.1508	23.0272	0.6506
	SCA	16.8193	0.9226	17.9044	2.4447	18.4463	2.7127
	SSA	16.0566	2.2109	19.7046	1.9156	22.2269	1.0931
	CS	17.4508	0.2761	20.0837	1.1871	20.9959	2.7628
BC08	AO	15.7121	0.6077	19.9249	1.1946	23.2118	0.9198
	RIME	15.5487	0.8135	19.9984	0.3892	23.0541	0.5775
	DE	15.5437	0.7951	19.8883	0.4203	22.8528	0.7428
	HHO	13.4367	2.6517	17.7358	1.7400	20.8830	2.0373
	WOA	14.7874	1.3877	18.2378	1.8374	21.0461	2.0219
	PSO	13.7662	1.4474	20.1901	0.4658	22.8771	1.1608
	SCA	15.4618	0.6822	16.9815	2.7294	18.5535	2.3134
	SSA	15.2994	0.9132	19.1641	1.4626	21.3634	1.3262
	CS	15.5633	0.8158	19.3000	0.8990	21.5278	1.5083
BC09	AO	16.4583	1.6344	21.5545	0.5940	23.3661	0.4766
	RIME	16.1171	1.7292	21.0031	1.0081	23.1860	0.9244
	DE	15.4248	1.7314	21.1955	0.6029	23.2850	0.5906
	HHO	14.3265	2.5918	18.7892	1.9962	21.8614	1.9799
	WOA	14.6133	2.5359	19.2005	2.1915	22.1777	2.0169
	PSO	13.8526	1.0961	20.3398	0.7264	22.9816	0.7897
	SCA	15.3772	2.4779	17.7125	1.6742	18.9344	2.2230
	SSA	15.2798	3.0315	19.1695	1.5100	21.3516	1.6312
	CS	13.8751	1.6505	19.4322	1.4820	22.5102	0.9743
BC10	AO	16.8143	0.8087	21.5120	1.0773	22.9591	0.8835
	RIME	16.3824	1.8850	21.0854	1.1929	22.9802	0.8523
	DE	16.5996	0.2416	20.5662	1.0437	22.6092	0.7587
	HHO	13.1335	3.3611	17.8954	2.5721	20.4412	3.8017
	WOA	14.9994	2.7542	18.7451	2.6464	21.4403	1.9866
	PSO	12.7175	2.0803	19.8793	1.5964	22.7904	1.0137
	SCA	15.8327	2.2826	17.6074	3.4091	19.5742	2.1369
	SSA	15.6789	2.6706	19.2042	1.4540	21.8889	1.2801
	CS	16.5445	0.4208	19.0575	1.7346	22.2825	1.4559
BC11	AO	14.6650	1.3233	20.3124	0.4883	23.0432	0.5367
	RIME	14.6510	1.0075	20.5834	0.3347	23.3802	0.6808
	DE	14.4335	1.0457	20.3821	0.3891	23.5939	0.4166
	HHO	13.9964	2.1690	18.3532	2.6372	21.3177	1.7637
	WOA	14.4055	1.3427	19.1104	1.3285	21.1308	2.4114
	PSO	14.9765	0.8457	20.6385	0.1449	23.5644	0.6017
	SCA	12.8882	2.8104	16.8396	1.9135	18.6901	1.9804
	SSA	14.4954	1.1117	19.1144	2.3365	21.3159	2.0039
	CS	14.2119	1.0188	19.3369	0.8387	22.3277	1.1786
BC12	AO	16.0955	0.3700	20.9623	0.5213	23.4994	0.3916
	RIME	15.6469	1.4706	20.9520	0.1308	23.6239	0.3281
	DE	16.2317	0.0000	21.0778	0.0375	23.5950	0.4644

	HHO	13.9171	1.9179	19.2074	1.2833	22.3011	1.2538
	WOA	14.7801	1.7783	19.5501	1.3237	22.3785	1.7314
	PSO	12.8783	1.8081	20.7048	0.2529	23.8429	0.4556
	SCA	15.7327	0.7348	17.9529	1.9416	18.7038	2.2956
	SSA	14.5092	2.1614	20.5221	0.4522	22.9978	1.0059
	CS	16.0679	0.3464	20.0876	1.3777	22.5218	1.2232
BC13	AO	15.4591	0.3214	21.0463	0.2954	23.5623	0.3732
	RIME	15.4494	0.3127	21.0144	0.2724	23.7797	0.5648
	DE	15.5030	0.0969	21.1021	0.2228	23.8668	0.2491
	HHO	14.1058	1.3798	19.8385	1.4028	22.2412	1.1341
	WOA	15.2234	0.5702	20.3832	0.8709	23.2027	0.9468
	PSO	14.1607	0.9164	20.9390	0.3354	23.7869	0.4816
	SCA	15.2538	0.8358	17.3605	2.2365	18.6701	3.0371
	SSA	15.2339	0.5932	20.2965	0.6998	22.8323	1.2805
	CS	15.5566	0.5114	20.4205	0.6934	22.7885	0.9844
BC14	AO	16.0574	0.2534	19.1048	0.9052	20.7540	0.7781
	RIME	16.2537	0.1144	19.2027	0.8934	20.6468	0.7497
	DE	16.2303	0.0983	19.9310	0.4625	20.9493	0.3503
	HHO	14.8387	1.8253	17.8811	2.1725	19.6659	1.4917
	WOA	15.1800	2.1493	17.7894	2.2282	20.1266	1.0566
	PSO	16.0846	0.1398	19.3118	0.5923	21.3863	0.6444
	SCA	11.2522	2.6964	14.2982	2.9164	16.5136	2.8607
	SSA	14.4385	2.0922	17.9486	1.4019	20.2840	1.9059
	CS	15.1312	1.5425	18.8941	0.7669	20.4101	1.0973
BC15	AO	14.1643	0.7935	19.3284	0.6980	22.9923	1.2185
	RIME	14.1479	0.3276	19.3533	0.8093	23.0058	0.9767
	DE	14.2109	0.6872	19.2051	0.7418	22.6499	1.1842
	HHO	13.8809	2.4190	17.5124	2.3791	21.7991	2.0294
	WOA	13.0414	2.1137	18.2056	2.2499	21.1481	1.6455
	PSO	14.0878	0.0971	19.3689	0.5388	23.1182	0.7508
	SCA	11.4715	3.9746	15.9721	2.7540	19.0266	2.5889
	SSA	13.8045	1.6219	18.2504	2.5425	21.7776	1.9525
	CS	13.9873	0.3343	18.9672	1.3213	21.4056	1.7351

Table A.8 SSIM evaluation results at low threshold

		2 thresholds		4 thresholds		6 thresholds	
Image	Method	AVG	STD	AVG	STD	AVG	STD
BC01	AO	0.6304	0.0694	0.8277	0.0220	0.8982	0.0123
	RIME	0.5589	0.0003	0.8211	0.0172	0.8953	0.0109
	DE	0.5807	0.0464	0.8169	0.0126	0.8991	0.0062
	HHO	0.5421	0.1149	0.7539	0.0756	0.8139	0.0803
	WOA	0.5748	0.0820	0.7806	0.0583	0.8502	0.0418
	PSO	0.5768	0.0313	0.8114	0.0115	0.8918	0.0156
	SCA	0.5068	0.1547	0.7309	0.1003	0.8032	0.0717
	SSA	0.5854	0.0714	0.7588	0.0712	0.8504	0.0338
	CS	0.5406	0.0468	0.7965	0.0377	0.8534	0.0491
BC02	AO	0.6879	0.0834	0.8578	0.0224	0.9041	0.0076
	RIME	0.6265	0.0776	0.8371	0.0289	0.8977	0.0109
	DE	0.6262	0.0688	0.8178	0.0228	0.9003	0.0088
	HHO	0.5535	0.1615	0.7706	0.0706	0.8578	0.0342

	WOA	0.6422	0.1134	0.7637	0.1069	0.8288	0.0655
	PSO	0.6314	0.0228	0.8228	0.0216	0.8928	0.0113
	SCA	0.5322	0.1729	0.7717	0.0874	0.7756	0.0924
	SSA	0.6168	0.1038	0.7730	0.0783	0.8594	0.0530
	CS	0.5933	0.0368	0.7866	0.0522	0.8718	0.0211
BC03	AO	0.5913	0.0825	0.7864	0.0349	0.8545	0.0225
	RIME	0.5481	0.0778	0.7869	0.0203	0.8438	0.0267
	DE	0.5529	0.0663	0.7789	0.0111	0.8416	0.0271
	HHO	0.4516	0.1874	0.7058	0.0907	0.7682	0.0904
	WOA	0.4404	0.1358	0.7287	0.0717	0.7766	0.0795
	PSO	0.4921	0.0715	0.7584	0.0336	0.8252	0.0539
	SCA	0.5089	0.1676	0.6803	0.1037	0.7157	0.1169
	SSA	0.4778	0.1658	0.7221	0.0640	0.8125	0.0654
	CS	0.4537	0.0622	0.7176	0.0638	0.7904	0.0617
BC04	AO	0.5982	0.0390	0.7924	0.0237	0.8852	0.0275
	RIME	0.5940	0.0277	0.7696	0.0276	0.8703	0.0312
	DE	0.5961	0.0340	0.7682	0.0186	0.8767	0.0225
	HHO	0.5388	0.1336	0.7190	0.1149	0.8069	0.0781
	WOA	0.5805	0.0807	0.7208	0.0963	0.8427	0.0500
	PSO	0.5873	0.0149	0.7676	0.0274	0.8802	0.0197
	SCA	0.5689	0.1341	0.6962	0.1083	0.7608	0.0989
	SSA	0.5858	0.0512	0.7627	0.0687	0.8352	0.0392
	CS	0.5911	0.0154	0.7578	0.0523	0.8295	0.0556
BC05	AO	0.6803	0.0347	0.8113	0.0148	0.8767	0.0113
	RIME	0.6767	0.0103	0.8030	0.0190	0.8721	0.0173
	DE	0.6777	0.0154	0.8069	0.0070	0.8773	0.0135
	HHO	0.6001	0.0775	0.7669	0.0452	0.8199	0.0422
	WOA	0.6250	0.0724	0.7638	0.0638	0.8271	0.0608
	PSO	0.6502	0.0549	0.8024	0.0175	0.8641	0.0250
	SCA	0.6300	0.0961	0.7280	0.0611	0.7980	0.0476
	SSA	0.6632	0.0541	0.7603	0.0718	0.8424	0.0349
	CS	0.6607	0.0337	0.7876	0.0368	0.8399	0.0261
BC06	AO	0.7060	0.0137	0.8267	0.0213	0.8813	0.0145
	RIME	0.7027	0.0153	0.8210	0.0254	0.8680	0.0271
	DE	0.7083	0.0079	0.8290	0.0051	0.8767	0.0115
	HHO	0.6291	0.0536	0.7601	0.0562	0.8041	0.0578
	WOA	0.6740	0.0376	0.7618	0.0761	0.8305	0.0398
	PSO	0.5879	0.0433	0.7478	0.0352	0.8462	0.0236
	SCA	0.6789	0.0267	0.7049	0.1209	0.7509	0.1174
	SSA	0.6839	0.0169	0.7647	0.0534	0.8154	0.0563
	CS	0.6954	0.0205	0.8028	0.0450	0.8241	0.0739
BC07	AO	0.6723	0.0003	0.7912	0.0194	0.8429	0.0266
	RIME	0.6723	0.0001	0.7722	0.0325	0.8429	0.0360
	DE	0.6724	0.0000	0.7915	0.0170	0.8340	0.0307
	HHO	0.5436	0.1064	0.7287	0.0539	0.7675	0.0932
	WOA	0.5686	0.1170	0.7525	0.0579	0.7953	0.0540
	PSO	0.5489	0.0954	0.7667	0.0277	0.8550	0.0153
	SCA	0.6396	0.0272	0.6911	0.1124	0.7086	0.1155
	SSA	0.6301	0.0658	0.7521	0.0747	0.8277	0.0339

	CS	0.6688	0.0051	0.7803	0.0418	0.7893	0.0986
BC08	AO	0.7060	0.0219	0.8550	0.0567	0.9195	0.0210
	RIME	0.6993	0.0292	0.8607	0.0111	0.9196	0.0087
	DE	0.6971	0.0288	0.8562	0.0115	0.9148	0.0119
	HHO	0.6030	0.1363	0.7872	0.0585	0.8671	0.0544
	WOA	0.6719	0.0497	0.7999	0.0619	0.8651	0.0803
	PSO	0.6377	0.0547	0.8646	0.0150	0.9121	0.0300
	SCA	0.6896	0.0383	0.7346	0.1399	0.7801	0.1024
	SSA	0.6929	0.0320	0.8268	0.0619	0.8804	0.0332
	CS	0.6985	0.0320	0.8370	0.0331	0.8799	0.0428
BC09	AO	0.5797	0.0803	0.8169	0.0236	0.8664	0.0135
	RIME	0.5635	0.0839	0.8036	0.0316	0.8617	0.0264
	DE	0.5300	0.0840	0.8037	0.0221	0.8630	0.0196
	HHO	0.5303	0.1210	0.7155	0.0838	0.8129	0.0876
	WOA	0.5221	0.1131	0.7404	0.0833	0.8239	0.0705
	PSO	0.4925	0.0591	0.7789	0.0205	0.8551	0.0229
	SCA	0.5443	0.1242	0.6781	0.0708	0.6990	0.0979
	SSA	0.5493	0.1408	0.7361	0.0578	0.8008	0.0685
	CS	0.4651	0.0936	0.7463	0.0538	0.8371	0.0296
BC10	AO	0.5945	0.0269	0.8128	0.0403	0.8513	0.0347
	RIME	0.5810	0.0646	0.8018	0.0381	0.8543	0.0223
	DE	0.5844	0.0106	0.7788	0.0361	0.8433	0.0217
	HHO	0.4828	0.1386	0.6776	0.1220	0.7618	0.1578
	WOA	0.5448	0.1013	0.7220	0.0966	0.7991	0.0742
	PSO	0.4672	0.0846	0.7458	0.0791	0.8471	0.0280
	SCA	0.5521	0.1047	0.6522	0.1595	0.7229	0.0896
	SSA	0.5538	0.1119	0.7257	0.0565	0.8207	0.0380
	CS	0.5845	0.0234	0.7228	0.0823	0.8313	0.0416
BC11	AO	0.6517	0.0530	0.8546	0.0173	0.9082	0.0108
	RIME	0.6587	0.0216	0.8646	0.0112	0.9169	0.0133
	DE	0.6610	0.0132	0.8610	0.0105	0.9182	0.0077
	HHO	0.6072	0.1020	0.7757	0.1215	0.8642	0.0540
	WOA	0.6296	0.0596	0.8128	0.0400	0.8559	0.0761
	PSO	0.6533	0.0397	0.8518	0.0053	0.9182	0.0136
	SCA	0.5369	0.1452	0.7085	0.0978	0.7826	0.0632
	SSA	0.6416	0.0494	0.8090	0.0856	0.8681	0.0488
	CS	0.6477	0.0427	0.8236	0.0281	0.8914	0.0274
BC12	AO	0.6741	0.0091	0.8641	0.0142	0.9089	0.0071
	RIME	0.6567	0.0549	0.8652	0.0037	0.9116	0.0064
	DE	0.6795	0.0000	0.8667	0.0011	0.9109	0.0089
	HHO	0.6078	0.0837	0.8169	0.0430	0.8865	0.0261
	WOA	0.6359	0.0722	0.8253	0.0378	0.8854	0.0399
	PSO	0.5691	0.0772	0.8562	0.0059	0.9141	0.0098
	SCA	0.6556	0.0437	0.7595	0.0741	0.7726	0.0866
	SSA	0.6203	0.0867	0.8530	0.0111	0.8975	0.0214
	CS	0.6718	0.0196	0.8330	0.0646	0.8887	0.0284
BC13	AO	0.6589	0.0039	0.8615	0.0080	0.9069	0.0076
	RIME	0.6575	0.0028	0.8648	0.0064	0.9131	0.0098
	DE	0.6559	0.0023	0.8629	0.0044	0.9128	0.0062

	HHO	0.6087	0.0806	0.8321	0.0389	0.8875	0.0243
	WOA	0.6570	0.0232	0.8495	0.0235	0.9039	0.0175
	PSO	0.6101	0.0583	0.8528	0.0084	0.9107	0.0109
	SCA	0.6463	0.0562	0.7295	0.1031	0.7625	0.1576
	SSA	0.6492	0.0313	0.8419	0.0231	0.8929	0.0299
	CS	0.6615	0.0265	0.8523	0.0218	0.8955	0.0218
BC14	AO	0.6827	0.0038	0.7630	0.0543	0.8224	0.0384
	RIME	0.6810	0.0048	0.7635	0.0551	0.8042	0.0410
	DE	0.6817	0.0033	0.8125	0.0287	0.8219	0.0185
	HHO	0.6062	0.1189	0.7118	0.1290	0.7982	0.0546
	WOA	0.6275	0.1237	0.7202	0.1115	0.8042	0.0413
	PSO	0.6762	0.0085	0.7781	0.0382	0.8468	0.0349
	SCA	0.4076	0.1815	0.5391	0.2033	0.6622	0.1610
	SSA	0.5690	0.1503	0.7336	0.0738	0.8178	0.0876
	CS	0.6139	0.0868	0.7601	0.0495	0.8071	0.0555
BC15	AO	0.6028	0.0436	0.7956	0.0267	0.8682	0.0280
	RIME	0.6070	0.0111	0.8015	0.0229	0.8671	0.0293
	DE	0.6099	0.0293	0.7997	0.0260	0.8551	0.0346
	HHO	0.5761	0.1161	0.7177	0.0988	0.8464	0.0626
	WOA	0.5431	0.1101	0.7418	0.0929	0.8345	0.0593
	PSO	0.6097	0.0032	0.8038	0.0212	0.8704	0.0191
	SCA	0.4392	0.2121	0.6509	0.1298	0.7563	0.1058
	SSA	0.5708	0.0885	0.7432	0.0965	0.8430	0.0580
	CS	0.5881	0.0252	0.7732	0.0513	0.8220	0.0524

Table A.9 FSIM evaluation results at high threshold

		16 thresholds		20 thresholds		24 thresholds	
Image	Method	AVG	STD	AVG	STD	AVG	STD
BC01	AO	0.9847	0.0031	0.9881	0.0019	0.9889	0.0037
	RIME	0.9802	0.0062	0.9835	0.0065	0.9868	0.0033
	DE	0.9801	0.0044	0.9849	0.0044	0.9876	0.0040
	HHO	0.9687	0.0173	0.9785	0.0079	0.9844	0.0068
	WOA	0.9766	0.0067	0.9845	0.0048	0.9900	0.0028
	PSO	0.9820	0.0042	0.9840	0.0050	0.9880	0.0031
	SCA	0.9492	0.0238	0.9586	0.0223	0.9658	0.0147
	SSA	0.9818	0.0044	0.9868	0.0047	0.9896	0.0026
	CS	0.9769	0.0081	0.9818	0.0059	0.9860	0.0057
BC02	AO	0.9853	0.0032	0.9890	0.0016	0.9907	0.0024
	RIME	0.9815	0.0048	0.9844	0.0069	0.9859	0.0044
	DE	0.9814	0.0054	0.9865	0.0032	0.9885	0.0028
	HHO	0.9682	0.0172	0.9789	0.0105	0.9812	0.0103
	WOA	0.9786	0.0070	0.9861	0.0034	0.9876	0.0044
	PSO	0.9836	0.0044	0.9852	0.0044	0.9883	0.0037
	SCA	0.9416	0.0294	0.9650	0.0147	0.9660	0.0189
	SSA	0.9825	0.0051	0.9869	0.0051	0.9911	0.0030
	CS	0.9788	0.0069	0.9835	0.0056	0.9871	0.0048
BC03	AO	0.9537	0.0345	0.9733	0.0118	0.9770	0.0109
	RIME	0.9640	0.0120	0.9679	0.0198	0.9707	0.0310
	DE	0.9601	0.0152	0.9636	0.0157	0.9657	0.0143
	HHO	0.9427	0.0264	0.9491	0.0333	0.9558	0.0380

	WOA	0.9595	0.0179	0.9615	0.0256	0.9743	0.0122
	PSO	0.9621	0.0193	0.9725	0.0121	0.9757	0.0126
	SCA	0.9006	0.0528	0.9430	0.0452	0.9549	0.0261
	SSA	0.9535	0.0196	0.9720	0.0133	0.9779	0.0107
	CS	0.9479	0.0191	0.9617	0.0276	0.9724	0.0186
BC04	AO	0.9792	0.0033	0.9836	0.0038	0.9865	0.0038
	RIME	0.9718	0.0099	0.9770	0.0121	0.9817	0.0060
	DE	0.9717	0.0112	0.9784	0.0064	0.9812	0.0084
	HHO	0.9611	0.0139	0.9709	0.0114	0.9718	0.0203
	WOA	0.9684	0.0119	0.9784	0.0089	0.9838	0.0075
	PSO	0.9783	0.0040	0.9801	0.0067	0.9844	0.0044
	SCA	0.9300	0.0296	0.9505	0.0209	0.9595	0.0301
	SSA	0.9703	0.0125	0.9801	0.0067	0.9847	0.0059
	CS	0.9619	0.0408	0.9702	0.0195	0.9804	0.0074
BC05	AO	0.9806	0.0035	0.9855	0.0025	0.9882	0.0023
	RIME	0.9766	0.0080	0.9810	0.0063	0.9822	0.0098
	DE	0.9754	0.0064	0.9810	0.0047	0.9847	0.0045
	HHO	0.9652	0.0137	0.9700	0.0162	0.9807	0.0103
	WOA	0.9740	0.0143	0.9793	0.0083	0.9863	0.0045
	PSO	0.9776	0.0059	0.9824	0.0040	0.9837	0.0058
	SCA	0.9485	0.0240	0.9450	0.0353	0.9664	0.0138
	SSA	0.9757	0.0080	0.9825	0.0069	0.9879	0.0039
	CS	0.9718	0.0109	0.9808	0.0060	0.9835	0.0055
BC06	AO	0.9778	0.0076	0.9850	0.0031	0.9869	0.0043
	RIME	0.9765	0.0069	0.9766	0.0111	0.9815	0.0076
	DE	0.9737	0.0085	0.9772	0.0074	0.9836	0.0065
	HHO	0.9614	0.0264	0.9738	0.0127	0.9733	0.0141
	WOA	0.9705	0.0150	0.9750	0.0200	0.9857	0.0059
	PSO	0.9784	0.0049	0.9819	0.0057	0.9844	0.0068
	SCA	0.9369	0.0261	0.9502	0.0242	0.9672	0.0206
	SSA	0.9731	0.0094	0.9821	0.0057	0.9840	0.0066
	CS	0.9721	0.0093	0.9781	0.0121	0.9806	0.0107
BC07	AO	0.9694	0.0350	0.9790	0.0162	0.9804	0.0135
	RIME	0.9554	0.0620	0.9685	0.0187	0.9803	0.0099
	DE	0.9646	0.0192	0.9689	0.0217	0.9755	0.0111
	HHO	0.9390	0.0439	0.9502	0.0369	0.9599	0.0220
	WOA	0.9606	0.0274	0.9743	0.0244	0.9701	0.0390
	PSO	0.9665	0.0254	0.9741	0.0162	0.9727	0.0174
	SCA	0.9030	0.0589	0.9493	0.0292	0.9589	0.0267
	SSA	0.9667	0.0163	0.9749	0.0077	0.9774	0.0179
	CS	0.9392	0.0418	0.9585	0.0366	0.9750	0.0099
BC08	AO	0.9864	0.0033	0.9858	0.0136	0.9911	0.0045
	RIME	0.9831	0.0087	0.9837	0.0068	0.9855	0.0066
	DE	0.9804	0.0095	0.9841	0.0050	0.9863	0.0050
	HHO	0.9682	0.0129	0.9780	0.0085	0.9828	0.0068
	WOA	0.9769	0.0105	0.9818	0.0152	0.9866	0.0056
	PSO	0.9794	0.0181	0.9861	0.0063	0.9880	0.0044
	SCA	0.9388	0.0255	0.9603	0.0248	0.9723	0.0117
	SSA	0.9784	0.0088	0.9867	0.0049	0.9899	0.0046

	CS	0.9693	0.0318	0.9840	0.0051	0.9842	0.0091
BC09	AO	0.9706	0.0056	0.9776	0.0060	0.9814	0.0039
	RIME	0.9638	0.0173	0.9699	0.0130	0.9793	0.0078
	DE	0.9643	0.0135	0.9734	0.0078	0.9741	0.0134
	HHO	0.9281	0.0436	0.9609	0.0188	0.9685	0.0127
	WOA	0.9591	0.0162	0.9671	0.0145	0.9767	0.0139
	PSO	0.9678	0.0112	0.9718	0.0115	0.9765	0.0082
	SCA	0.9196	0.0416	0.9142	0.0493	0.9503	0.0238
	SSA	0.9641	0.0103	0.9771	0.0067	0.9830	0.0059
	CS	0.9537	0.0218	0.9650	0.0148	0.9730	0.0146
BC10	AO	0.9761	0.0037	0.9775	0.0066	0.9818	0.0057
	RIME	0.9672	0.0164	0.9697	0.0178	0.9752	0.0129
	DE	0.9648	0.0127	0.9685	0.0107	0.9776	0.0070
	HHO	0.9387	0.0422	0.9603	0.0225	0.9689	0.0120
	WOA	0.9618	0.0230	0.9713	0.0147	0.9783	0.0108
	PSO	0.9663	0.0134	0.9770	0.0065	0.9754	0.0096
	SCA	0.9048	0.0361	0.9263	0.0519	0.9483	0.0329
	SSA	0.9690	0.0099	0.9760	0.0084	0.9802	0.0077
	CS	0.9526	0.0259	0.9609	0.0207	0.9702	0.0142
BC11	AO	0.9817	0.0089	0.9885	0.0014	0.9894	0.0049
	RIME	0.9799	0.0100	0.9848	0.0048	0.9840	0.0069
	DE	0.9803	0.0047	0.9863	0.0023	0.9876	0.0039
	HHO	0.9608	0.0204	0.9745	0.0137	0.9727	0.0141
	WOA	0.9708	0.0178	0.9758	0.0105	0.9783	0.0166
	PSO	0.9800	0.0054	0.9824	0.0079	0.9868	0.0033
	SCA	0.9442	0.0285	0.9571	0.0223	0.9673	0.0150
	SSA	0.9795	0.0068	0.9862	0.0035	0.9898	0.0026
	CS	0.9676	0.0150	0.9793	0.0096	0.9822	0.0059
BC12	AO	0.9863	0.0024	0.9878	0.0064	0.9925	0.0009
	RIME	0.9825	0.0057	0.9818	0.0128	0.9860	0.0067
	DE	0.9823	0.0038	0.9855	0.0044	0.9887	0.0032
	HHO	0.9695	0.0150	0.9762	0.0125	0.9784	0.0123
	WOA	0.9805	0.0077	0.9865	0.0053	0.9866	0.0111
	PSO	0.9833	0.0069	0.9853	0.0047	0.9886	0.0031
	SCA	0.9496	0.0223	0.9609	0.0210	0.9695	0.0162
	SSA	0.9822	0.0041	0.9871	0.0036	0.9903	0.0040
	CS	0.9703	0.0184	0.9748	0.0232	0.9843	0.0091
BC13	AO	0.9850	0.0022	0.9892	0.0012	0.9911	0.0019
	RIME	0.9807	0.0093	0.9846	0.0046	0.9876	0.0039
	DE	0.9813	0.0047	0.9850	0.0036	0.9888	0.0027
	HHO	0.9721	0.0166	0.9731	0.0133	0.9787	0.0148
	WOA	0.9797	0.0059	0.9848	0.0067	0.9864	0.0068
	PSO	0.9831	0.0046	0.9839	0.0046	0.9871	0.0045
	SCA	0.9340	0.0300	0.9582	0.0271	0.9597	0.0319
	SSA	0.9779	0.0072	0.9838	0.0076	0.9891	0.0031
	CS	0.9744	0.0099	0.9755	0.0136	0.9841	0.0061
BC14	AO	0.9355	0.0627	0.9791	0.0224	0.9803	0.0256
	RIME	0.9504	0.0455	0.9706	0.0281	0.9808	0.0186
	DE	0.9573	0.0263	0.9807	0.0060	0.9866	0.0038

	HHO	0.9084	0.0707	0.9429	0.0454	0.9511	0.0421
	WOA	0.9217	0.0628	0.9495	0.0504	0.9603	0.0376
	PSO	0.9539	0.0367	0.9705	0.0212	0.9792	0.0103
	SCA	0.9163	0.0588	0.9390	0.0298	0.9543	0.0286
	SSA	0.9714	0.0205	0.9844	0.0045	0.9897	0.0033
	CS	0.9337	0.0452	0.9617	0.0349	0.9731	0.0186
BC15	AO	0.9714	0.0085	0.9827	0.0031	0.9830	0.0048
	RIME	0.9654	0.0296	0.9756	0.0124	0.9776	0.0094
	DE	0.9674	0.0125	0.9773	0.0078	0.9797	0.0066
	HHO	0.9462	0.0458	0.9647	0.0177	0.9672	0.0166
	WOA	0.9614	0.0255	0.9763	0.0088	0.9791	0.0135
	PSO	0.9744	0.0071	0.9732	0.0361	0.9742	0.0295
	SCA	0.9472	0.0217	0.9323	0.0507	0.9611	0.0211
	SSA	0.9701	0.0105	0.9747	0.0121	0.9800	0.0078
	CS	0.9659	0.0116	0.9714	0.0158	0.9759	0.0142

Table A.10 PSNR evaluation results at high threshold

		16 thresholds		20 thresholds		24 thresholds	
Image	Method	AVG	STD	AVG	STD	AVG	STD
BC01	AO	29.4571	0.6052	30.9928	0.4686	31.9056	0.7631
	RIME	28.9339	1.1033	30.2569	1.5058	31.2484	1.0824
	DE	28.7195	0.8641	30.4419	0.6816	31.3911	1.0593
	HHO	27.7542	1.8548	29.3215	1.5960	31.2209	1.4360
	WOA	28.5004	1.0752	30.6207	1.3392	32.1084	1.1823
	PSO	29.4130	0.6863	30.0838	1.3570	31.6459	0.9892
	SCA	25.1334	2.0487	26.3718	2.5041	27.5386	2.1293
	SSA	28.7346	1.0961	30.5838	1.2316	31.8098	1.0928
	CS	28.5712	1.2748	29.7931	1.2055	31.2915	1.3162
BC02	AO	29.2503	0.6375	30.7592	0.5309	31.9010	0.7232
	RIME	28.6791	0.9793	30.3118	1.1367	31.0113	1.6509
	DE	28.9611	0.7404	30.5337	0.8732	31.3456	0.9044
	HHO	27.7976	2.0718	29.4450	1.4446	30.1775	1.9402
	WOA	28.5400	1.4739	30.5696	1.0786	31.4528	1.4521
	PSO	29.3817	0.6733	30.4045	1.0355	31.7072	0.8871
	SCA	24.5997	2.2787	26.6534	2.1247	28.1208	2.0348
	SSA	28.6195	0.9233	30.3600	1.2809	32.1898	0.9401
	CS	28.6204	1.0572	30.0081	1.4003	31.2334	1.1403
BC03	AO	27.2945	2.5622	29.4957	1.6186	30.5724	1.5364
	RIME	28.0008	1.3136	29.2809	2.0297	30.4343	2.7276
	DE	27.7982	1.1838	28.6339	1.6821	29.1583	1.7584
	HHO	26.3049	1.8932	27.2665	2.4223	28.5296	2.9732
	WOA	27.6376	1.8924	28.6788	2.5365	30.5022	1.8165
	PSO	27.8870	1.8523	29.6066	1.5785	30.6061	1.6082
	SCA	23.6612	2.7781	26.8615	2.6717	27.9426	2.0511
	SSA	26.8794	1.5676	29.4403	1.5304	30.5745	1.6371
	CS	26.7646	1.6865	28.5236	2.5678	30.3732	2.1139
BC04	AO	29.5096	0.6363	30.9900	0.8119	31.9711	0.9467
	RIME	28.5740	1.4411	30.1435	1.8364	31.0492	1.3189
	DE	28.5369	1.3081	30.0813	1.0752	30.9854	1.5600
	HHO	27.4712	1.5750	29.0924	1.7819	29.5899	2.3440

	WOA	28.2350	1.5660	30.0312	1.6367	31.6458	1.5422
	PSO	29.5624	0.8549	30.5633	1.2314	31.6975	0.9890
	SCA	25.2915	2.1542	26.5386	2.1035	28.1775	2.6121
	SSA	28.2180	1.5554	30.3234	1.1871	31.6124	1.4077
	CS	28.1983	2.6314	29.4594	2.3170	30.9755	1.5657
BC05	AO	29.2940	0.7634	30.8437	0.7423	32.0174	0.8861
	RIME	29.2435	0.9450	30.3727	1.2998	31.2895	2.0056
	DE	29.0331	1.0445	30.3332	0.9678	31.5496	1.1280
	HHO	28.0983	1.7244	28.9723	2.1882	31.1230	1.9723
	WOA	29.2033	1.6944	30.2582	1.3941	32.1801	1.1932
	PSO	29.1582	1.0981	30.6457	1.0219	31.4664	1.1137
	SCA	26.1946	2.1743	26.3338	3.0031	28.7189	1.5634
	SSA	28.8402	1.2184	30.3903	1.4495	32.2300	1.2132
	CS	28.6778	1.1812	30.5928	1.2813	31.6183	1.0818
BC06	AO	29.2077	1.0742	30.9706	0.8476	31.9454	1.1375
	RIME	29.3905	1.2924	29.9920	1.8952	31.1907	1.6919
	DE	28.9677	1.2167	29.7890	1.2945	31.5917	1.2906
	HHO	27.9380	2.7446	29.6573	1.7335	30.2830	1.9478
	WOA	28.5122	1.9962	30.1508	2.6347	32.3015	1.5520
	PSO	29.6694	0.9824	30.8781	1.4131	32.0570	1.5092
	SCA	25.3560	2.3211	27.0663	2.2900	29.3184	2.3392
	SSA	28.7809	1.4033	30.6777	1.3221	31.6399	1.4322
	CS	28.9272	1.2852	30.4000	1.8165	31.4844	1.9140
BC07	AO	28.7976	2.4246	30.4019	1.8861	31.3015	2.0119
	RIME	28.1537	3.6168	29.9576	2.1297	31.4751	1.7522
	DE	28.3464	1.6039	29.5726	2.1137	30.5998	1.7666
	HHO	26.7298	3.3658	27.8191	2.9227	28.5450	2.6077
	WOA	28.0383	2.6949	30.3147	2.3994	30.5779	3.3250
	PSO	28.8227	2.4534	30.1616	2.1246	30.4009	2.5464
	SCA	24.1038	3.7347	27.3625	2.6871	28.8620	2.6608
	SSA	28.2210	1.8744	29.5253	1.4084	30.7777	2.3328
	CS	26.3710	3.1275	28.9419	3.0553	30.3882	2.1427
BC08	AO	29.6183	0.7552	30.6001	2.0112	32.3599	1.0404
	RIME	29.5421	1.3037	30.1886	1.2032	31.3983	1.4657
	DE	29.0370	0.8625	30.1208	0.9958	31.4019	0.7954
	HHO	27.4113	1.5456	29.2898	1.3713	30.2937	1.5682
	WOA	28.7887	1.4340	30.3174	2.4032	31.3638	1.7204
	PSO	29.1742	2.1316	30.6575	1.1808	31.7045	1.2472
	SCA	24.4862	1.9248	26.5228	2.3505	28.4123	1.3644
	SSA	28.0315	1.5208	30.3427	1.0081	31.8939	1.0920
	CS	28.1048	2.6676	29.9547	1.3020	30.9644	2.0995
BC09	AO	28.7727	0.6773	30.4020	0.9392	31.4265	0.9051
	RIME	28.8007	1.8266	29.8414	1.7424	31.6641	1.4281
	DE	28.5891	1.2901	30.0726	1.0461	31.1184	1.2673
	HHO	26.3650	2.4056	29.3547	1.7951	30.4729	1.8238
	WOA	28.6690	1.2913	29.7004	1.8505	31.3771	2.1488
	PSO	29.0186	1.1006	30.2089	1.4933	31.2866	1.4200
	SCA	25.4280	2.4211	25.4343	2.8323	28.3165	2.1868
	SSA	28.4026	1.1280	30.3264	1.1894	31.8637	1.3124

	CS	28.0193	1.8643	29.7328	1.6098	30.9176	1.6933
BC10	AO	29.3159	0.6825	30.2096	1.1340	31.3653	1.3920
	RIME	29.0962	1.7346	29.8070	1.7693	31.2317	2.0534
	DE	28.5956	1.3477	29.4603	1.3043	31.3972	1.1187
	HHO	26.6203	2.8654	29.3686	2.2765	30.3515	1.6087
	WOA	28.9577	2.2696	30.2265	1.8214	31.6892	1.9065
	PSO	28.9271	1.3341	30.7205	1.1651	31.1780	1.2258
	SCA	24.8622	1.9609	26.6349	3.1441	28.6860	2.1657
	SSA	28.5831	1.3741	30.1921	1.3285	31.4349	1.5618
	CS	27.6955	2.2701	29.1647	2.1083	30.4698	1.8582
BC11	AO	29.2756	0.8698	31.0603	0.5875	32.1955	0.9682
	RIME	29.3180	1.5760	30.9713	1.1716	31.3558	1.5801
	DE	29.4597	0.9205	31.1115	0.6414	31.7749	1.0690
	HHO	27.4550	2.0043	29.6215	1.7656	29.8512	1.8746
	WOA	28.6784	2.1252	29.7756	2.0376	30.6304	2.9286
	PSO	29.5627	0.7590	30.5814	1.5415	31.7557	1.0841
	SCA	25.0557	2.1157	26.7467	2.1711	28.3380	1.6148
	SSA	28.4349	1.6233	30.2553	1.1925	31.6959	1.2306
	CS	28.1095	1.7185	29.8581	1.7677	30.5583	1.5161
BC12	AO	29.9294	0.6876	30.9171	1.2252	32.5864	0.5533
	RIME	29.6783	0.9151	30.1351	2.1716	31.6271	1.5249
	DE	29.3787	0.7951	30.6540	1.0073	31.5925	1.1571
	HHO	28.3649	1.7271	29.3495	1.9521	30.2627	2.1537
	WOA	29.9630	1.3589	31.6654	1.6202	32.6135	1.8584
	PSO	30.0772	1.0571	30.8026	1.2245	31.9845	0.9961
	SCA	25.8980	1.9175	27.0176	2.4918	28.5552	1.8134
	SSA	28.9472	0.9506	30.3181	1.1750	31.9326	1.0434
	CS	28.3234	2.1074	29.4627	2.4855	31.3148	1.6042
BC13	AO	29.7520	0.6255	31.2644	0.5937	32.2851	0.8575
	RIME	29.4629	1.3844	30.8897	1.2884	31.9296	1.1476
	DE	29.3947	1.0483	30.5116	1.0166	31.8388	0.8428
	HHO	28.7322	2.1041	29.2346	1.9210	30.5704	2.2201
	WOA	29.8751	1.2401	31.4306	1.1211	32.2749	1.8709
	PSO	30.0252	0.9081	30.1923	1.2918	31.6055	1.4335
	SCA	24.9359	2.5399	27.1209	2.4514	27.6444	2.4413
	SSA	28.3912	1.1366	29.9920	1.6282	31.6453	1.0971
	CS	28.8081	1.4432	29.3783	2.1532	31.2805	1.6669
BC14	AO	26.7695	2.3417	29.5795	1.9300	30.4507	2.1791
	RIME	27.8545	2.0275	29.6409	1.7091	30.7655	1.4572
	DE	28.0318	1.0893	30.0654	0.6269	31.0392	1.0017
	HHO	25.2302	3.0652	27.2964	2.3138	27.7162	2.6570
	WOA	26.0562	2.8937	28.1716	2.5395	29.0337	2.7886
	PSO	27.9216	1.6046	29.1346	1.6083	30.5744	1.3470
	SCA	23.9785	2.8666	25.5307	2.0752	27.2522	2.2546
	SSA	27.8656	1.5721	29.7405	1.4017	31.4189	1.2437
	CS	26.4505	2.2353	28.4457	2.0461	29.3873	1.6756
BC15	AO	28.7846	0.7096	30.8731	0.7509	31.6406	1.1571
	RIME	28.4731	1.7807	30.1402	1.6780	31.0823	1.4009
	DE	28.4478	1.1373	30.3615	0.9416	31.1229	0.9557

	HHO	27.1343	2.7354	29.1122	2.1326	29.8001	2.1616
	WOA	28.2330	1.9819	30.5605	1.6208	31.5565	1.6657
	PSO	29.4305	0.9362	30.3887	2.5138	31.5929	2.4009
	SCA	26.6371	1.7458	26.1983	2.9899	28.7027	2.1582
	SSA	28.6559	1.1632	30.2134	1.4980	31.2212	1.4671
	CS	28.3490	1.4549	29.7916	1.7793	31.0736	1.8625

Table A.11 SSIM evaluation results at high threshold

		16 thresholds		20 thresholds		24 thresholds	
Image	Method	AVG	STD	AVG	STD	AVG	STD
BC01	AO	0.9685	0.0043	0.9765	0.0032	0.9795	0.0041
	RIME	0.9629	0.0118	0.9690	0.0184	0.9751	0.0074
	DE	0.9606	0.0116	0.9716	0.0071	0.9744	0.0086
	HHO	0.9477	0.0287	0.9609	0.0179	0.9746	0.0094
	WOA	0.9591	0.0125	0.9728	0.0093	0.9794	0.0070
	PSO	0.9665	0.0069	0.9663	0.0143	0.9761	0.0075
	SCA	0.9133	0.0455	0.9228	0.0469	0.9385	0.0329
	SSA	0.9609	0.0116	0.9721	0.0126	0.9778	0.0074
	CS	0.9577	0.0170	0.9648	0.0133	0.9739	0.0109
BC02	AO	0.9679	0.0054	0.9756	0.0040	0.9800	0.0044
	RIME	0.9613	0.0120	0.9729	0.0076	0.9718	0.0151
	DE	0.9649	0.0071	0.9731	0.0090	0.9760	0.0069
	HHO	0.9520	0.0278	0.9659	0.0147	0.9669	0.0198
	WOA	0.9599	0.0174	0.9737	0.0084	0.9765	0.0102
	PSO	0.9686	0.0068	0.9717	0.0082	0.9778	0.0059
	SCA	0.9060	0.0409	0.9313	0.0352	0.9509	0.0250
	SSA	0.9624	0.0095	0.9718	0.0105	0.9811	0.0055
	CS	0.9607	0.0127	0.9686	0.0131	0.9755	0.0084
BC03	AO	0.9286	0.0394	0.9555	0.0158	0.9622	0.0149
	RIME	0.9438	0.0155	0.9522	0.0246	0.9551	0.0358
	DE	0.9372	0.0169	0.9441	0.0189	0.9470	0.0177
	HHO	0.9228	0.0309	0.9245	0.0409	0.9364	0.0465
	WOA	0.9394	0.0210	0.9457	0.0295	0.9631	0.0121
	PSO	0.9397	0.0236	0.9545	0.0172	0.9613	0.0133
	SCA	0.8703	0.0582	0.9189	0.0508	0.9307	0.0339
	SSA	0.9248	0.0233	0.9521	0.0177	0.9623	0.0143
	CS	0.9194	0.0244	0.9380	0.0399	0.9567	0.0238
BC04	AO	0.9562	0.0068	0.9660	0.0067	0.9705	0.0083
	RIME	0.9484	0.0187	0.9591	0.0243	0.9640	0.0135
	DE	0.9445	0.0194	0.9565	0.0133	0.9602	0.0189
	HHO	0.9367	0.0200	0.9511	0.0217	0.9513	0.0337
	WOA	0.9457	0.0240	0.9588	0.0171	0.9708	0.0118
	PSO	0.9573	0.0094	0.9601	0.0138	0.9694	0.0094
	SCA	0.9003	0.0398	0.9161	0.0302	0.9308	0.0544
	SSA	0.9415	0.0225	0.9592	0.0123	0.9669	0.0123
	CS	0.9361	0.0589	0.9487	0.0314	0.9628	0.0148
BC05	AO	0.9487	0.0097	0.9611	0.0080	0.9676	0.0081
	RIME	0.9492	0.0143	0.9572	0.0145	0.9589	0.0236
	DE	0.9450	0.0167	0.9553	0.0128	0.9627	0.0126
	HHO	0.9320	0.0279	0.9379	0.0346	0.9610	0.0230

	WOA	0.9480	0.0233	0.9560	0.0176	0.9694	0.0111
	PSO	0.9444	0.0168	0.9582	0.0100	0.9624	0.0115
	SCA	0.9076	0.0424	0.9006	0.0640	0.9372	0.0237
	SSA	0.9429	0.0165	0.9549	0.0177	0.9687	0.0107
	CS	0.9404	0.0188	0.9568	0.0174	0.9632	0.0103
BC06	AO	0.9407	0.0161	0.9576	0.0087	0.9637	0.0098
	RIME	0.9449	0.0183	0.9453	0.0249	0.9554	0.0206
	DE	0.9380	0.0202	0.9431	0.0186	0.9589	0.0159
	HHO	0.9278	0.0497	0.9455	0.0254	0.9465	0.0261
	WOA	0.9379	0.0302	0.9467	0.0414	0.9673	0.0135
	PSO	0.9464	0.0140	0.9562	0.0159	0.9629	0.0178
	SCA	0.8873	0.0481	0.9073	0.0383	0.9313	0.0397
	SSA	0.9332	0.0224	0.9539	0.0152	0.9593	0.0154
	CS	0.9382	0.0194	0.9498	0.0247	0.9571	0.0245
BC07	AO	0.9317	0.0536	0.9509	0.0254	0.9599	0.0157
	RIME	0.9207	0.0799	0.9477	0.0236	0.9558	0.0243
	DE	0.9298	0.0227	0.9366	0.0372	0.9502	0.0186
	HHO	0.9048	0.0589	0.9183	0.0530	0.9216	0.0383
	WOA	0.9218	0.0485	0.9481	0.0365	0.9438	0.0595
	PSO	0.9316	0.0378	0.9479	0.0270	0.9433	0.0312
	SCA	0.8477	0.0835	0.9103	0.0454	0.9258	0.0471
	SSA	0.9245	0.0353	0.9409	0.0195	0.9479	0.0368
	CS	0.8919	0.0627	0.9309	0.0448	0.9439	0.0271
BC08	AO	0.9757	0.0044	0.9769	0.0189	0.9852	0.0041
	RIME	0.9733	0.0115	0.9747	0.0076	0.9797	0.0091
	DE	0.9696	0.0071	0.9741	0.0078	0.9805	0.0047
	HHO	0.9546	0.0180	0.9696	0.0092	0.9735	0.0115
	WOA	0.9686	0.0115	0.9732	0.0230	0.9790	0.0114
	PSO	0.9667	0.0368	0.9766	0.0103	0.9803	0.0084
	SCA	0.9155	0.0386	0.9390	0.0387	0.9608	0.0127
	SSA	0.9622	0.0155	0.9768	0.0060	0.9825	0.0055
	CS	0.9529	0.0542	0.9720	0.0095	0.9742	0.0186
BC09	AO	0.9491	0.0080	0.9617	0.0093	0.9679	0.0073
	RIME	0.9425	0.0281	0.9517	0.0203	0.9665	0.0127
	DE	0.9408	0.0221	0.9554	0.0128	0.9615	0.0140
	HHO	0.8994	0.0528	0.9458	0.0238	0.9534	0.0202
	WOA	0.9427	0.0187	0.9500	0.0242	0.9616	0.0256
	PSO	0.9465	0.0162	0.9550	0.0170	0.9627	0.0166
	SCA	0.8839	0.0546	0.8744	0.0677	0.9278	0.0326
	SSA	0.9405	0.0153	0.9590	0.0122	0.9691	0.0135
	CS	0.9303	0.0333	0.9498	0.0200	0.9579	0.0206
BC10	AO	0.9519	0.0075	0.9577	0.0123	0.9656	0.0119
	RIME	0.9454	0.0225	0.9494	0.0277	0.9605	0.0200
	DE	0.9389	0.0206	0.9446	0.0185	0.9620	0.0134
	HHO	0.9014	0.0573	0.9419	0.0311	0.9516	0.0164
	WOA	0.9382	0.0356	0.9535	0.0215	0.9648	0.0186
	PSO	0.9422	0.0181	0.9590	0.0128	0.9599	0.0120
	SCA	0.8700	0.0468	0.8913	0.0696	0.9305	0.0404
	SSA	0.9404	0.0197	0.9554	0.0148	0.9628	0.0139

	CS	0.9224	0.0417	0.9378	0.0283	0.9520	0.0226
BC11	AO	0.9733	0.0046	0.9810	0.0028	0.9844	0.0034
	RIME	0.9687	0.0150	0.9784	0.0066	0.9774	0.0133
	DE	0.9709	0.0080	0.9794	0.0046	0.9801	0.0081
	HHO	0.9500	0.0242	0.9691	0.0134	0.9682	0.0157
	WOA	0.9626	0.0261	0.9689	0.0162	0.9689	0.0340
	PSO	0.9725	0.0056	0.9744	0.0147	0.9808	0.0062
	SCA	0.9160	0.0431	0.9391	0.0324	0.9555	0.0187
	SSA	0.9618	0.0189	0.9748	0.0077	0.9812	0.0061
	CS	0.9590	0.0202	0.9703	0.0147	0.9730	0.0110
BC12	AO	0.9703	0.0055	0.9743	0.0085	0.9820	0.0025
	RIME	0.9676	0.0085	0.9660	0.0173	0.9753	0.0112
	DE	0.9640	0.0078	0.9709	0.0082	0.9743	0.0079
	HHO	0.9573	0.0204	0.9612	0.0179	0.9637	0.0206
	WOA	0.9700	0.0099	0.9769	0.0110	0.9806	0.0107
	PSO	0.9697	0.0080	0.9716	0.0114	0.9774	0.0076
	SCA	0.9249	0.0303	0.9338	0.0380	0.9489	0.0248
	SSA	0.9615	0.0092	0.9682	0.0093	0.9771	0.0071
	CS	0.9521	0.0311	0.9572	0.0355	0.9729	0.0104
BC13	AO	0.9714	0.0041	0.9788	0.0035	0.9820	0.0045
	RIME	0.9671	0.0137	0.9739	0.0101	0.9788	0.0069
	DE	0.9660	0.0116	0.9718	0.0071	0.9780	0.0057
	HHO	0.9558	0.0313	0.9600	0.0187	0.9676	0.0221
	WOA	0.9697	0.0108	0.9780	0.0063	0.9792	0.0111
	PSO	0.9718	0.0069	0.9681	0.0124	0.9759	0.0119
	SCA	0.9058	0.0525	0.9354	0.0441	0.9385	0.0493
	SSA	0.9581	0.0117	0.9673	0.0183	0.9778	0.0073
	CS	0.9599	0.0165	0.9598	0.0251	0.9734	0.0133
BC14	AO	0.9368	0.0513	0.9697	0.0260	0.9712	0.0353
	RIME	0.9535	0.0318	0.9694	0.0149	0.9741	0.0117
	DE	0.9608	0.0111	0.9736	0.0053	0.9764	0.0077
	HHO	0.9059	0.0626	0.9432	0.0290	0.9435	0.0348
	WOA	0.9235	0.0520	0.9514	0.0356	0.9578	0.0368
	PSO	0.9573	0.0207	0.9660	0.0165	0.9741	0.0104
	SCA	0.8963	0.0818	0.9255	0.0394	0.9421	0.0315
	SSA	0.9576	0.0209	0.9712	0.0113	0.9790	0.0085
	CS	0.9374	0.0387	0.9571	0.0239	0.9640	0.0159
BC15	AO	0.9497	0.0091	0.9672	0.0061	0.9687	0.0088
	RIME	0.9430	0.0361	0.9579	0.0176	0.9657	0.0121
	DE	0.9473	0.0148	0.9621	0.0112	0.9657	0.0104
	HHO	0.9230	0.0564	0.9460	0.0290	0.9529	0.0239
	WOA	0.9432	0.0312	0.9627	0.0156	0.9645	0.0167
	PSO	0.9551	0.0100	0.9557	0.0482	0.9634	0.0355
	SCA	0.9291	0.0226	0.9012	0.0678	0.9406	0.0244
	SSA	0.9497	0.0137	0.9616	0.0122	0.9659	0.0122
	CS	0.9467	0.0162	0.9545	0.0218	0.9625	0.0180

10. Reference

1. Yang, M., et al., *A new approach to system design optimization of underwater gliders.* IEEE/ASME Transactions on Mechatronics, 2022. **27**(5): p. 3494-3505.
2. Sharma, S., et al., *mLBOA: A Modified Butterfly Optimization Algorithm with Lagrange Interpolation for Global Optimization.* JOURNAL OF BIONIC ENGINEERING, 2022. **19**(4): p. 1161-1176.
3. Jiang, F., L. Wang, and L. Bai, *An Improved Whale Algorithm and Its Application in Truss Optimization.* JOURNAL OF BIONIC ENGINEERING, 2021. **18**(3): p. 721-732.
4. Van Den Berg, E. and M.P.J.S.j.o.s.c. Friedlander, *Probing the Pareto frontier for basis pursuit solutions.* 2009. **31**(2): p. 890-912.
5. Hinton, G.E. and R.R.J.s. Salakhutdinov, *Reducing the dimensionality of data with neural networks.* 2006. **313**(5786): p. 504-507.
6. Li, Y., X. Yu, and J. Liu, *Enhanced Butterfly Optimization Algorithm for Large-Scale Optimization Problems.* JOURNAL OF BIONIC ENGINEERING, 2022. **19**(2): p. 554-570.
7. Başaran, E., *A new brain tumor diagnostic model: Selection of textural feature extraction algorithms and convolution neural network features with optimization algorithms.* Computers in Biology and Medicine, 2022. **148**: p. 105857.
8. Beheshti, Z. and S.M.H.J.I.j.a.s.c.a. Shamsuddin, *A review of population-based meta-heuristic algorithms.* 2013. **5**(1): p. 1-35.
9. Emam, M.M., E.H. Houssein, and R.M. Ghoniem, *A modified reptile search algorithm for global optimization and image segmentation: Case study brain MRI images.* Computers in Biology and Medicine, 2023. **152**: p. 106404.
10. Emam, M.M., et al., *Optimized deep learning architecture for brain tumor classification using improved Hunger Games Search Algorithm.* Computers in Biology and Medicine, 2023. **160**: p. 106966.
11. Houssein, E.H., et al., *Boosted sooty tern optimization algorithm for global optimization and feature selection.* Expert Systems with Applications, 2023. **213**: p. 119015.
12. Črepinšek, M., S.-H. Liu, and M. Mernik, *Exploration and exploitation in evolutionary algorithms.* ACM Computing Surveys, 2013. **45**(3): p. 1-33.
13. David H. Wolpert and W.G. Macready, *No Free Lunch Theorems for Optimization.* IEEE Trans, 1997: p. 67–82.
14. Hashim, F.A., et al., *Henry gas solubility optimization: A novel physics-based algorithm.* FUTURE GENERATION COMPUTER SYSTEMS-THE INTERNATIONAL JOURNAL OF ESCIENCE, 2019. **101**: p. 646-667.
15. Su, H., et al., *RIME: A physics-based optimization.* NEUROCOMPUTING, 2023. **532**: p. 183-214.
16. Anita and A. Yadav, *AEFA: Artificial electric field algorithm for global optimization.* Swarm and Evolutionary Computation, 2019. **48**: p. 93-108.
17. Holland, J.H., *Genetic Algorithms.* Scientific american, 1992. **267**: p. 66-73.
18. Hirsh, H., *Genetic programming.* IEEE INTELLIGENT SYSTEMS & THEIR APPLICATIONS, 2000. **15**(3): p. 74-74.
19. Storn, R. and K.J.J.o.G.O. Price, *Differential Evolution – A Simple and Efficient Heuristic for global Optimization over Continuous Spaces.* 1997. **11**(4): p. 341-359.
20. Simon, D.J.I.t.o.e.c., *Biogeography-based optimization.* 2008. **12**(6): p. 702-713.
21. Beyer, H.-G. and H.-P.J.N.c. Schwefel, *Evolution strategies–a comprehensive introduction.* 2002. **1**: p. 3-52.
22. Kuo, R.J. and F.E. Zulvia, *The gradient evolution algorithm: A new metaheuristic.* Information Sciences, 2015. **316**: p. 246-265.
23. Akay, B., *A study on particle swarm optimization and artificial bee colony algorithms for multilevel thresholding.* APPLIED SOFT COMPUTING, 2013. **13**(6): p. 3066-3091.
24. Karaboga, D. and B. Basturk, *A powerful and efficient algorithm for numerical function optimization: artificial bee colony (ABC) algorithm.* JOURNAL OF GLOBAL OPTIMIZATION, 2007. **39**(3): p. 459-471.
25. Socha, K. and M. Dorigo, *Ant colony optimization for continuous domains.* European Journal of Operational Research, 2008. **185**(3): p. 1155-1173.
26. Mirjalili, S., et al., *Grey Wolf Optimizer: Theory, Literature Review, and Application in Computational Fluid Dynamics Problems*, in *Nature-Inspired Optimizers: Theories, Literature Reviews and Applications*, S. Mirjalili, J. Song Dong, and A. Lewis, Editors. 2020, Springer International Publishing: Cham. p. 87-105.
27. Arora, S. and P. Anand, *Chaotic grasshopper optimization algorithm for global optimization.* NEURAL COMPUTING & APPLICATIONS, 2019. **31**(8): p. 4385-4405.
28. Chen, H., et al., *Slime mould algorithm: a comprehensive review of recent variants and applications.* International Journal of Systems Science,

2022: p. 1-32.
29. Li, S., et al., *Slime mould algorithm: A new method for stochastic optimization.* Future Generation Computer Systems, 2020. **111**: p. 300-323.
30. Tu, J., et al., *The Colony Predation Algorithm.* Journal of Bionic Engineering, 2021. **18**(3): p. 674-710.
31. Heidari, A.A., et al., *Harris hawks optimization: Algorithm and applications.* Future Generation Computer Systems-the International Journal of Escience, 2019. **97**: p. 849-872.
32. Mirjalili, S., et al., *Salp Swarm Algorithm: A bio-inspired optimizer for engineering design problems.* Advances in Engineering Software, 2017. **114**: p. 163-191.
33. Yang, X.-S., *A new metaheuristic bat-inspired algorithm*, in *Nature inspired cooperative strategies for optimization (NICSO 2010)*. 2010, Springer. p. 65-74.
34. Chu, S.-C., P.-w. Tsai, and J.-S. Pan. *Cat Swarm Optimization*. in *PRICAI 2006: Trends in Artificial Intelligence*. 2006. Berlin, Heidelberg: Springer Berlin Heidelberg.
35. Lian, J., et al., *Parrot optimizer: Algorithm and applications to medical problems.* Computers in Biology and Medicine, 2024: p. 108064.
36. Yang, Y., et al., *Hunger games search: Visions, conception, implementation, deep analysis, perspectives, and towards performance shifts.* Expert Systems with Applications, 2021. **177**: p. 114864.
37. Rashedi, E., H. Nezamabadi-Pour, and S. Saryazdi, *GSA: A Gravitational Search Algorithm.* INFORMATION SCIENCES, 2009. **179**(13): p. 2232-2248.
38. Hatamlou, A., *Black hole: A new heuristic optimization approach for data clustering.* Information Sciences, 2013. **222**: p. 175-184.
39. Recioui, A., *Application of a Galaxy-Based Search Algorithm to MIMO System Capacity Optimization.* ARABIAN JOURNAL FOR SCIENCE AND ENGINEERING, 2016. **41**(9): p. 3407-3414.
40. Faramarzi, A., et al., *Equilibrium optimizer: A novel optimization algorithm.* KNOWLEDGE-BASED SYSTEMS, 2020. **191**.
41. Kirkpatrick, S., C.D. Gelatt, and M.P. Vecchi, *Optimization by Simulated Annealing.* Science, 1983. **220**(4598): p. 671-680.
42. Mirjalili, S., S.M. Mirjalili, and A. Hatamlou, *Multi-Verse Optimizer: a nature-inspired algorithm for global optimization.* NEURAL COMPUTING & APPLICATIONS, 2016. **27**(2): p. 495-513.
43. Formato, R.A., *Central Force Optimization: A New Nature Inspired Computational Framework for Multidimensional Search and Optimization*, in *NATURE INSPIRED COOPERATIVE STRATEGIES FOR OPTIMIZATION (NICSO 2007)*. 2008. p. 221-238.
44. Ahmadianfar, I., et al., *INFO: An Efficient Optimization Algorithm based on Weighted Mean of Vectors.* Expert Systems with Applications, 2022: p. 116516.
45. Ahmadianfar, I., et al., *RUN Beyond the Metaphor: An Efficient Optimization Algorithm Based on Runge Kutta Method.* Expert Systems with Applications, 2021: p. 115079.
46. Rao, R.V., V.J. Savsani, and D.P. Vakharia, *Teaching–learning-based optimization: A novel method for constrained mechanical design optimization problems.* Computer-Aided Design, 2011. **43**(3): p. 303-315.
47. Askari, Q., I. Younas, and M. Saeed, *Political Optimizer: A novel socio-inspired meta-heuristic for global optimization.* Knowledge-Based Systems, 2020. **195**: p. 105709.
48. Kim, J.H., *Harmony Search Algorithm: A Unique Music-inspired Algorithm.* Procedia Engineering, 2016. **154**: p. 1401-1405.
49. Ghorbani, N. and E. Babaei, *Exchange market algorithm.* Applied Soft Computing, 2014. **19**: p. 177-187.
50. Satapathy, S. and A. Naik, *Social group optimization (SGO): a new population evolutionary optimization technique.* Complex & Intelligent Systems, 2016. **2**(3): p. 173-203.
51. Venkata Rao, R., *Jaya: A simple and new optimization algorithm for solving constrained and unconstrained optimization problems.* International Journal of Industrial Engineering Computations, 2016: p. 19-34.
52. Houssein, E.H., et al., *Liver Cancer Algorithm: A novel bio-inspired optimizer.* Computers in Biology and Medicine, 2023. **165**: p. 107389.
53. Dong, R., et al., *Boosting Kernel Search Optimizer with Slime Mould Foraging Behavior for Combined Economic Emission Dispatch Problems.* Journal of Bionic Engineering, 2023.
54. Dong, R., et al., *Multi-strategy enhanced kernel search optimization and its application in economic emission dispatch problems.* Journal of Computational Design and Engineering, 2024. **11**(1): p. 135-172.
55. Zhou, X., et al., *Boosted local dimensional mutation and all-dimensional neighborhood slime mould algorithm for feature selection.* Neurocomputing, 2023. **551**: p. 126467.
56. Liu, Y., et al., *Simulated annealing-based dynamic step shuffled frog leaping algorithm: Optimal performance design and feature selection.*

Neurocomputing, 2022. **503**: p. 325-362.
57. Zhou, H.M., et al., *A modified particle swarm optimization algorithm for a batch-processing machine scheduling problem with arbitrary release times and non-identical job sizes.* COMPUTERS & INDUSTRIAL ENGINEERING, 2018. **123**: p. 67-81.
58. Hussain, M., et al., *Energy and performance-efficient task scheduling in heterogeneous virtualized cloud computing.* SUSTAINABLE COMPUTING-INFORMATICS & SYSTEMS, 2021. **30**.
59. Lakhan, A., et al., *Deadline aware and energy-efficient scheduling algorithm for fine-grained tasks in mobile edge computing.* INTERNATIONAL JOURNAL OF WEB AND GRID SERVICES, 2022. **18**(2): p. 168-193.
60. Zhang, Y., et al., *Towards augmented kernel extreme learning models for bankruptcy prediction: algorithmic behavior and comprehensive analysis.* Neurocomputing, 2021. **430**: p. 185-212.
61. Yang, X., et al., *An optimized machine learning framework for predicting intradialytic hypotension using indexes of chronic kidney disease-mineral and bone disorders.* Computers in Biology and Medicine, 2022. **145**: p. 105510.
62. Liu, J., et al., *Chaotic simulated annealing multi-verse optimization enhanced kernel extreme learning machine for medical diagnosis.* Computers in Biology and Medicine, 2022. **144**: p. 105356.
63. Deng, W., et al., *An enhanced fast non-dominated solution sorting genetic algorithm for multi-objective problems.* INFORMATION SCIENCES, 2022. **585**: p. 441-453.
64. Tu, Y., *Artemisinin—A Gift from Traditional Chinese Medicine to the World (Nobel Lecture).* Angewandte Chemie International Edition, 2016. **55**(35): p. 10210-10226.
65. Wang, J., et al., *Artemisinin, the Magic Drug Discovered from Traditional Chinese Medicine.* Engineering, 2019. **5**(1): p. 32-39.
66. Tu, Y., *The discovery of artemisinin (qinghaosu) and gifts from Chinese medicine.* Nature Medicine, 2011. **17**(10): p. 1217-1220.
67. Bridgford, J.L., et al., *Artemisinin kills malaria parasites by damaging proteins and inhibiting the proteasome.* Nature Communications, 2018. **9**(1).
68. Visser, B.J., et al., *Efficacy and safety of artemisinin combination therapy (ACT) for non-falciparum malaria: a systematic review.* Malaria Journal, 2014. **13**(1): p. 463.
69. Isacchi, B., et al., *Conventional and long-circulating liposomes of artemisinin: preparation, characterization, and pharmacokinetic profile in mice.* Journal of Liposome Research, 2010. **21**(3): p. 237-244.
70. Beyer, H.G. and D.V. Arnold, *Theory of evolution strategies - A tutorial*, in *THEORETICAL ASPECTS OF EVOLUTIONARY COMPUTING*. 2001. p. 109-133.
71. Huang, H., et al., *SLNL: A novel method for gene selection and phenotype classification.* International Journal of Intelligent Systems, 2022. **37**(9): p. 6283-6304.
72. Li, J., et al., *MS2OD: outlier detection using minimum spanning tree and medoid selection.* Machine Learning: Science and Technology, 2024. **5**(1): p. 015025.
73. Chang, X., et al., *Unified Low-Rank Matrix Estimate via Penalized Matrix Least Squares Approximation.* IEEE TRANSACTIONS ON NEURAL NETWORKS AND LEARNING SYSTEMS, 2019. **30**(2): p. 474-485.
74. Jiang, X., et al., *Android Malware Detection Using Fine-Grained Features.* SCIENTIFIC PROGRAMMING, 2020. **2020**.
75. Garcia, S., et al., *Advanced nonparametric tests for multiple comparisons in the design of experiments in computational intelligence and data mining: Experimental analysis of power.* INFORMATION SCIENCES, 2010. **180**(10): p. 2044-2064.
76. Derrac, J., et al., *A practical tutorial on the use of nonparametric statistical tests as a methodology for comparing evolutionary and swarm intelligence algorithms.* SWARM AND EVOLUTIONARY COMPUTATION, 2011. **1**(1): p. 3-18.
77. Hussain, M., et al., *A multi-objective quantum-inspired genetic algorithm for workflow healthcare application scheduling with hard and soft deadline constraints in hybrid clouds.* Applied Soft Computing, 2022. **128**: p. 109440.
78. Lakhan, A., et al., *Federated Learning-Aware Multi-Objective Modeling and blockchain-enable system for IIoT applications.* Computers and Electrical Engineering, 2022. **100**: p. 107839.
79. Kennedy, J., R.C. Eberhart, and Ieee, *A discrete binary version of the particle swarm algorithm*, in *SMC '97 CONFERENCE PROCEEDINGS - 1997 IEEE INTERNATIONAL CONFERENCE ON SYSTEMS, MAN, AND CYBERNETICS, VOLS 1-5: CONFERENCE THEME: COMPUTATIONAL CYBERNETICS AND SIMULATION*. 1997. p. 4104-4108.
80. Mirjalili, S. and A. Lewis, *The Whale Optimization Algorithm.* Advances in Engineering Software, 2016. **95**: p. 51-67.
81. Mirjalili, S., *Moth-flame optimization algorithm: A novel nature-inspired heuristic paradigm.* Knowledge-based systems, 2015. **89**: p. 228-249.
82. Heidari, A.A., et al., *Harris hawks optimization: Algorithm and applications.* Future Generation Computer Systems, 2019. **97**: p. 849-

872.
83. Rawat, A., S. Singh, and J.C. Bansal, *Sine Cosine Algorithm: Introduction and Advances*, in *The Palgrave Handbook of Operations Research*, S. Salhi and J. Boylan, Editors. 2022, Springer International Publishing: Cham. p. 447-467.
84. Li, C.Y., et al., *Enhanced Harris hawks optimization with multi-strategy for global optimization tasks.* EXPERT SYSTEMS WITH APPLICATIONS, 2021. **185**.
85. Zhu, A., et al., *Hybridizing grey wolf optimization with differential evolution for global optimization and test scheduling for 3D stacked SoC*. Journal of Systems Engineering and Electronics, 2015. **26**(2): p. 317-328.
86. Iacca, G., V.C. dos Santos, and V.V. de Melo, *An improved Jaya optimization algorithm with Levy flight.* EXPERT SYSTEMS WITH APPLICATIONS, 2021. **165**.
87. Cai, Z., et al., *Evolving an optimal kernel extreme learning machine by using an enhanced grey wolf optimization strategy.* Expert Systems with Applications, 2019. **138**.
88. Kumar, N., et al., *Single Sensor-Based MPPT of Partially Shaded PV System for Battery Charging by Using Cauchy and Gaussian Sine Cosine Optimization.* Ieee Transactions on Energy Conversion, 2017. **32**(3): p. 983-992.
89. Heidari, A.A., R. Ali Abbaspour, and H. Chen, *Efficient boosted grey wolf optimizers for global search and kernel extreme learning machine training.* Applied Soft Computing, 2019. **81**: p. 105521.
90. Nenavath, H. and R.K. Jatoth, *Hybridizing sine cosine algorithm with differential evolution for global optimization and object tracking.* Applied Soft Computing, 2018. **62**: p. 1019-1043.
91. Qu, C., et al., *A Modified Sine-Cosine Algorithm Based on Neighborhood Search and Greedy Levy Mutation.* Computational intelligence and neuroscience, 2018. **2018**: p. 4231647-4231647.
92. Chen, C., et al., *Dealing with multi-modality using synthesis of Moth-flame optimizer with sine cosine mechanisms.* Mathematics and Computers in Simulation, 2021. **188**: p. 291-318.
93. Chen, H., et al., *An efficient double adaptive random spare reinforced whale optimization algorithm.* Expert Systems with Applications, 2019.
94. Zhan, G., et al., *Auto-CSC: A Transfer Learning Based Automatic Cell Segmentation and Count Framework.* Cyborg and Bionic Systems, 2022. **2022**.
95. Kapur, J.N., P.K. Sahoo, and A.K.C. Wong, *A new method for gray-level picture thresholding using the entropy of the histogram.* Computer Vision, Graphics, and Image Processing, 1985. **29**(3): p. 273-285.
96. Otsu, N.J.I.t.o.s., man, and cybernetics, *A threshold selection method from gray-level histograms.* 1979. **9**(1): p. 62-66.
97. Buades, A., B. Coll, and J.M. Morel, *A non-local algorithm for image denoising*, in *2005 IEEE COMPUTER SOCIETY CONFERENCE ON COMPUTER VISION AND PATTERN RECOGNITION, VOL 2, PROCEEDINGS*. 2005. p. 60-65.
98. Shi, M.R., et al., *A grade-based search adaptive random slime mould optimizer for lupus nephritis image segmentation.* COMPUTERS IN BIOLOGY AND MEDICINE, 2023. **160**.
99. Hu, C., et al., *Trustworthy multi-phase liver tumor segmentation via evidence-based uncertainty.* Engineering Applications of Artificial Intelligence, 2024. **133**: p. 108289.
100. Oliva, D., et al., *Image segmentation by minimum cross entropy using evolutionary methods.* SOFT COMPUTING, 2019. **23**(2): p. 431-450.
101. Mehmet, S. and S. Bülent, *Survey over image thresholding techniques and quantitative performance evaluation.* Journal of Electronic Imaging, 2004. **13**(1): p. 146-165.
102. Liao, P.S., Chen, T. S., & Chung, P. C., *A fast algorithm for multilevel thresholding.* Journal of Information Science and Engineering, 2001. **17**: p. 713-727.
103. Storn, R. and K. Price, *Differential evolution - A simple and efficient heuristic for global optimization over continuous spaces.* JOURNAL OF GLOBAL OPTIMIZATION, 1997. **11**(4): p. 341-359.
104. Yang, X.S. and S. Deb, *Cuckoo Search via Levey Flights*, in *2009 WORLD CONGRESS ON NATURE & BIOLOGICALLY INSPIRED COMPUTING (NABIC 2009)*. 2009. p. 210-+.
105. Horé, A. and D. Ziou. *Image Quality Metrics: PSNR vs. SSIM*. in *2010 20th International Conference on Pattern Recognition*. 2010.
106. Wang, Z., et al., *Image quality assessment: From error visibility to structural similarity.* IEEE TRANSACTIONS ON IMAGE PROCESSING, 2004. **13**(4): p. 600-612.
107. Zhang, L., et al., *FSIM: A Feature Similarity Index for Image Quality Assessment.* IEEE TRANSACTIONS ON IMAGE PROCESSING, 2011. **20**(8): p. 2378-2386.
108. Tong, Y., et al., *Research of spatial context convolutional neural networks for early diagnosis of Alzheimer's disease.* The Journal of Supercomputing, 2024. **80**(4): p. 5279-5297.

109. Yang, N., et al., *Cooperative multi-population Harris Hawks optimization for many-objective optimization.* Complex & Intelligent Systems, 2022. **8**(4): p. 3299-3332.
110. Li, Y., et al., *Spatio-Temporal-Spectral Hierarchical Graph Convolutional Network With Semisupervised Active Learning for Patient-Specific Seizure Prediction.* IEEE Transactions on Cybernetics, 2022. **52**(11): p. 12189-12204.